SYNTHESIS OF HEPTAKIS-2-*O*-SULFO-CYCLOMALTOHEPTAOSE, A SINGLE-ISOMER CHIRAL RESOLVING AGENT FOR ENANTIOMER SEPARATIONS IN CAPILLARY ELECTROPHORESIS

A Dissertation

by

EDWARD TUTU

Submitted to the Office of Graduate Studies of
Texas A&M University
in partial fulfillment of the requirements for the degree of

DOCTOR OF PHILOSOPHY

December 2010

Major Subject: Chemistry

SYNTHESIS OF HEPTAKIS-2-*O*-SULFO-CYCLOMALTOHEPTAOSE, A SINGLE-ISOMER CHIRAL RESOLVING AGENT FOR ENANTIOMER SEPARATIONS IN CAPILLARY ELECTROPHORESIS

A Dissertation

by

EDWARD TUTU

Submitted to the Office of Graduate Studies of
Texas A&M University
in partial fulfillment of the requirements for the degree of

DOCTOR OF PHILOSOPHY

Approved by:

Chair of Committee,	Gyula Vigh
Committee Members,	David H. Russell
	Emile A. Schweikert
	Surya Waghela
Head of Department,	David H. Russell

December 2010

Major Subject: Chemistry

ABSTRACT

Synthesis of Heptakis-2-*O*-Sulfo-Cyclomaltoheptaose, a Single-Isomer Chiral Resolving Agent for Enantiomer Separations in Capillary Electrophoresis.

(December 2010)

Edward Tutu, B.S., University of Cape Coast; M.S., University of Minnesota

Chair of Advisory Committee: Dr. Gyula Vigh

Single-isomer sulfated cyclodextrins (SISCDs) have proven to be reliable, effective, robust means for separation of enantiomers by capillary electrophoresis (CE). SISCD derivatives used as chiral resolving agents in CE can carry the sulfo groups either at the C2, C3 or C6 positions of the glucopyranose subunits which provides varied intermolecular interactions to bring about favorable enantioselectivities.

The first single-isomer, sulfated β-CD that carries the sulfo group at the C2 position, the sodium salt of heptakis(2-*O*-sulfo-3-*O*-methyl-6-*O*-acetyl)cyclomaltoheptaose (HAMS) has been synthesized. The purity of each synthetic intermediate and of the final product was determined by HILIC and reversed phase HPLC. The structural identity of each intermediate and the final product was verified by 1D, and 2D NMR, and MALDI-TOF mass spectrometry.

HAMS has been used as chiral resolving agent for the CE separation of a set of nonionic, weak base and strong acid enantiomers in pH 2.5 background electrolytes. Rapid separations with satisfactory peak resolution values were obtained for the

enantiomers of most of the nonionic and weak base analytes. Typically, low concentrations of HAMS were required to effect good enantiomer resolution.

The trends in the effective mobilities and separation selectivities as a function of HAMS concentrations followed the predictions of the ionic strength-corrected charged resolving agent migration model (CHARM model). HAMS showed poor complexation with the anionic strong electrolyte enantiomers for which no peak resolution was observed. The separation patterns observed with HAMS as chiral resolving agent were compared with those of other β-cyclodextrin analogues, including heptakis(2-*O*-methyl-3-*O*-acetyl-6-*O*-sulfo)-β-cyclodextrin (HMAS), heptakis(2-*O*-methyl-3,6-di-*O*-sulfo)-β-cyclodextrin (HMdiSu), heptakis(2,3-di-*O*-acetyl-6-*O*-sulfo)-β-cyclodextrin (HDAS) and heptakis(2,3-di-*O*-methyl-6-*O*-sulfo)-β-cyclodextrin (HDMS).

DEDICATION

To my wife, Ingri, my parents, Emmanuel and Victoria, my brothers, Rexford, Ernest and Raymond, and my parents-in-law, Marvin and Shirley for their unconditional support.

ACKNOWLEDGEMENTS

I would like to give thanks to Almighty God for all his blessings. Thanks to Dr. Shane Tichy, Dr. Yohannes Rezenom and Vanessa Santiago of the Laboratory for Biological Mass Spectrometry for their contributions to this body of work. Many thanks to Dr. Steve Silber and Dr. Sarathy, for assistance with NMR.

I would like to thank my fellow research group members of the TAMU Separation Science group, past and present, including Brent Busby, Sanjiv Lalwani, Kingsley Nzeadibe, Ann Hwang, Evan Shaves, Peniel Lim, Omar Maldonando, Helen Craver, Brian Sinajon, Roy Estrada, Robert North and Ming-Chien Li for their insight and support.

I really appreciate the time and effort of my committee members: Dr. David H. Russell, Dr. Emile A. Schweikert, and Dr. Surya Waghela. The help from the Chemistry Department is also greatly appreciated.

Finally, I would like to express my gratitude to my advisor Dr. Gyula Vigh for his guidance, and everything he did for me during my studies at Texas A&M University.

NOMENCLATURE

Ac_2O	acetic anhydride
CE	capillary electrophoresis
DMF	*N*,*N*-dimethylformamide
DMSO	dimethylsulfoxide
EOF	electroosmotic flow
EtOAc	ethylacetate
EtOH	ethanol
MeOH	methanol
Py	pyridine
$Pyr.SO_3$	pyridine sulfur trioxide
SISCD	single-isomer sulfated cyclodextrin
TBAI	tetrabutylammonium iodide
TBDMS	tert-butyldimethylchlorosilane
THF	tetrahydrofuran

TABLE OF CONTENTS

CHAPTER Page

LIST OF FIGURES

Page

Page

Page

Page

LIST OF TABLES

CHAPTER I

INTRODUCTION

1.1 Enantiomers and Separation Techniques

It has been reported that among 523 natural and semi-synthetic drugs, approximately 99% are chiral and about 98% of them are sold as a single isomer. In the case of synthetic drugs, about 12% of them are sold as a single isomer.[1] Enantiomers can have different biological or pharmacological activity. Thus one enantiomer may be the effective agent with a useful therapeutic value, while the other enantiomer might be inactive or active in a different way, contributing to side-effects, or be even toxic.[2] These differences in the biological activity of enantiomers stem from their different mode of protein binding and transport, rate of metabolism as well as mechanism of action.[3] Therefore, the pharmacological effects and metabolic pathways for each enantiomer of a new chiral drug must be thoroughly studied before it is approved for human consumption.[4] However, in order to study these properties effectively, a suitable method for separation of enanantiomers should be developed.

Most common methods used in enantioseparation include gas chromatography (GC),[5,6] high performance liquid chromatography (HPLC), including both normal and reversed phase,[7, 8, 9] ion-chromatography[10] and thin-layer chromatography (TLC),[11,12]

This dissertation follows the style of *Analytical Chemistry*.

supercritical fluid chromatography (SFC)[13,14] and capillary electrophoresis (CE)[15]. Though the separation efficiency of capillary GC is high, it is limited to the analysis of volatile analytes or their derivatives. HPLC has lower separation efficiency than capillary GC. The utility of TLC is limited by its low separation efficiency and narrow linear range in detection.

CE has proven to be a powerful tool for the separation of enantiomers. In addition to its high resolving power and low consumption of sample and solvent, it demonstrates flexibility with regards to using and changing chiral resolving agents.[16] The main advantages of this technique include: (i) the broad variety of chiral resolving agents and (ii) the high efficiency attainable by CE.[17]

1.2 Fundamentals of Capillary Electrophoresis (CE)

In CE, molecules that are charged migrate under the influence of an electric field, with a certain electrophoretic velocity, ν. This velocity is proportional to the electric field strength, E:

$$\nu = \mu E \qquad (1)$$

where the constant of proportionality, μ, called electrophoretic mobility, is a function of the ratio of the ionic charge (q) to the hydrodynamic radius (r) of the analyte ion, and viscosity (η) of the solution, expressed as:

$$\mu = \frac{q}{6\eta\pi r} \qquad (2)$$

Zone electrophoretic separation is based upon the electrophoretic mobility differences among the analytes.

1.2.1 Significance of Electroosmotic Flow (EOF)

In CE, fused silica capillaries are most commonly used for separation. When the capillary is filled with background electrolyte (BGE), the silanol groups on the surface of the fused silica capillary partially dissociate forming SiO^- and hydronium ions. The extent of the dissociation of the silanol groups depends on the pH of the BGE. Thus, immobilized negative charges can be created on the inner wall of the capillary. In order to maintain electric neutrality, some of the positive ions in the BGE are strongly attracted to the wall forming a "fixed" or Stern layer. The remaining cations which are less-tightly held are in the diffused (Gouy-Chapman) layer farther out into the solution. This leads to the formation of a double layer. The potential at the shear plane between the two layers is known as the zeta (ζ) potential.[18] Upon application of a potential across the length of the capillary, the solvated cations in the diffuse layer migrate toward the cathode at a constant velocity, dragging along their hydrated layer (bulk solvent molecules). Thus, a bulk flow of the BGE, electroosmotic flow, is obtained in the capillary.

The electroosmotic velocity (v^{eo}), relates to the permittivity of the medium (ε), the dielectric constant (ε_0), the zeta potential (ζ), the dynamic viscosity of the medium (η), and the applied electric field strength (E) as:[19]

$$v^{eo} = -\frac{\varepsilon_0 \varepsilon \zeta}{\eta} \mathrm{E} = \mu^{eo} \mathrm{E} \qquad (3)$$

The negative sign is an indication of the direction of the bulk flow toward the cathode. The most pronounced property of EOF is its flat or plug-like flow profile, compared to the parabolic flow profile of pressure-driven flow observed in HPLC.[20] This eliminates the most significant band broadening mechanism, related to the parabolic flow profile observed in HPLC, which leads to high separation efficiency in CE than in HPLC.

With a sufficiently high EOF, it is possible to detect cations, anions and uncharged molecules in a single CE run.

1.2.2 Significance of BGE

The BGE regulates the pH of the system in addition to conducting electric current for the separation of analytes. As such, BGEs must contain enough ions to transport the electric current. Furthermore, the BGE must have significant buffering capacity at the selected pH.[21] When electric current is generated by the application of voltage across the capillary, the temperature of the solution inside the capillary increases due to Joule heating. As a result, the properties of the BGE including its viscosity and

the mobility of the EOF are affected. According to, e.g., Ryslavy et al.,[22] Joule heat will also cause temperature differences (ΔT) between the walls and the center of the capillary. They reported that ΔT depends on the electric field strength (E), the conductivity of the solution (k) and the radius of the capillary (r) as:

$$\Delta T \sim E^2 k r^2 \qquad (4)$$

The radial temperature difference leads to a radial velocity distribution that causes extra peak broadening which, in turn, decreases separation efficiency and peak resolution. From equation 4, low conductance BGEs and small internal diameter capillaries are preferred.

The mobility of EOF depends on the pH and the ionic strength (*I*) of the BGEs. Likewise, the effective mobility of an analyte depends on the ionic strength of the BGE and the effective charge, z of the analyte as expressed by the equation:[18,23]

$$\frac{\mu^{eff}}{\mu_0} = \exp(-0.77)(zI)^{1/2} \qquad (5)$$

where μ_0 is the ionic mobility at infinite dilution. The ionic strength[19] of the BGE, *I*, is defined as

$$I = \frac{1}{2}\sum c_i z_i^2 \qquad (6)$$

where c is the concentration and z is the charge of the ionic species of the BGE.

Charged analytes migrate with their observed mobility, μ^{obs}, which is a combination of their effective electrophoretic mobility, μ^{eff}, and the non-selective electroosmotic mobility, μ^{eo}, given by

$$\mu^{obs} = \mu^{eff} + \mu^{eo} \qquad (7)$$

1.3 Chiral Resolving Agents Used in CE

Several chiral resolving agents have been used in CE separations. Examples include macrocyclic antibiotics,[24-29] proteins,[30-32] chiral crown ethers,[28, 30, 33] linear oligo- and polysaccharides,[34, 35] and cyclodextrins (CDs). Although proteins and macrocyclic antibiotics are good chiral resolving agents, they adsorb on the capillary wall and also absorb UV light. Linear oligosaccharides complex with analytes weakly compared with cyclodextrins.[30, 35] Chiral crown ethers bind only enantiomers that contain primary amino groups which limits their applicability. Moreover, BGEs used for separations involving chiral crown ethers are restricted to cations other than potassium and ammonium ions.[33] Up to date[36], CDs still remain the most dominant chiral resolving agents employed in CE enantioseparations.

1.4 Cyclodextrins and Principle of Chiral Recognition

CDs are neutral, cyclic, non-reducing oligosaccharides that contain 6, 7 or 8 D (+) - glucopyranose units bonded through α-1,4-glycosidic linkages.[37] CDs having 6, 7 and 8 glucopyranose units are called α-, β- and γ-cyclodextrins, respectively. The native CD, shown in idealized form in Figure 1 is a hallow, truncated cone having an axial cavity with primary hydroxyl groups around its narrower rim and, secondary hydroxyl groups on the opposite, wider rim.[38] The outside of CD is hydrophilic due to the presence of primary and secondary hydroxyl groups, which allow dissolution in the aqueous BGE while the cavity of the CD is hydrophobic.[16] The crystallographic diameter of the hydrophobic cavity is 0.57, 0.78 and 0.95 nm for α-, β-, and γ-CD, respectively.[39] Chiral recognition in CDs comes from the five asymmetric chiral carbon atoms on each glucopyranose unit.[40] Enantioselectivity, which is based on the formation of temporal diastereoisomer complexes can be rationalized with the help of a three-point interaction model.[41] Depending on the inner diameter of the cavity of the CDs and the size of the enantiomer, the enantiomer can form host-guest complexes in dynamic equilibrium with CDs through full or partial inclusion into cavities of the CDs. Stabilization of these complexes is influenced by steric parameters of the enantiomer, and also by the possibility of creating intermolecular interactions, including van der Waals, charge transfer type (π-π), dipole-type, hydrophobic, hydrogen bonding or electrostatic interactions between substituents of the CD and the enantiomers.[42] The strength of interaction of the two enantiomers with the CD molecule can be different

from each other, which leads to different complexation constants. This, in turn, leads to different electrophoretic mobilities and possibly CE separation.

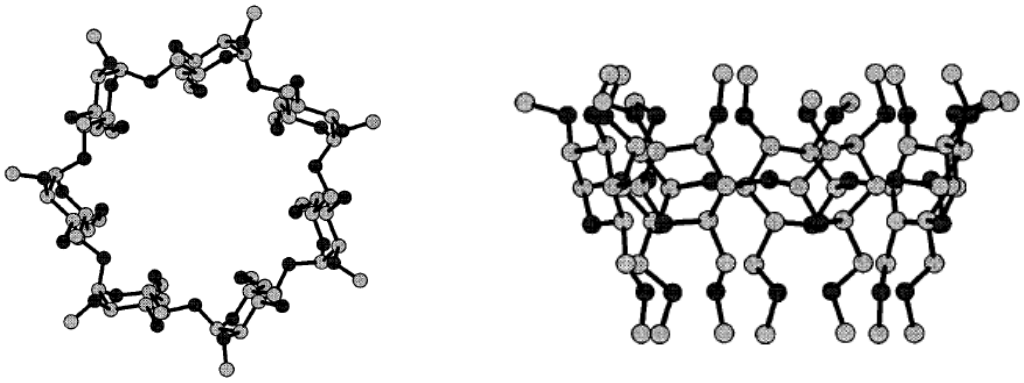

Top view Side view

Figure 1. Idealized structure of β-cyclodextrin

Accurate description of the chiral recognition mechanism is still lacking at the molecular level,[43] though NMR spectroscopy and X-ray crystallography have been used to provide direct evidence for the binding of enantiomers to chiral selectors.[44]

1.5 Cyclodextrins as Chiral Resolving Agents in CE

The advantages of CDs compared to other resolving agents include their UV transparency and solubility in aqueous solutions.[45] CDs used for enantioseparation in CE include the native species as well as those modified with charged and non-charged

functional groups. Neutral CDs include native α-, β-, and γ-CDs and those derivatized with methyl, acetyl or hydroxypropyl groups. Neutral CDs are, however, not applicable for analysis of neutral enantiomers. Also, native CDs exhibit lower aqueous solubilities compared to their functionalized derivatives: the solubility of β–cyclodextrin is 16mM[38] while 40mM[46] has been reported for heptakis(2,6-di-*O*-methyl)-β-CD. Carboxylic acids, dialkyl- and trialkylamine derivatives are examples of weakly acidic and weakly basic charged CDs. The major limitation of these derivatives is that their charge state is pH dependent.[47] Sulfated and sulfoalkyl ether CDs and quaternary ammonium CDs are examples of strongly acidic and strongly basic charged CDs. The charge state of these permanently charged CDs is pH independent. Quaternary ammonium CDs however do adsorb onto the walls of the fused silica capillary. Therefore, sulfated CDs are preferred for CE separations.

Sulfated CDs that are commercially available are random mixtures of isomers with different degrees of substitution. For a given enantiomer pair, each CD isomer exhibits a unique binding characteristics. As a result, it would be difficult to predict the outcome of interactions with a particular analyte. In addition, the possibility of conducting a systematic study of chiral CE enantioseparation at the molecular level as well as robust method development would be hindered.[48] In order to eliminate problems associated with the randomly sulfated CDs, single-isomer, sulfated cyclodextrins (SISCDs) need to be synthesized.

1.5.1 Synthetic Strategies for Selective Modification of Cyclodextrins

Generally, SISCDs are made by adopting protecting and deprotecting synthetic schemes. It is reported[49] that the selective functionalization of the primary and secondary hydroxyl groups of CD is not trivial. However, several synthetic strategies have been developed to selectively functionalize either all the primary hydroxyl groups[50] or all the secondary hydroxyl groups.[51] These include: i) one step extensive per-functionalization of 6-hydroxyl groups; ii) two step bi-functionalization of hydroxyl groups at C-2 and C-6 positions with identical groups; iii) two step modification of the hydroxyl groups at C-2 and C-6 with different substituents. Complexity of the problem is increased if selective functionalization of all the hydroxyl groups at the 2-position and none at the 3-position, is desired. Methods available to achieve such control are often cumbersome or provide low yield of the desired product.[52] The hydroxyl groups at the 6-position with pK_a = 15-16 are the most reactive due to low steric hinderance. The hydroxyl groups at the 2-position are the most acidic with a pK_a of 12.1. The hydroxyl group at the 3-position are the least reactive and resist functionalization. This has been attributed to hydrogen bond formation between the protons of the hydroxyl groups at the 3-position and the oxygen atoms of the hydroxyl groups at the 2-position.[53]

The *tert*-butyldimethylsilyl (TBDMS) group has proved to be a valuable protecting group in CDs because it can be selectively attached to the primary 6-hydroxyl groups of CDs.[54] Rong and D'Souza[55] reported a new convenient strategy for functionalization of the 2-position of CDs by NaH to form an alkoxide that readily reacts with an electrophile. This strategy offers regioselective persubstitution of the 2-

hydroxyl groups. Subsequent protection and deprotection steps can be performed to allow the functionalization of hydroxyl groups in the 3-position and 6-position, independently of one another.

These regioselective persubstitution modification techniques were exploited in the synthesis of the novel SISCD described in this dissertation.

1.5.2 Use of SISCD for Enantioseparation by CE

SISCDs are reliable and effective resolving agents for robust CE enantioseparations.[56] Several SISCDs have been synthesized and employed for the electrophoretic separation of enantiomers including acids, bases, neutrals and ampholytics using different concentrations of CDs and pH in aqueous[57] and methanolic[58] BGEs. Heptakis(2,3-di-*O*-acetyl-6-*O*-sulfo)-β-CD,[59] heptakis(6-*O*-sulfo)-β-CD ,[60] and heptakis(2,3-di-*O*-methyl-6-*O*-sulfo)-β-CD [61] analogs were the first SISCDs used for CE enantioseparations. Further research led to the development of the corresponding α-[57, 62, 63] and γ-CD[64-67] derivatives. Recently, the first set of SISCDs carrying non-identical substituents at all the C2, C3, and C6 positions, namely heptakis(2-*O*-methyl-3-*O*-acetyl-6-*O*-sulfo)-β-CD[68] and heptakis(2-*O*-methyl-6-*O*-sulfo)-β-CD[69] were reported. Another derivative carrying sulfate groups at both the C3 and C6 positions, heptakis(2-*O*-methyl-3,6-di-*O*-sulfo)-β-CD has been synthesized and its enantiorecognition behavior has also been investigated.[70] All these derivatives thus far carry the sulfate group at either the C3 or C6 positions. In order to have a better understanding of the role of the sulfate moiety

in enantiorecognition, SISCDs that carry the sulfate group exclusively at C2 position of the glucopyranose units have to be synthesized.

1.5.3 SISCDs and Separation Models

To better understand the different factors (including type of CD, the concentration of CD and pH) involved in enantiorecognition and also aid method development for CE enantiomer separations, two major theoretical models were developed. The first model, reported by Wren and Rowe[71-74] for neutral cyclodextrins and based on secondary equilibria, showed that the difference in the apparent electrophoretic mobility between enantiomers is related to the differences between the complexation contants of the enantiomers, the mobilities of the free and the complexed analytes, and the concentration of the chiral resolving agent expressed as:

$$\Delta\mu = \frac{[C](\mu_1 - \mu_2)(K_2 - K_1)}{1 + [C](K_1 + K_2) + K_1 K_2 [C]^2} \qquad (8)$$

where $\Delta\mu$ is the apparent mobility difference between the enantiomers, C is the concentration of the chiral selector, μ_1 is the mobility of the analyte in free solution, μ_2 is the mobility of the analyte-chiral selector complex and K_1 and K_2 are binding constants of the enantiomers. From equation 8, they indicated that there exits an optimum CD concentration expressed as a function of the two enantiomer-CD binding constants as:

$$[C]^{opt} = \frac{1}{\sqrt{K_1 K_2}} \qquad (9)$$

where K_1 and K_2 are the binding constants for the enantiomer-CD complexes. This model was verified experimentally by native β-CD and randomly methylated β-CD. This approach considers mobility difference rather than peak resolution.

Major limitation of the model include the exclusion of important operational parameters such as pH of the BGE, electric field strength and electroosmotic mobility.

The second model, called the Charged Resolving Agent Migration model (CHARM model) developed by Williams et al.[47] for the rational, predictable design of the separation of chiral weak electrolyte (including weak acids and weak bases) and neutral analytes with charged chiral resolving agents takes into account the effect of pH on separation selectivity. This secondary equilibra-based model looks at resolution and separation selectivity as a function of the concentration of the charged single-isomer cyclcodextrin (CCD) and pH of the BGE. For a 1:1 complex between the CCD and the analyte, the resulting effective mobility of one of the enantiomers can be expressed as:

$$\mu_R^{eff} = \frac{\mu_R^0 + \mu_{RCD}^0 K_{RCD}[CD] + K[H_3O](\mu_{HR}^0 + \mu_{HRCD}^0 K_{HRCD}[CD])}{1 + K_{RCD}[CD] + K[H_3O](1 + K_{HRCD}[CD])} \qquad (10)$$

where μ^o_R and μ^o_{RCD}, μ^o_{HR} and μ^o_{HRCD} are the ionic mobilities of the uncomplexed and fully complexed species, K_{RCD} and K_{HRCD} are the complexation coefficients for the non-

protonated and the protonated forms of the enantiomer, *K* is the acid dissociation constant for the enantiomer, and [H_3O] and [CD] are the concentrations of the hydronium ion and the resolving agent.

Separation selectivity, α, for a given enantiomer pair, offered by a particular CD concentration is described as:

$$\alpha = \frac{\mu_1^{eff}}{\mu_2^{eff}} \tag{11}$$

where subscripts 1 and 2 refer to the more and less mobile enantiomer, respectively. In an ideal CE system, where peak dispersion is caused only by longitudinal diffusion, peak resolution[47] is expressed as:

$$R_s = \sqrt{\frac{ELe_o}{8kT}} \times \frac{|\alpha - 1|\sqrt{|\alpha + \beta|}\sqrt{|1 + \beta|}\sqrt{z_1^{eff}}\sqrt{z_2^{eff}}}{\sqrt{|\alpha + \beta|^3}\sqrt{z_1^{eff}} + \sqrt{\alpha|1 + \beta|^3}\sqrt{z_2^{eff}}} \tag{12}$$

Here, E is the electric field strength, k is the Boltzman contant, e_0 is the electric charge, T is the absolute temperature, l is the capillary length from injector to the detector, z_i^{eff} is the effective charge of the solutes, and β is the normalized electroosmotic mobility calculated as:

$$\beta = \frac{\mu^{eo}}{\mu_2^{eff}} \tag{13}$$

Thus, peak resolution depends on α, β and z^{eff} as shown in Figure 2. In addition to selectivity optimization, the key to the development of enantiomer separations lies in optimizing the β term through the use of a coated capillary and/or appropriate background electrolyte constituents. By optimizing β and knowing the dependence of α, and z_i^{eff} on the composition of the BGE, resolution can be achieved.

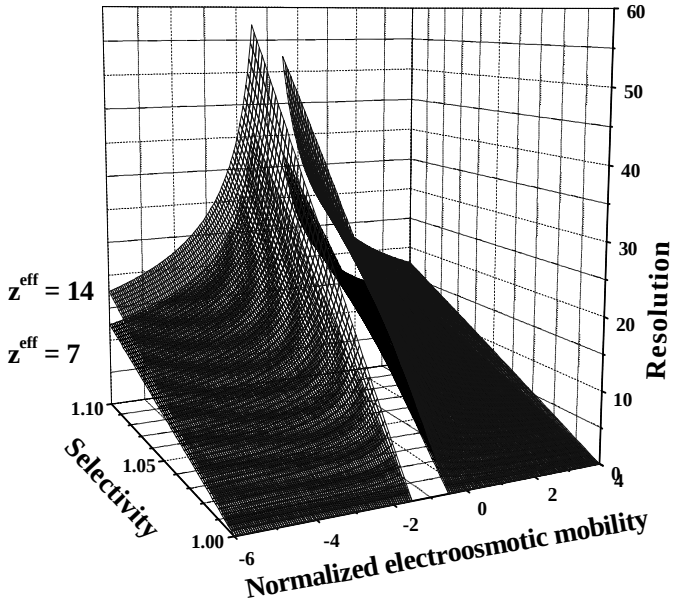

Figure 2. Peak resolution surfaces for 7-charged and 14-charged cyclodextrins as a function of separation selectivity and normalized electroosmotic mobility

According to equation 12 when all other parameters are equal, resolution increases with the square root of z_i^{eff}. The three-dimensional resolution surface in Figure 2 indicates that resolution increases with the effective charge as long as the other parameters remain the same. Under identical α and z^{eff}, peak resolution increases towards infinitely high values as β approaches -1. As long as the cyclodextrin shows some selectivity for the enantiomers, peak resolution can be improved by optimizing β at the expense of increasing analysis time. It also shows that initially, peak resolution increases linearly with α.

According to the predictions of the CHARM model, three types of enantiomer separations are possible for weakly basic and acidic analytes: ionoselective, desionoselective and duoionoselective separations. Ionoselective separation occurs when only the dissociated forms of the enantiomers complex selectively with the charged CD. On the other hand, desionoselective separation is achieved when the nondissociated forms of the enantiomers complex selectively with the charged CD. When both the dissociated and nondissociated forms complex selectively with the charged CD, duoselective separation is achieved.[47] Peak resolution, according to the CHARM model for weak electrolytes, depends on the pH of the BGE. For ionoselective separation of weak bases and desionoselective separation of weak acids, peak resolution is high at low pH. For desionoselective separation of weak bases and ionoselective separation of weak acids peak resolution is high at high pH. Peak resolution for duoselective separation of both weak acids and weak bases is high at both low and high pH. For neutrals and permanently charged analytes, peak resolution values are similar at all pH values.

Practically, the most efficient approach to chiral CE separation method development is the use of only two stock BGEs: one at low pH and the other at high pH.[47]

This dissertation will discuss the synthesis and characterization of the first single-isomer sulfated CD that carriers the sulfate group exclusively at C2 position, heptakis(6-*O*-acetyl-3-*O*-methyl-2-*O*-sulfo)-β-CD. The possibility for unique separation selectivity offered by charged sulfate groups on the chiral face of the cyclodextrin is of particular interest. A single-isomer, 2-sulfated CD would add to the arsenal of chiral resolving agents available for separations and permit the study of selectivity and resolution for various enantiomers, and aid in the rational design of chiral separations according to the CHARM model.

CHAPTER II

SYNTHESIS AND CHARACTERIZATION OF HEPTAKIS(2-*O*-SULFO-3-*O*-METHYL-6-*O*-ACETYL)CYCLOMALTOHEPTAOSE (HAMS)

Single-isomer CD derivatives used as chiral resolving agents in capillary electrophoresis can carry the sulfo groups either at the C2, C3 or C6 positions. There are no reports on the synthesis or use of a single-isomer cyclodextrin that carries the sulfo moiety at the C2 position. This chapter describes the synthesis of the first single-isomer β-CD derivative that is sulfated at the C2 position, the sodium salt of heptakis(2-*O*-sulfo-3-*O*-methyl-6-*O*-acetyl)cyclomaltoheptaose (HAMS).

2.1 Materials and General Methods

β-cyclodextrin was purchased from Cerestar, (Cedar Rapids, IA). *tert*-Butyldimethylsilyl chloride (TBDMS) was obtained from FMC Lithium Div. (Bessemer City, NC). Imidazole (Im) was obtained from ChemImpex (Wood Dale, IL). Tetrabutylammonium iodide (TBAI), sodium hydride (60% dispersion in oil), iodomethane and sulfur trioxide pyridine complex were purchased from Aldrich Chemical Co. (Milwaukee, WI). Hydrofluoric acid, acetic anhydride and all reaction solvents were obtained from Mallinckrodt Chemical Co. (St. Louis, MO). Activated, 4Å-molecular sieves from Fischer Scientific, Inc. (Fairlawn, NJ) were used to dry the solvents. For some of the β-CD intermediates, progress of the reaction was monitored by aluminium backed Silica-60 TLC plates, obtained from E.M. Science (Gibbstown,NJ). A

staining solution, composed of 35g α-napthol, 140 ml conc. sulfuric acid, 420ml ethanol and 88ml deionized water was used to visualize spots of the cyclodextrin derivatives. Visualization was accomplished by dipping the developed TLC plates into the staining solution, then heating them in an oven at 110ºC for 10 minutes. An HPLC system containing a programmable solvent delivery module 126 (Beckman-Coulter, Fullerton, CA), a Sedex Model 55 evaporative light scattering detector (S.E.D.E.R.E., Alfortville, France), and an AD 406 data acquisition system operated under Gold 8.1 software control (Beckman-Coulter) running on a 486DX4 personal computer (Computer Associates, College Station, TX) was used to establish the purity of all intermediates. Separations were obtained on a 4.6 mm I. D. × 250 mm analytical column packed with a 5μm Luna C18 stationary phase (Phenomenex, Torrance, CA). The purity values reported in this dissertation were calculated with the assumption that the response factors of the evaporative light scattering detector were the same for all CD isomers. The progress of the sulfation reaction and the purity of the sulfated β-CD product were monitored by hydrophilic interaction chromatography (HILIC) using a 4.6 mm I. D. × 150 mm analytical column packed with a 3μm Luna HILIC stationary phase (Phenomenex, Torrance, CA).

^{1}H, ^{13}C and DEPT NMR spectra were obtained on Varian 300 and 500 MHz UnityPlus Spectrometers equipped with a $^{1}H/^{19}F/^{31}P/^{13}C$ quad probe, using VnmrJ 2.2 C/D and Red Hat Linux softwares. 2-D NMR experiments including ^{1}H-^{1}H correlation spectroscopy (^{1}H-^{1}H COSY) and ^{1}H-^{13}C heteronuclear correlation spectroscopy were used for assignment of the proton and carbon signals.

The molecular mass of the intermediates was obtained by high resolution MALDI-TOF-MS. A Voyager Elite XL TOF mass spectrometer equipped with delayed extraction capability (PerSeptive Biosystems, Framingham, MA) and operated in reflectron mode with an acceleration voltage of 25 kV, 70% grid voltage, 0.035% guide wire voltage, and a delay time of 180 μs, was used to collect the high-resolution mass spectra. The analytes were spotted onto a Teflon target plate using the dried droplet method.[75] The matrix was prepared by dissolving 10 mg 2,4,6-trihydroxyacetophenone (THAP) in 1 mL acetonitrile.[76]

The molecular mass of the final product was obtained by ESI-TOF-MS with a Vestec Model 201-A single quadrupole mass spectrometer equipped with a Vestec electrospray ion source (PerSeptive Biosystems). The sample was prepared at a concentration of 2 mg/mL in an acetonitrile : water 1:1 (v/v) solvent mixture.

All electrophoretic measurements were made using a P/ACE 5010 system (Beckman-Coulter) equipped with a variable wavelength UV detector operated at 214 nm and a 26.4 / 19.6 cm long, 25 μm I. D. bare fused silica capillary column (Polymicro Technologies, Phoenix, AZ). The applied potential was varied between 5 and 25 kV. The cartridge coolant of the P/ACE 5010 was thermostated at 20^{o}C. The P/ACE 5010 system was interfaced with a 486DX-66 IBM personal computer.

2.2 Synthesis and Characterization of HAMS

Regioselective protection and deprotection methods were employed for functionalization of the hydroxyl groups at the 2, 3 and 6-C positions of β-CD. HAMS

was synthesized according to the scheme shown in Figure 3. The details of the synthetic procedure are outlined in the Appendix.

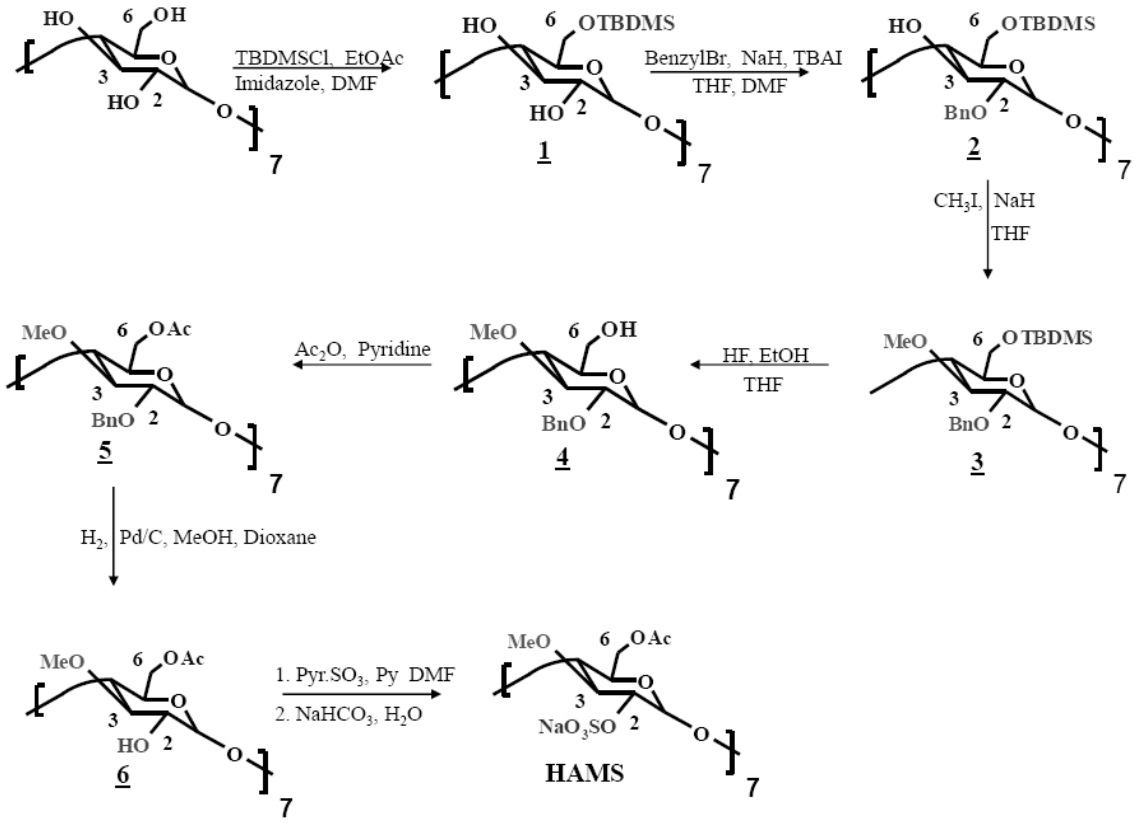

Figure 3. Synthesis scheme for HAMS

2.2.1 Heptakis(6-*O*-*t*-butyldimethylsilyl)cyclomaltoheptaose, Intermediate (1)

According to a modified procedure of Takeo,[54] the primary hydroxyl groups at the C-6 positions of β-CD were reacted in DMF with *t*-butyldimethylchlorosilane dissolved in ethyl acetate. The progress of the reaction was monitored by isocratic non-aqueous RP-HPLC using a 5µm Luna, C18 column and a 70 : 30 MeOH : EtOAc mobile phase at a flow rate of 2 ml/min, at ambient temperature. ImHCl generated in the reaction was filtered out at the end and the solvent was removed under vacuum. The crude product was recrystallized from a DMF/acetone/water solvent mixture and dried in vacuo. The isomeric purity of intermediate (**1**) was > 99%. Figure 4 shows a chromatogram of the recrystallized product overlaid with a chromatogram of the mother liquor.

^{1}H and ^{13}C NMR spectra are shown in Figures 5 and 6, respectively. Peak assignments were determined from the DEPT and 2-dimensional ^{1}H-^{1}H COSY and ^{1}H-^{13}C HMQC NMR spectra shown in Figures 6, 7 and 8, respectively. ^{1}H NMR data in $CDCl_3$: δ 6.73, 5.27 (singlet, exchangeable, OH-3 and OH-2); δ 4.89 (doublet, 7 H, $J_{1\text{-}2}$ = 3.5 Hz, H-1); δ 4.03 (triplet, 7 H, $J_{3\text{-}4}$ = 9.0 Hz, H-3); δ 3.90 (doublet, 7 H, $J_{6\text{-}6'}$ = 10.8 Hz, H-6); δ 3.71 (doublet, 7 H, $J_{6'\text{-}6}$ = 10.8 Hz, H-6′6); δ 3.63 (multiplet, 14 H, H-2,5); δ 3.55 (triplet, 7 H, $J_{4\text{-}3}$ = 9.0 Hz, H-4); δ 0.86 (singlet, 63 H, $Si(CH_3)_2(C(C\mathbf{H}_3)_3)$); δ 0.04 and δ 0.03 (two sets of singlets, 42 H, $Si(C\mathbf{H}_3)_2(C(CH_3)_3)$.

^{13}C NMR data in $CDCl_3$: δ 102.13 (C-1); δ 81.89 (C-4); δ 73.73 (C-2); δ 73.53 (C-3); δ 72.67 (C-5); δ 61.75 (C-6); δ 26.04 ($Si(CH_3)_2(C(\mathbf{C}H_3)_3)$); δ 18.41 ($Si(CH_3)_2(\mathbf{C}(CH_3)_3)$); δ -4.93, -5.05 ($Si(\mathbf{C}H_3)_2(C(CH_3)_3)$).

The ^1H-^1H COSY and ^1H-^{13}C HMQC NMR spectra show the proton and carbon contour signals that correspond to the glucopyranose subunits. The portion belonging to the *t*-butyldimethylsilyl group was omitted, because it is far away from those corresponding to the glucopyranose units, and can be assigned unambiguously.

High resolution MALDI-TOF mass spectrometry was used to determine the molecular mass of intermediate (**1**). The Na^+ and K^+ ion-adduct portion of the mass spectrum of intermediate (**1**) is shown in Figure 9. The calculated monoisotopic m/z values for the Na^+ and K^+ ion-adducts are 1955.96 and 1971.94 and agree well with the values obtained using MALDI-TOF-MS, 1955.61 and 1971.55, indicating the presence of seven *t*-butyldimethylsilyl groups on intermediate (**1**).

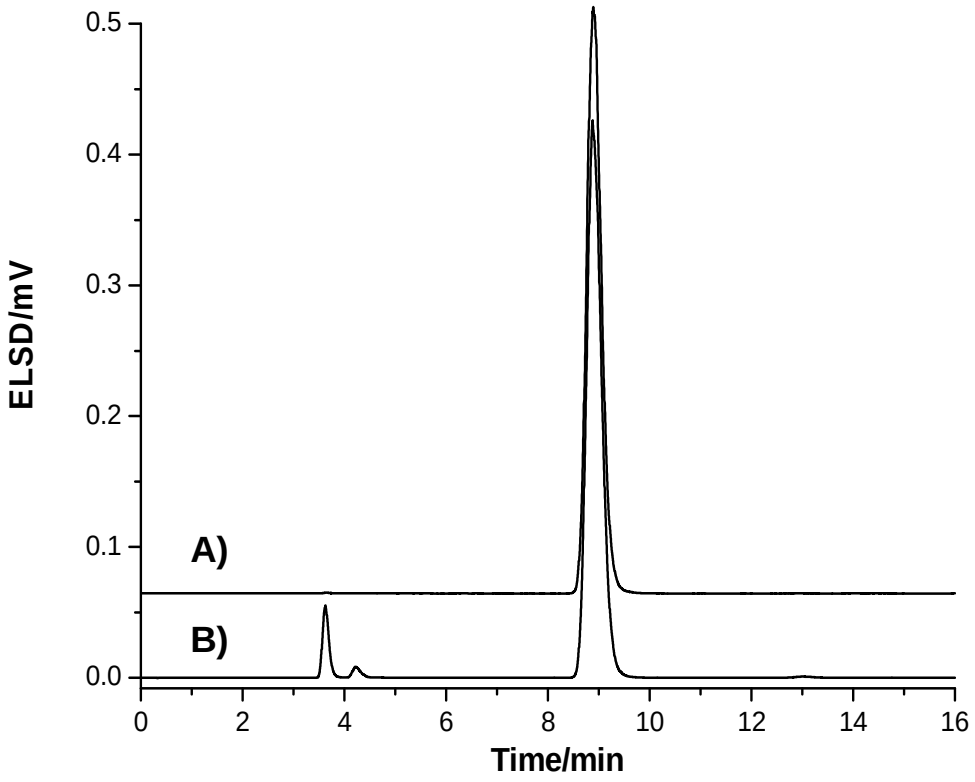

Figure 4. HPLC-ELSD chromatogram of A) recrystallized intermediate (**1**) and B) mother liquor

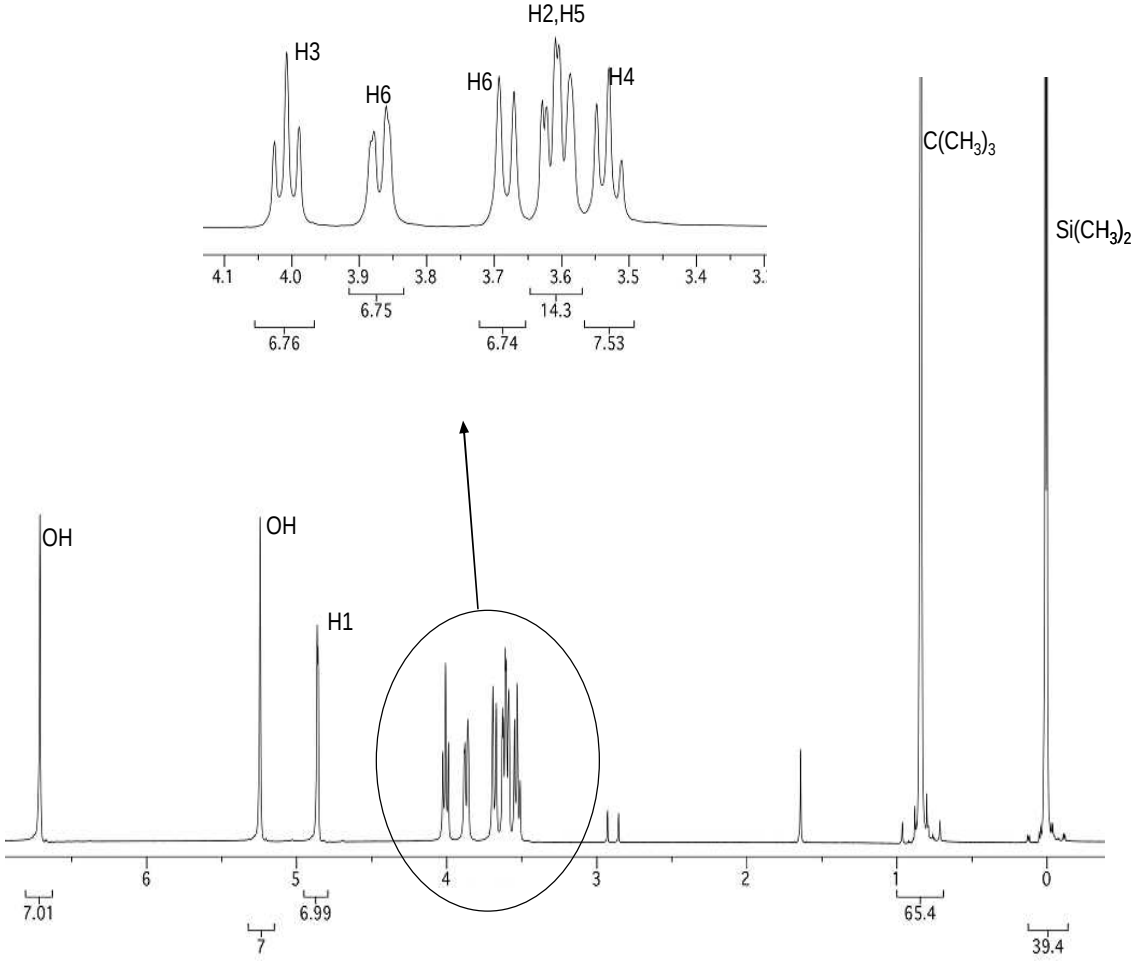

Figure 5. ^{1}H NMR spectrum of intermediate (**1**) in $CDCl_3$

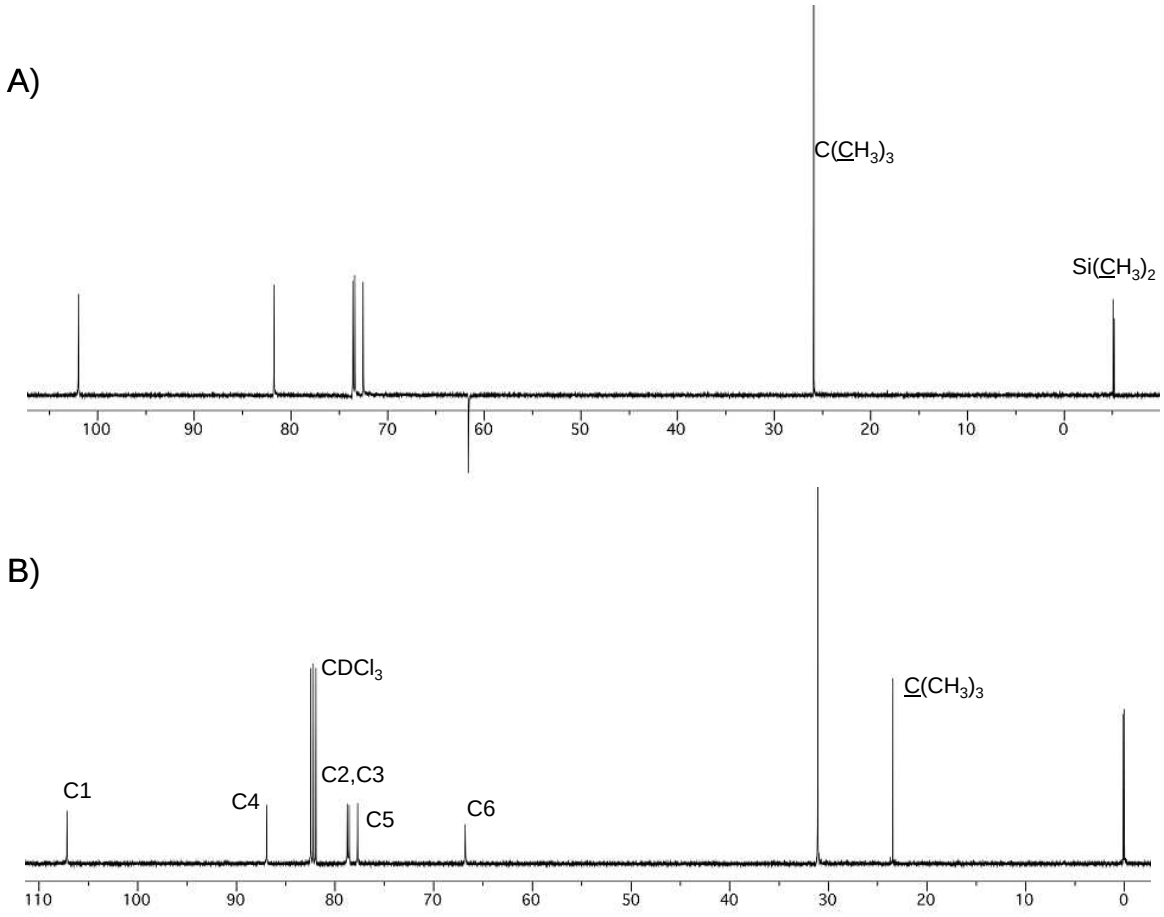

Figure 6. A) DEPT and B) ^{13}C NMR spectra of intermediate (**1**) in $CDCl_3$

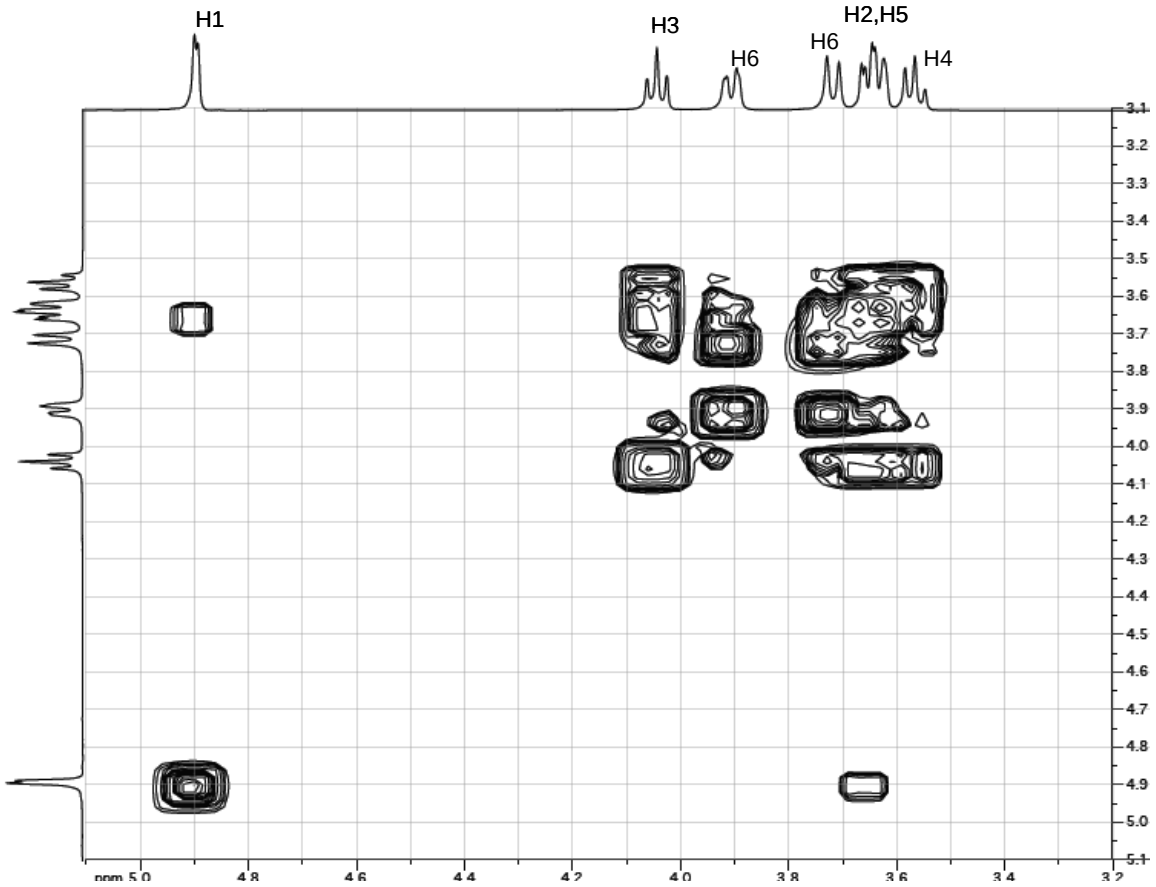

Figure 7. 2D COSY NMR spectrum of intermediate (**1**) in $CDCl_3$

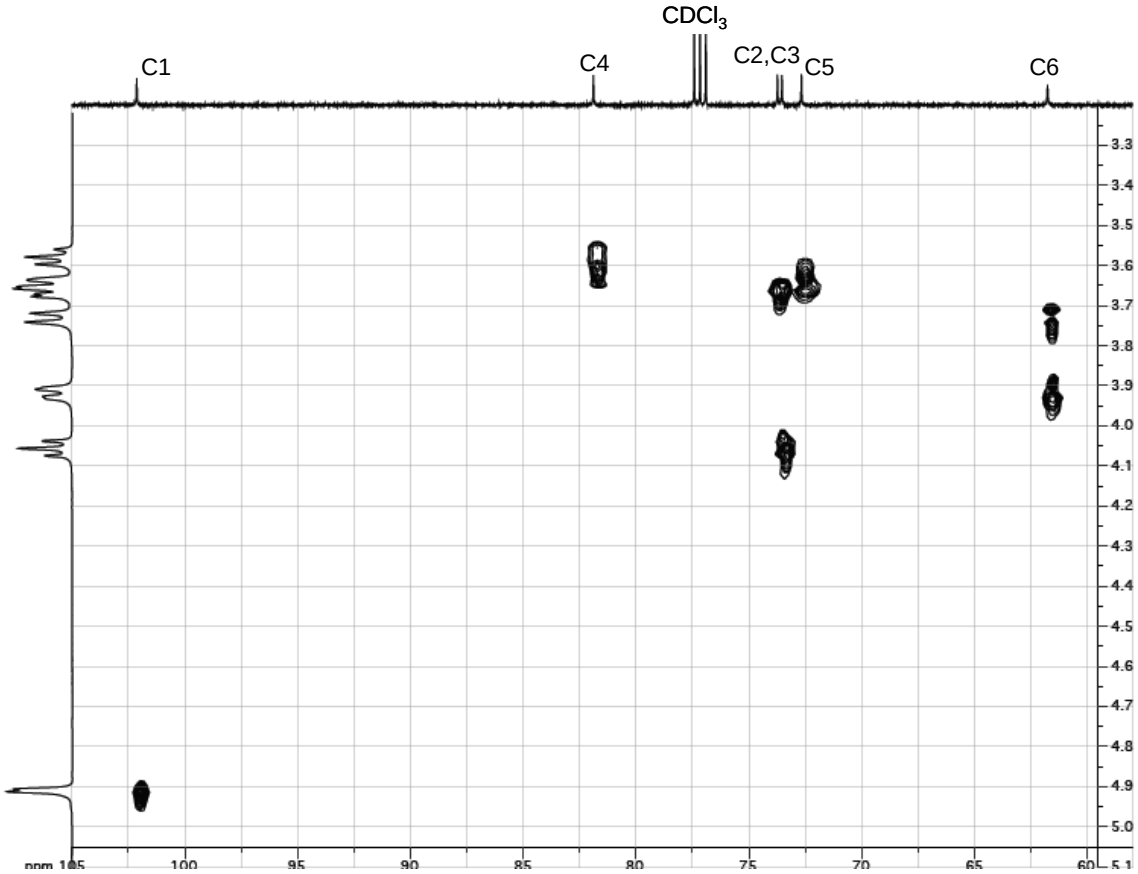

Figure 8. ^{1}H-^{13}C HMQC NMR spectrum of intermediate (**1**) in $CDCl_3$

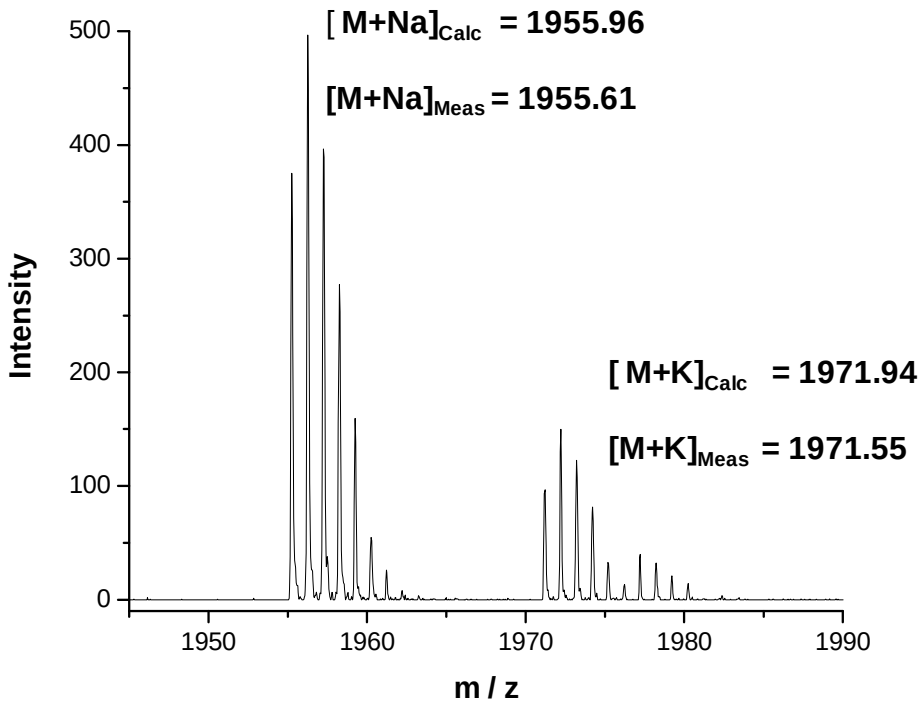

Figure 9. The Na^+ and K^+ ion-adduct portion of the MALDI-TOF mass spectrum of intermediate (**1**)

2.2.2 Heptakis(2-*O*-benzyl-6-*O*-*t*-butyldimethylsilyl)cyclomaltoheptaose, Intermediate (2)

Attempts to use a benzyl moiety as a protecting group for the hydroxyl group at C2 with BaO and $Ba(OH)_2$ as bases in DMF lead to: i) long reaction time (18h), ii) incomplete substitution at the C2 positions and iii) poor regioselectivity over the hydroxyl groups at the C3 positions[54] which, in turn, require extensive purification of the product. Instead, the procedure reported by Rong and D'Souza[55] that relies on NaH as the base was adopted. Thus, the secondary hydroxyl groups at the C2 position were reacted in THF, at room temperature, with benzyl bromide using NaH as the base and TBAI as the catalyst. A conversion rate over 80% was achieved under 3 hours. Progress of the reaction was monitored by isocratic non-aqueous RP-HPLC using a 5µm Luna, C18 column and a 55 : 45 MeOH : EtOAc mobile phase, at a flow rate of 2 ml/min, at ambient temperature. The reaction was quenched by adding methanol to the reaction mixture. The NaI precipitate was filtered and the reaction solvent was removed under reduced pressure. The crude product was dissolved in dichloromethane and the target material precipitated out of solution with methanol. The isomeric purity of the product was determined to be greater than 99 %. Selective benzylation of the hydroxyl group at the C-2 position over the C-3 position was greatly influenced by the amount of excess NaH used in the reaction.

Figure 10 shows a chromatogram of the recrystallized product overlaid with a chromatogram of the mother liquor.

The structure of intermediate (**2**) was verified by high-resolution ^{1}H and ^{13}C NMR spectroscopy. Peak assignments for the ^{1}H and ^{13}C NMR spectra shown in Figures 11 and 12 were determined by DEPT and 2-dimensional ^{1}H-^{1}H COSY and ^{1}H-^{13}C HMQC NMR spectroscopy (spectra shown in Figures 12, 13 and 14, respectively). ^{1}H NMR data in $CDCl_3$: δ 7.40-7.30 (multiplet, 35 H, Ph); δ 4.97 (doublet, 7H, J = 11.5 Hz, CH_2Ph); δ 4.93 (singlet, exchangeable, OH-3); δ 4.77 (doublet, 7 H, J_{1-2} = 3.5 Hz, H-1); δ 4.72 (doublet, 7H, J = 11.5 Hz, CH_2Ph); δ 4.01 (triplet, 7 H, J_{3-4} = 9.0 Hz, J_{3-2} = 9.5 Hz, H-3); δ 3.86 (doublet, 7 H, $J_{6-6'}$ = 10.5 Hz, H-6); δ 3.61 (doublet, 7 H, $J_{6'-5}$ = 9.5 Hz, $J_{6'-6}$ = 10.5 Hz, H-6′6); δ 3.55 (doublet, 7 H, J_{5-4} = 9.5 Hz, $J_{5-6'}$ = 9.5 Hz, H-5); δ 3.55 (triplet, 7 H, J_{4-3} = 9.0 Hz, J_{4-5} = 9.5 Hz, H-4); δ 3.33 (doublet of doublets, 7 H, J_{2-1} = 3.5 Hz, J_{2-3} = 9.5 Hz, H-2); δ 0.84 (singlet, 63 H, $Si(CH_3)_2(C(C\mathbf{H}_3)_3)$); δ -0.02 and δ -0.03 (two sets of singlets, 42 H, $Si(C\mathbf{H}_3)_2(C(CH_3)_3)$. ^{13}C NMR data in $CDCl_3$: δ 137.88 (C_{Ph}); δ 128.85 (C_{Ph}); δ 128.49 (C_{Ph}); δ 128.02 (C_{Ph}); δ 101.36 (C-1); δ 82.21 (C-4); δ 79.15 (C-2); δ 74.09 ($\mathbf{C}H_2Ph$); δ 73.72 (C-3); δ 71.78 (C-5); δ 61.85 (C-6); δ 26.04 ($Si(CH_3)_2(C(\mathbf{C}H_3)_3)$); δ 18.40 ($Si(CH_3)_2(\mathbf{C}(CH_3)_3)$); δ -4.98, -5.09 ($Si(\mathbf{C}H_3)_2(C(CH_3)_3)$).

The ^{1}H-^{1}H COSY and ^{1}H-^{13}C HMQC NMR spectra show only the signals that correspond to the glucopyranose subunits. The portion belonging to the aromatic ring was omitted because it is far away from the portion corresponding to the glucose subunits, and can be unambiguously assigned. The resonance position of C-2 in intermediate (**1**) shifted from 73.73 ppm to 79.12 ppm in intermediate (**2**), which is significant compared to the shift observed for the other carbon atoms. This indicates that the benzyl group was attached at the C-2 position.

High resolution MALDI-TOF mass spectrometry was used to determine the molecular mass of intermediate (**2**). The Na^{+} and K^{+}ion-adduct portion of the mass spectrum of intermediate (**2**) is shown in Figure 15. The calculated monoisotopic m/z values for the Na^{+} and K^{+} ion-adducts, 2586.29 and 2602.27, agree well with the values obtained by MALDI-TOF-MS, 2586.58 and 2602.55, indicating the presence of seven benzyl groups on intermediate (**2**).

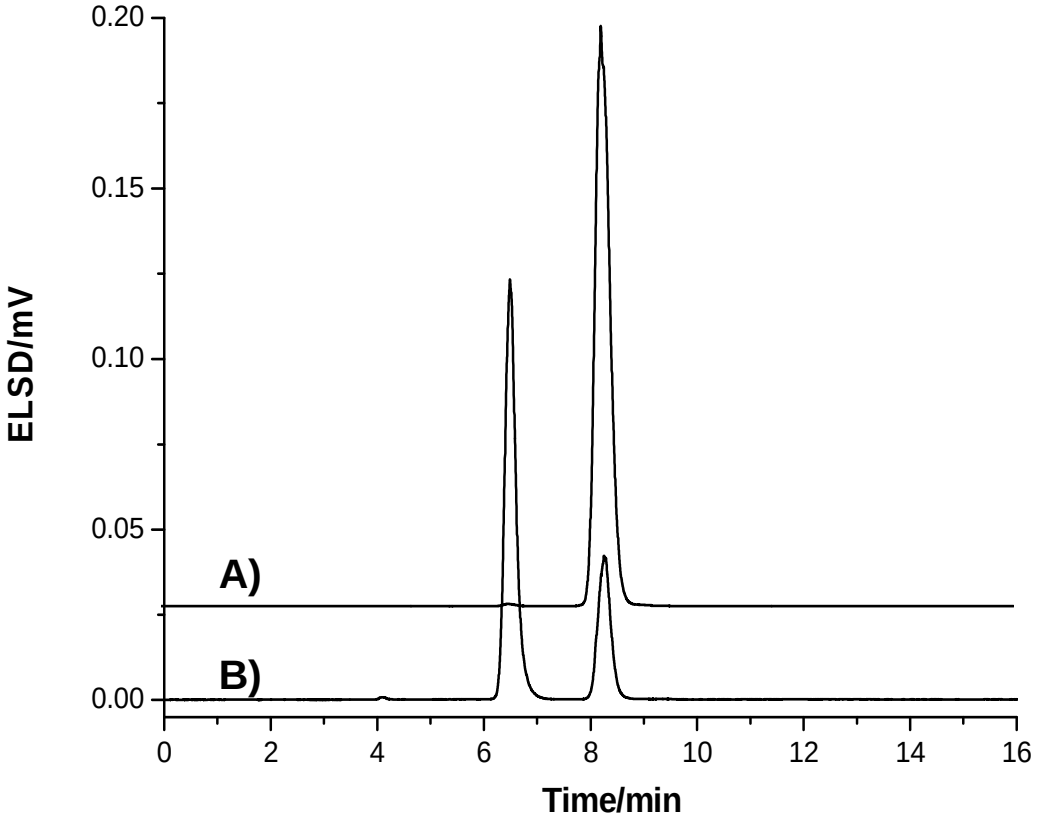

Figure 10. HPLC-ELSD chromatogram of A) recrystallized intermediate (**2**) and B) mother liquor

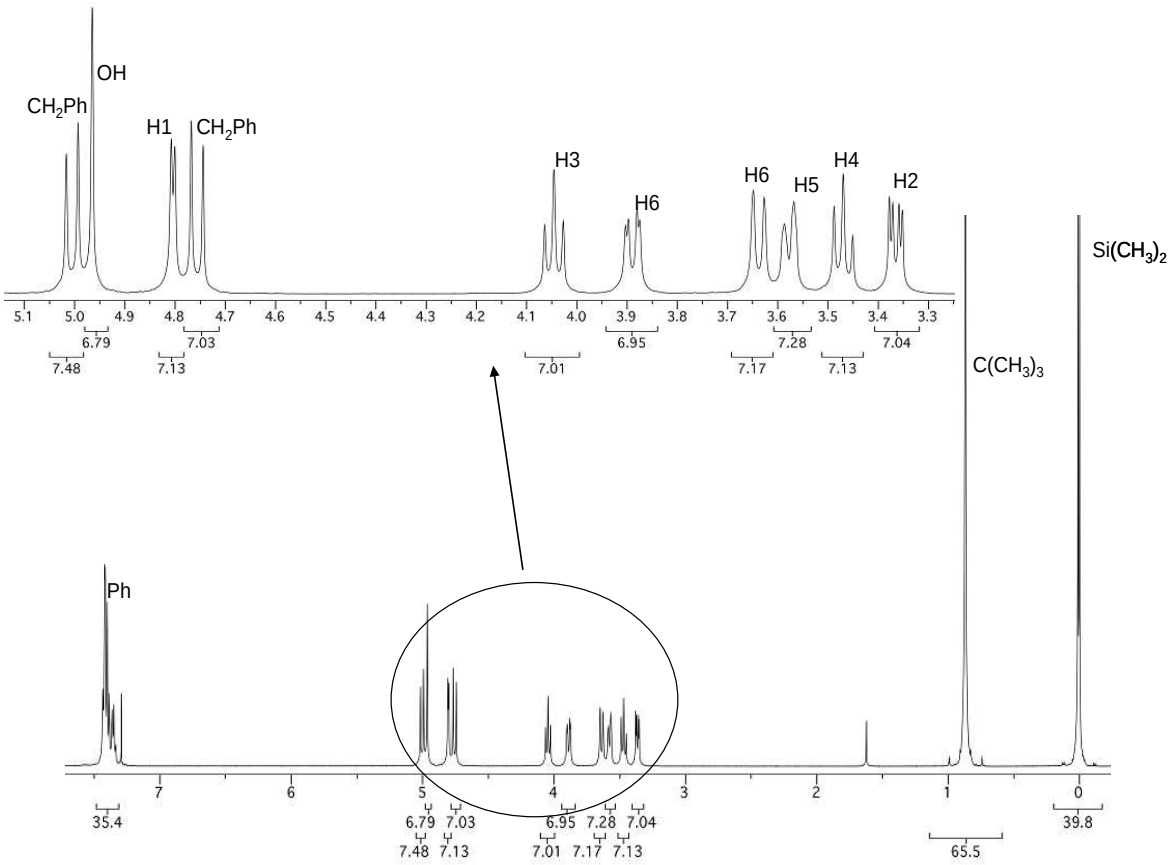

Figure 11. ^{1}H NMR spectrum of intermediate (**2**) in $CDCl_3$

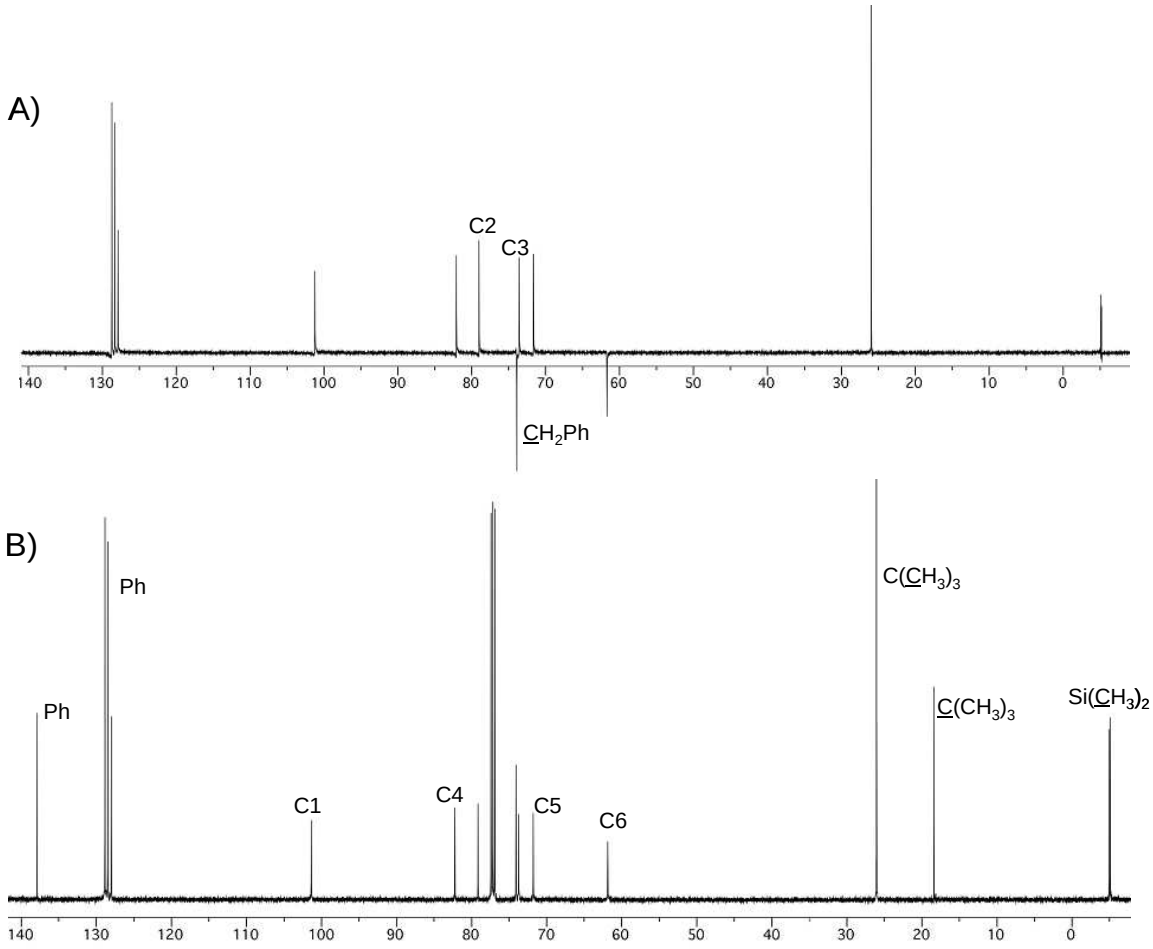

Figure 12. A) DEPT and B) ^{13}C NMR spectra of intermediate (**2**) in $CDCl_3$

Figure 13. 2D COSY NMR spectrum of intermediate (**2**) in $CDCl_3$

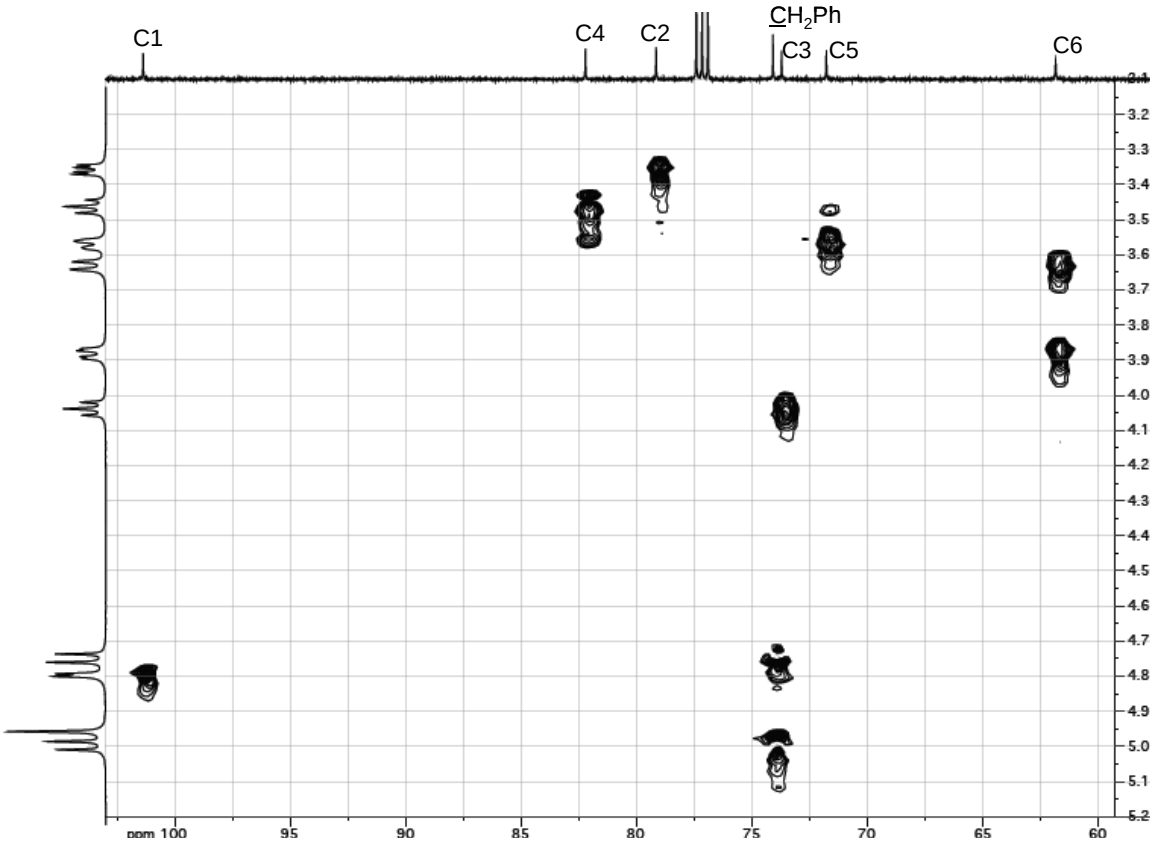

Figure 14. ^{1}H-^{13}C HMQC NMR spectrum of intermediate (**2**) in $CDCl_3$

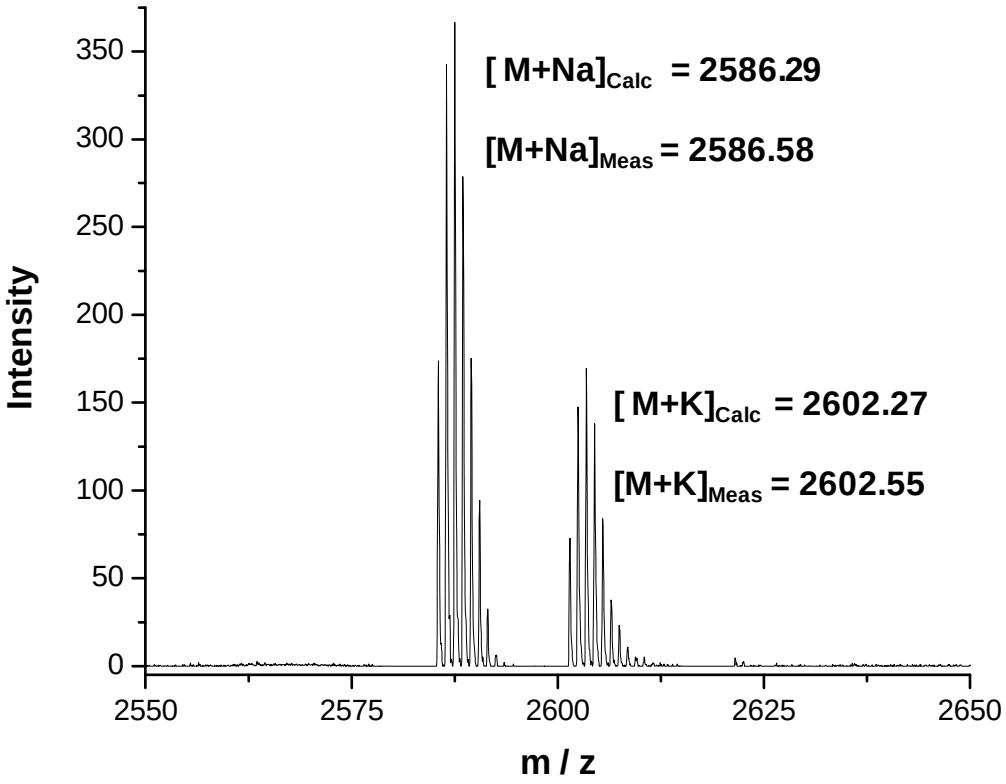

Figure 15. The Na^+ and K^+ ion-adduct portion of the MALDI-TOF mass spectrum of intermediate (**2**)

2.2.3 Heptakis(2-*O*-benzyl-3-*O*-methyl-6-*O*-*t*-butyldimethylsilyl)cyclomaltoheptaose, Intermediate (3)

Methylation of intermediate (**2**) was accomplished in THF using methyl iodide and sodium hydride, at room temperature, following a modified procedure reported by Cai and coworkers.[77] The reaction was monitored by TLC using a developing solvent mixture of hexane : EtOAc 8 : 1. The reaction was quenched by methanol and the solvent was removed under reduced pressure. The crude product was digested in dichloromethane and NaI was filtered. The crude product was recrystallized from a mixture of ethanol and H_2O. The purity of the final product was determined by isocratic non-aqueous RP-HPLC using a 5µm Luna, C18 column and a 55 : 45 MeOH : EtOAc mobile phase, at a flow rate of 2 ml/min, at ambient temperature. The isomeric purity of the product was determined to be greater than 99 %. Figure 16 shows a chromatogram of the recrystallized product.

Structural identity of intermediate (**3**) was established by high-resolution ^{1}H and ^{13}C NMR spectroscopy. Peak assignments for the ^{1}H and ^{13}C NMR spectra shown in Figures 17 and 18 were determined by DEPT and 2-dimensional ^{1}H-^{1}H COSY and ^{1}H-^{13}C HMQC NMR spectroscopy (spectra shown in Figures 18, 19 and 20, respectively). ^{1}H NMR data in $CDCl_3$: δ 7.42-7.25 (multiplet, 35 H, Ph); δ 5.22 (doublet, 7 H, $J_{1\text{-}2}$ = 3.5 Hz, H-1); δ 4.79 (doublet, 7H, J = 12.0 Hz, CH_2Ph); δ 4.72 (doublet, 7H, J = 12.0 Hz, CH_2Ph); δ 4.13 (doublet, 7 H, $J_{6\text{-}6'}$ = 9.5 Hz, H-6); δ 3.79 (triplet, 7 H, $J_{4\text{-}3}$ = 9.0 Hz, H-4); δ 3.68-3.63 (multiplet, 21 H, H-3, H-5, H-6′); δ 3.54 (singlet, 21 H, CH_3); δ 3.32 (doublet of doublets, 7 H, $J_{2\text{-}1}$ = 3.5 Hz, H-2); δ 0.86 (singlet, 63 H, $Si(CH_3)_2(C(C\mathbf{H}_3)_3)$);

δ 0.12 and δ 0.00 (two sets of singlets, 42 H, $Si(C\mathbf{H}_3)_2(C(CH_3)_3)$. ^{13}C NMR data in $CDCl_3$: δ 139.06 (C_{Ph}); δ 128.22 (C_{Ph}); δ 127.65 (C_{Ph}); δ 127.33 (C_{Ph}); δ 98.44 (C-1); δ 82.24 (C-3); δ 79.97 (C-2); δ 78.47 (C-4); δ 72.53 ($\mathbf{C}H_2Ph$) δ 72.36 (C-5); δ 62.45 (C-6); δ 61.59 ($\underline{C}H_3$); δ 26.06 ($Si(CH_3)_2(C(\mathbf{C}H_3)_3)$); δ 18.44 ($Si(CH_3)_2(\mathbf{C}(CH_3)_3)$); δ -4.71, -5.05 ($Si(\mathbf{C}H_3)_2(C(CH_3)_3)$).

The ^1H-^1H COSY and ^1H-^{13}C HMQC NMR spectra show only the signals corresponding to the glucopyranose subunits. shift in the resonance position observed for C-3 (to 82.24 ppm in intermediate (**3**) from 73.72 ppm in intermediate (**2**)) indicated the attachment of the methyl group at the C-3 position.

High resolution MALDI-TOF mass spectrometry was used to determine the molecular mass of intermediate (**3**). The Na^+ and K^+ion-adduct portion of the mass spectrum of intermediate (**3**) is shown in Figure 21. The calculated monoisotopic m/z values of the Na^+ and K^+ ion-adducts of 2684.40 and 2700.38 agree well with the values obtained using MALDI-TOF-MS, 2684.46 and 2700.30, respectively, indicating the presence of seven methyl groups on intermediate (**3**).

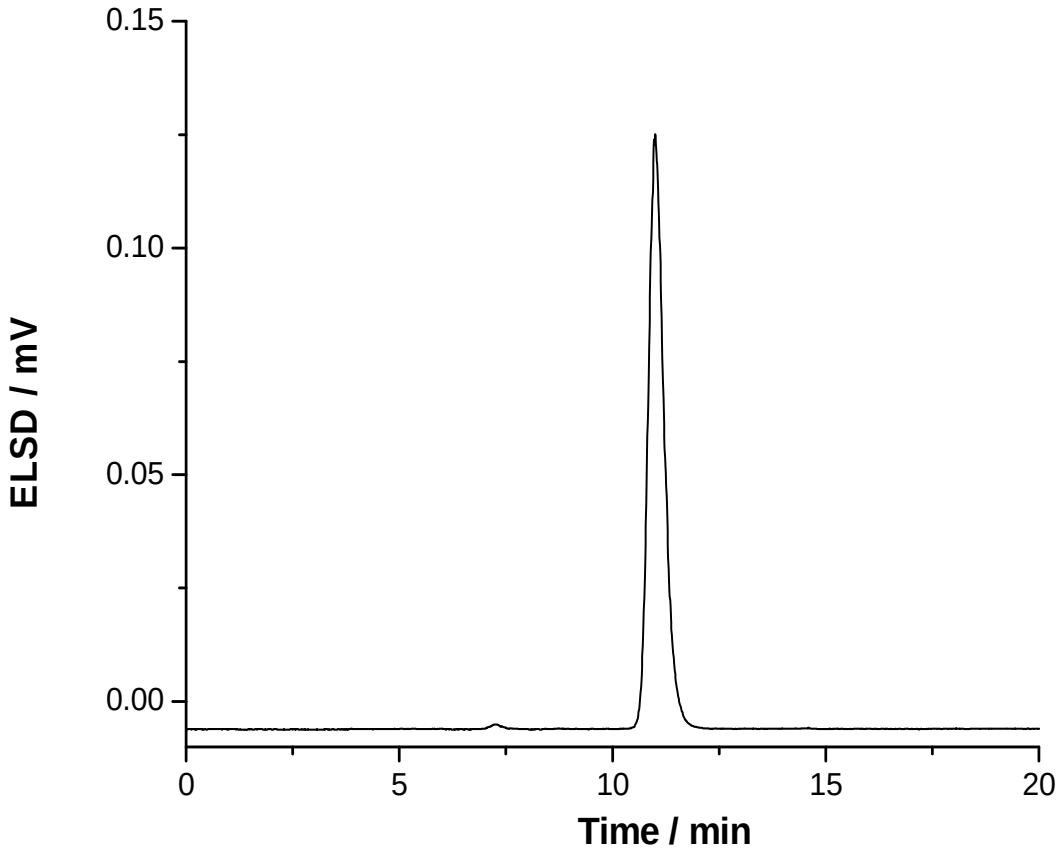

Figure 16. HPLC-ELSD chromatogram of recrystallized intermediate (**3**)

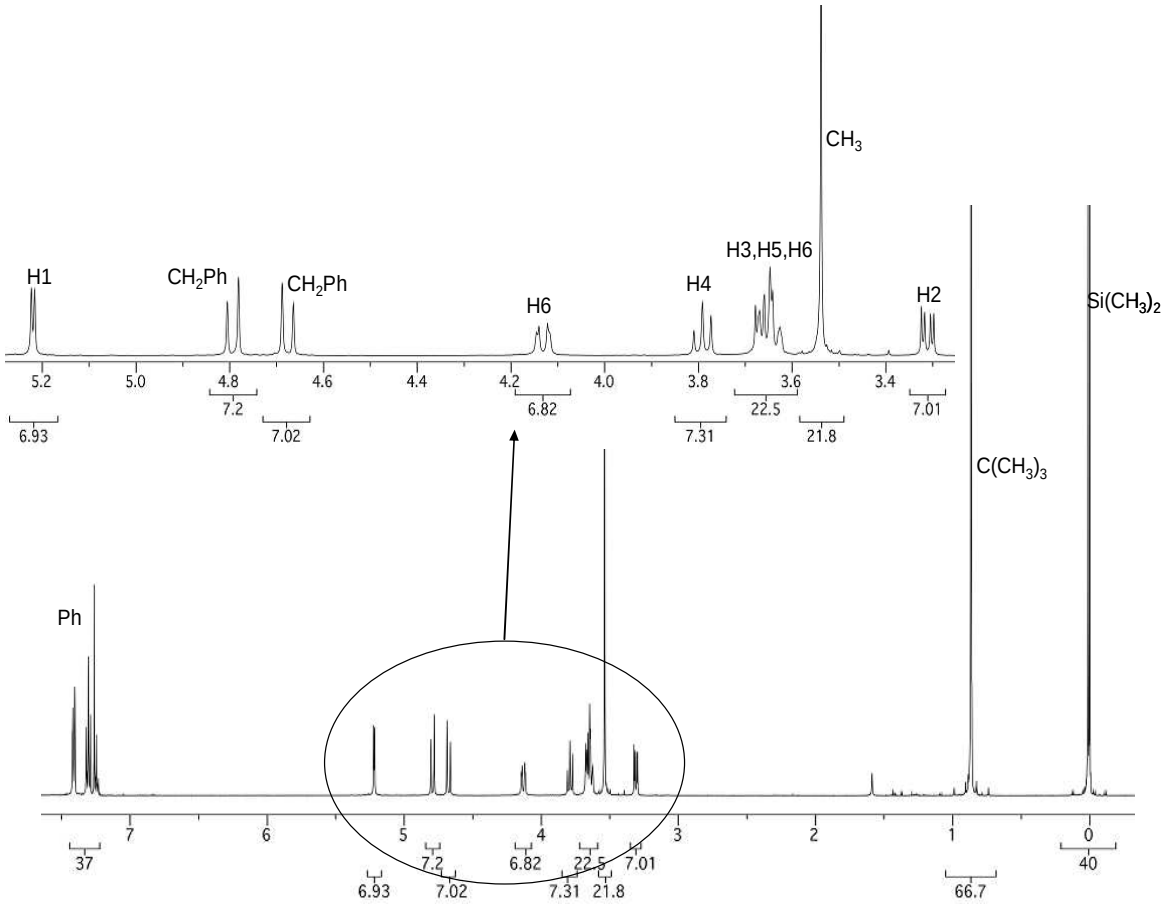

Figure 17. ^{1}H NMR spectrum of intermediate (**3**) in $CDCl_3$

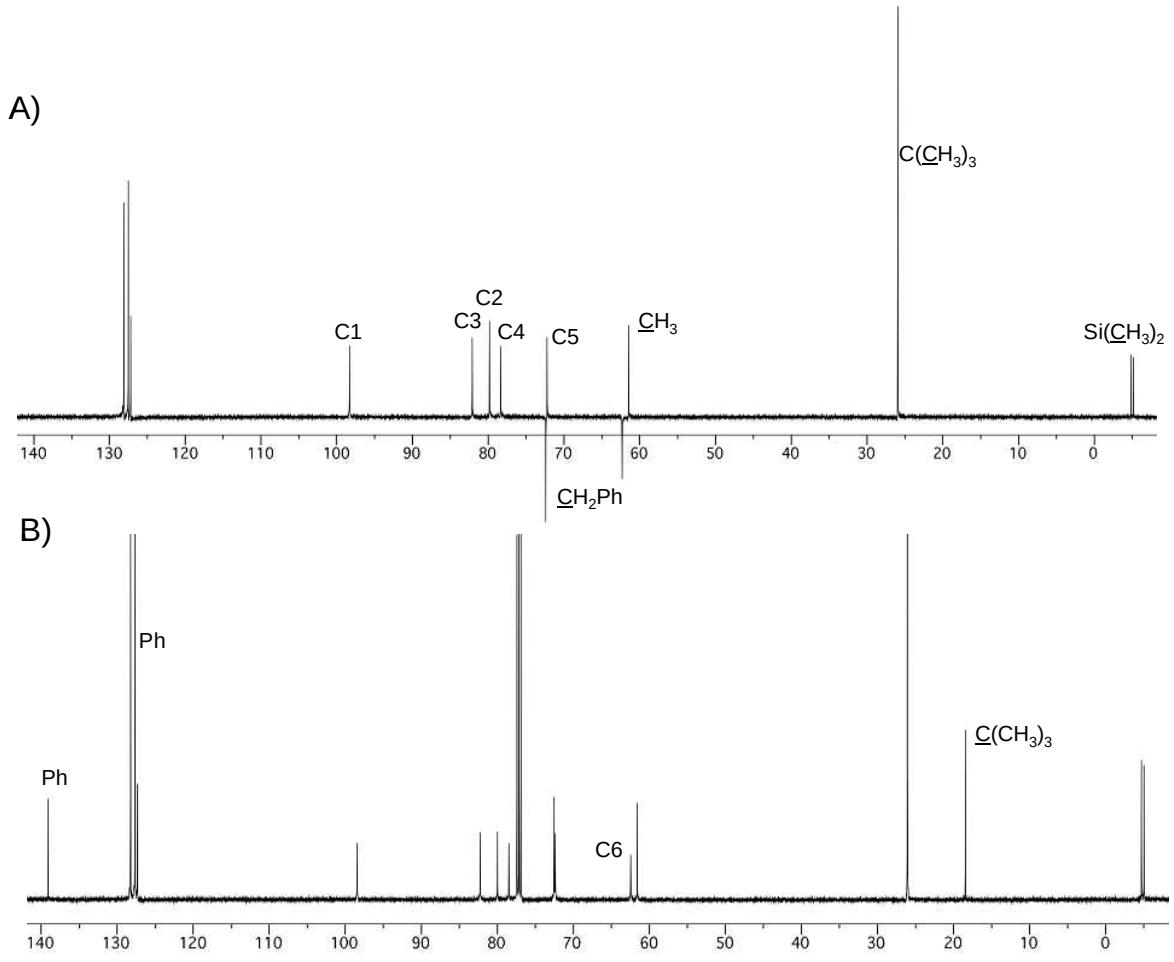

Figure 18. A) DEPT and B) ^{13}C NMR spectra of intermediate (**3**) in $CDCl_3$

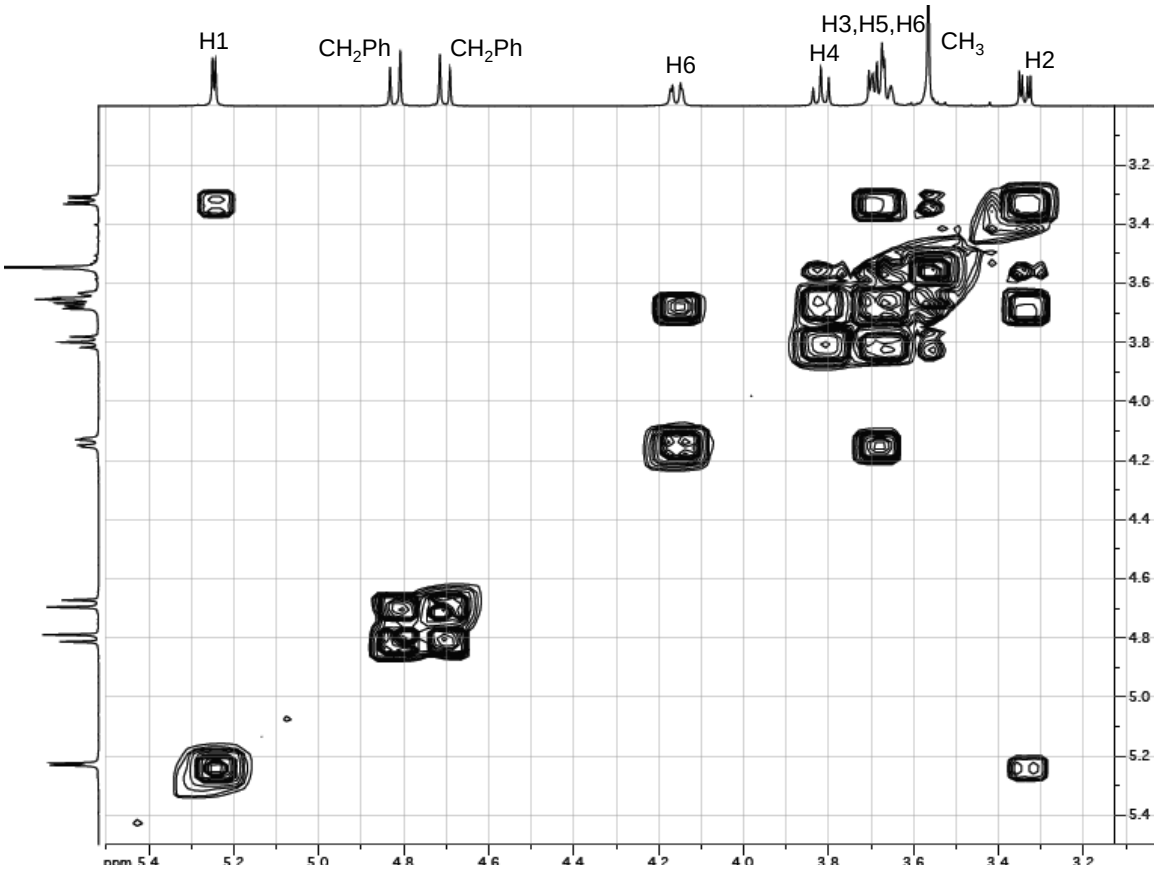

Figure 19. 2D COSY NMR spectrum of intermediate (**3**) in $CDCl_3$

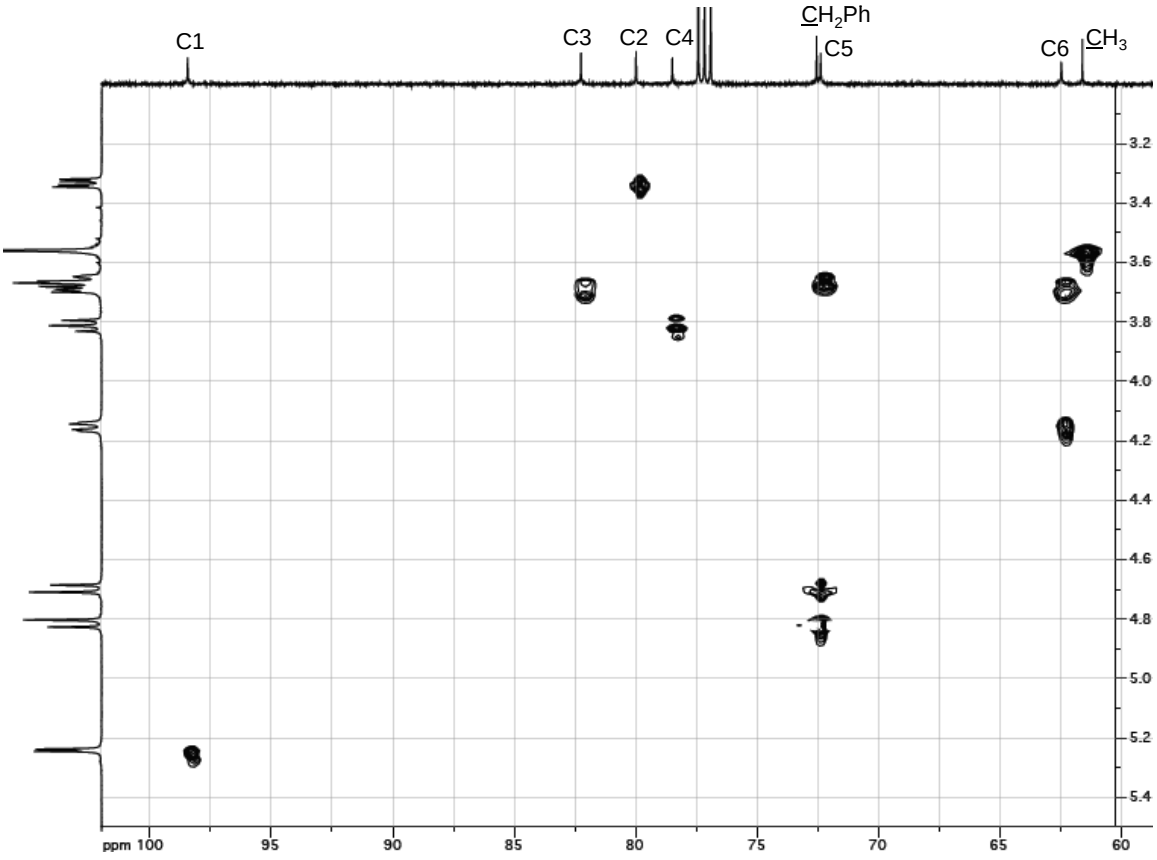

Figure 20. ^{1}H-^{13}C HMQC NMR spectrum of intermediate (**3**) in $CDCl_3$

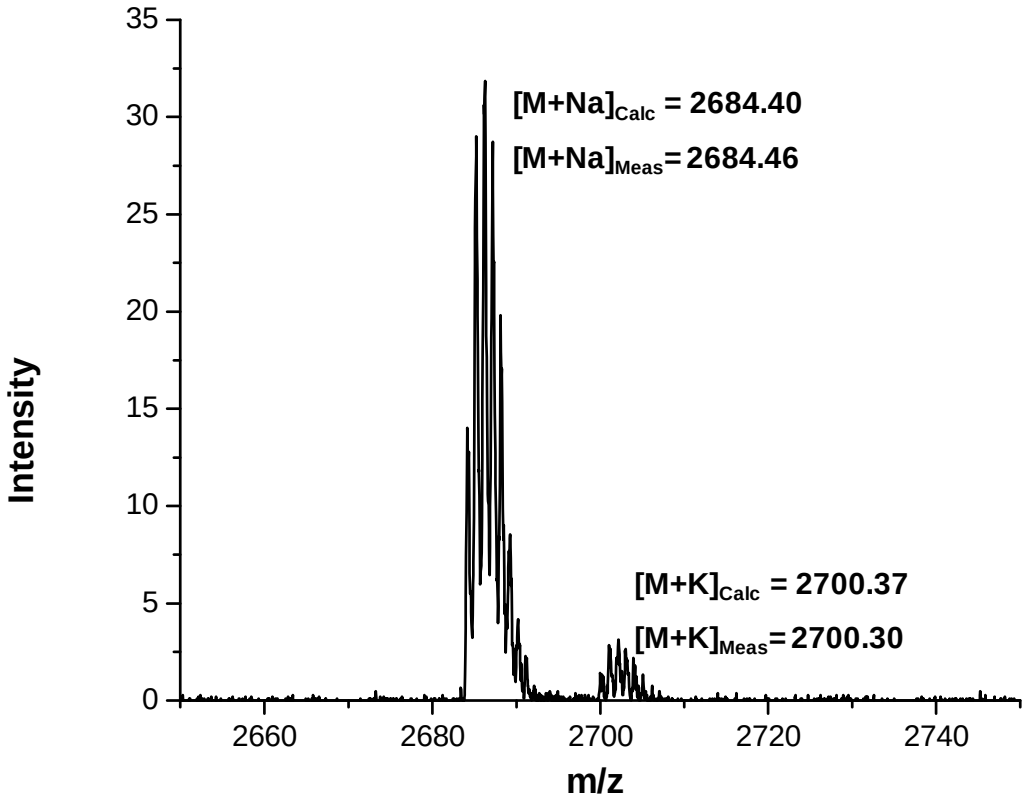

Figure 21. The Na^+ and K^+ion-adduct portion of the MALDI-TOF mass spectrum of intermediate (**3**)

2.2.4 Heptakis(2-*O*-benzyl-3-*O*-methyl)cyclomaltoheptaose, Intermediate (4)

Intermediate (**3**) was desilylated using 48% aqueous HF added to a mixture of THF and ethanol, in 24 hrs at room temperature. The reaction was monitored by TLC using a mobile phase of 50 : 10 : 1 $CHCl_3$: MeOH : H_2O. Once desilylation was complete, NaOH dissolved in aqueous ethanol was added to neutralize the excess HF. The NaF precipitate was filtered and the solvent was removed under reduced pressure. The crude product was recrystallized from acetone. The isomeric purity of the final product, which is greater than 98 %, was determined by isocratic aqueous RP-HPLC using a 5µm Luna, C18 column and a 95 : 5 MeOH : H_2O mobile phase, at a flow rate of 2 ml/min, at ambient temperature. Figure 22 shows a chromatogram of the recrystallized product. The structure of intermediate (**4**) was confirmed by high-resolution ^1H and ^{13}C NMR spectroscopy. Peak assignments for the ^1H and ^{13}C NMR spectra shown in Figures 23 and 24 were determined by DEPT and 2-dimensional ^1H-^1H COSY and ^1H-^{13}C HMQC NMR spectroscopy (spectra shown in Figures 24, 25 and 26). ^1H NMR data in $CDCl_3$: δ 7.43-7.27 (multiplet, 35 H, Ph); δ 5.03 (doublet, 7 H, $J_{1\text{-}2}$ = 3.5 Hz, H-1); δ 4.87 (broad, exchangeable, OH-6); δ 4.78 (doublet, 7H, J = 12.0 Hz, CH_2Ph); δ 4.71 (doublet, 7H, J = 12.0 Hz, CH_2Ph); δ 3.94 (doublet, 7 H, $J_{6\text{-}6'}$ = 10.0 Hz, H-6); δ 3.85-3.82 (multiplet, 14 H, H-5, H-6′); δ 3.61 (triplet, 7 H, $J_{3\text{-}4}$ = 9.0 Hz, H-3); δ 3.56-3.52 (multiplet, 28 H, H-4, CH_3,); δ 3.46 (doublet of doublets, 7 H, $J_{2\text{-}1}$ = 3.5 Hz, H-2).

^{13}C NMR data in $CDCl_3$: δ 138.83 (C_{Ph}); δ 128.34 (C_{Ph}); δ 127.76 (C_{Ph}); δ 127.56 (C_{Ph}); δ 99.32 (C-1); δ 82.10 (C-3); δ 80.01 (C-4); δ 79.30 (C-2); δ 72.82 (**C**H_2Ph); δ 72.66 (C-5); δ 61.52 (C-6); δ 61.40(<u>C</u>H_3).

The ^1H-^1H COSY and ^1H-^{13}C HMQC NMR spectra (Figures 25 and 26) show only the signals that correspond to the CD backbone. Figure 23 clearly shows the complete removal of the *t*-butyldimethylsilyl group at the C-6 position from intermediate (**3**) while the benzyl and methyl groups at the C-2 and C-3 positions remain intact.

High resolution MALDI-TOF mass spectrometry was used to determine the molecular mass of intermediate (**4**). The Na^+ and K^+ion-adduct portion of the mass spectrum of intermediate (**4**) is shown in Figure 27. The calculated monoisotopic m/z values for the Na^+ and K^+ ion-adducts are 1885.80 and 1909.77, and agree well with the values obtained using MALDI-TOF-MS, 1885.78 and 1909.75, respectively, indicating the complete removal of the *t*-butyldimethylsilyl groups from intermediate (**3**).

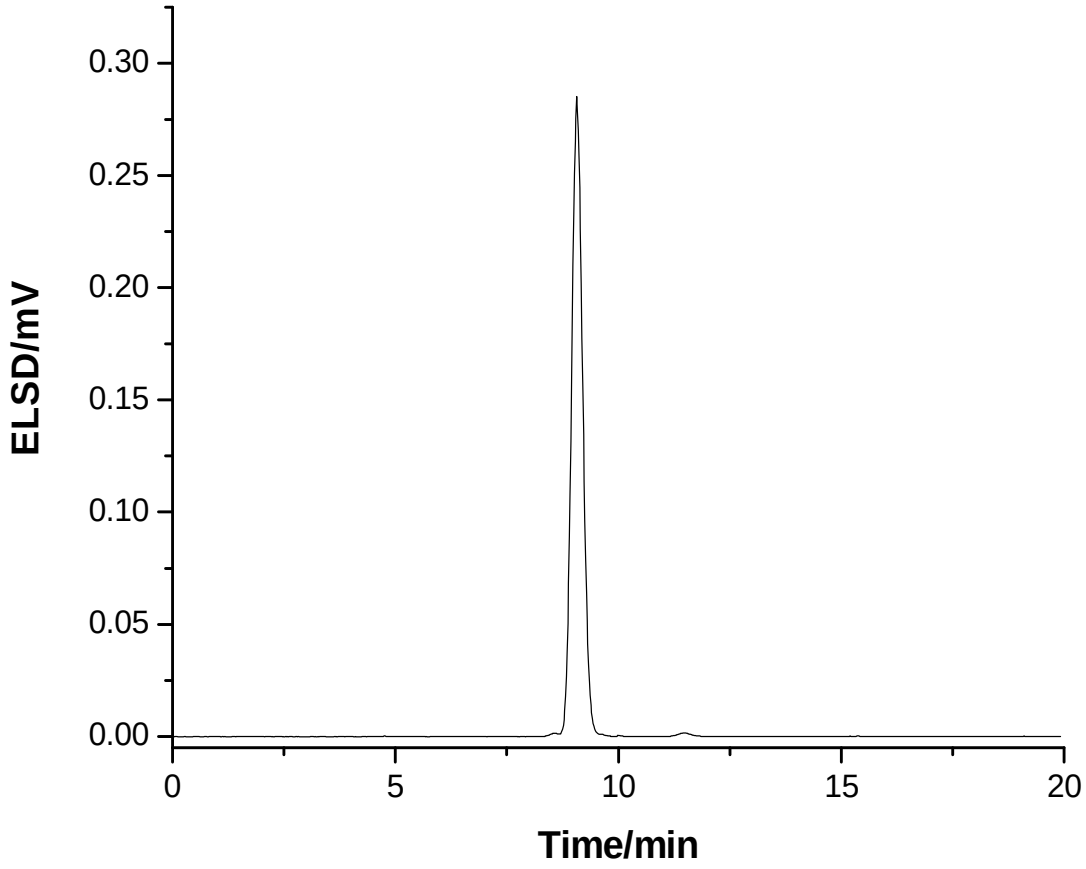

Figure 22. HPLC-ELSD chromatogram of recrystallized intermediate (**4**)

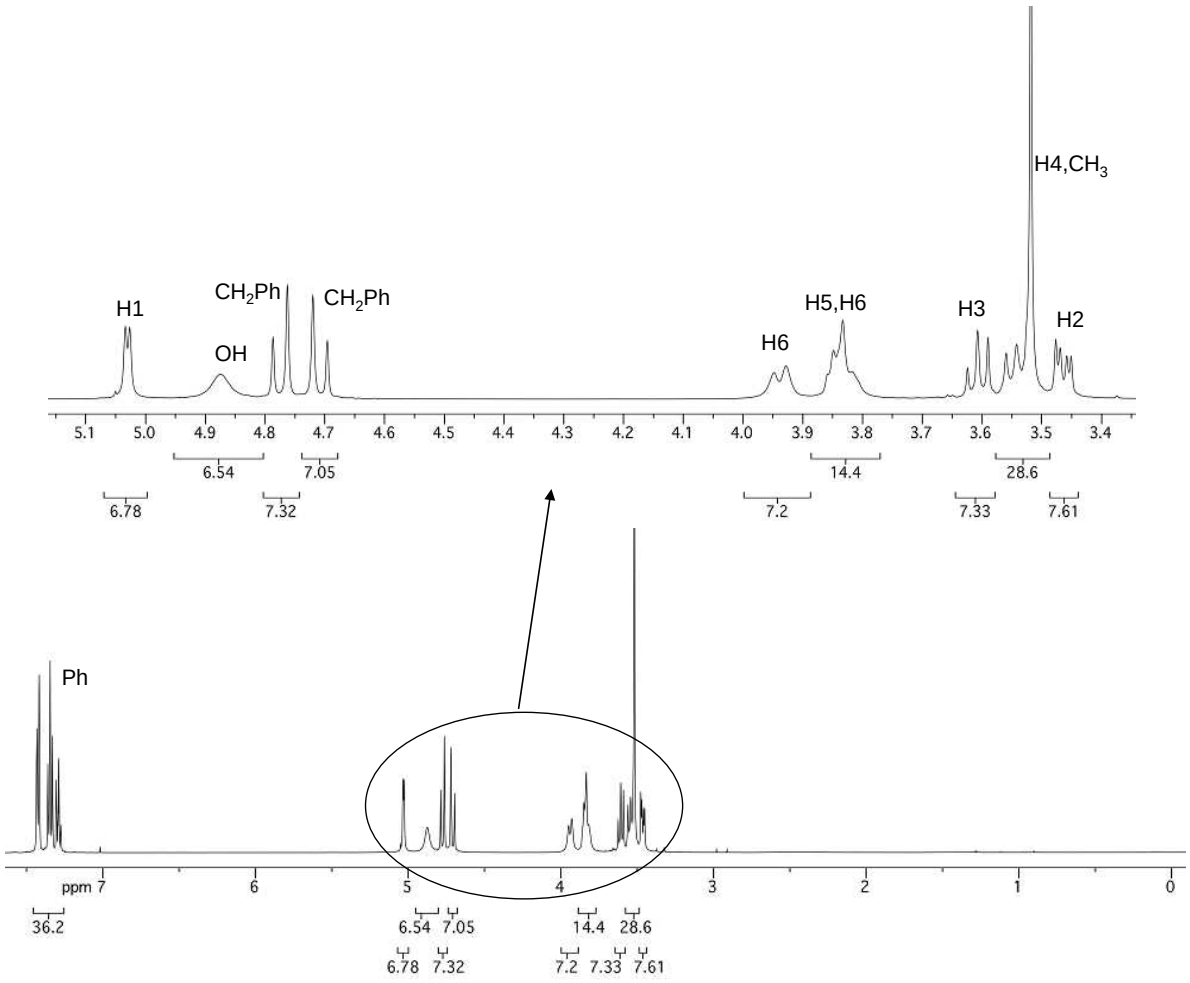

Figure 23. ^{1}H NMR spectrum of intermediate (**4**) in $CDCl_3$

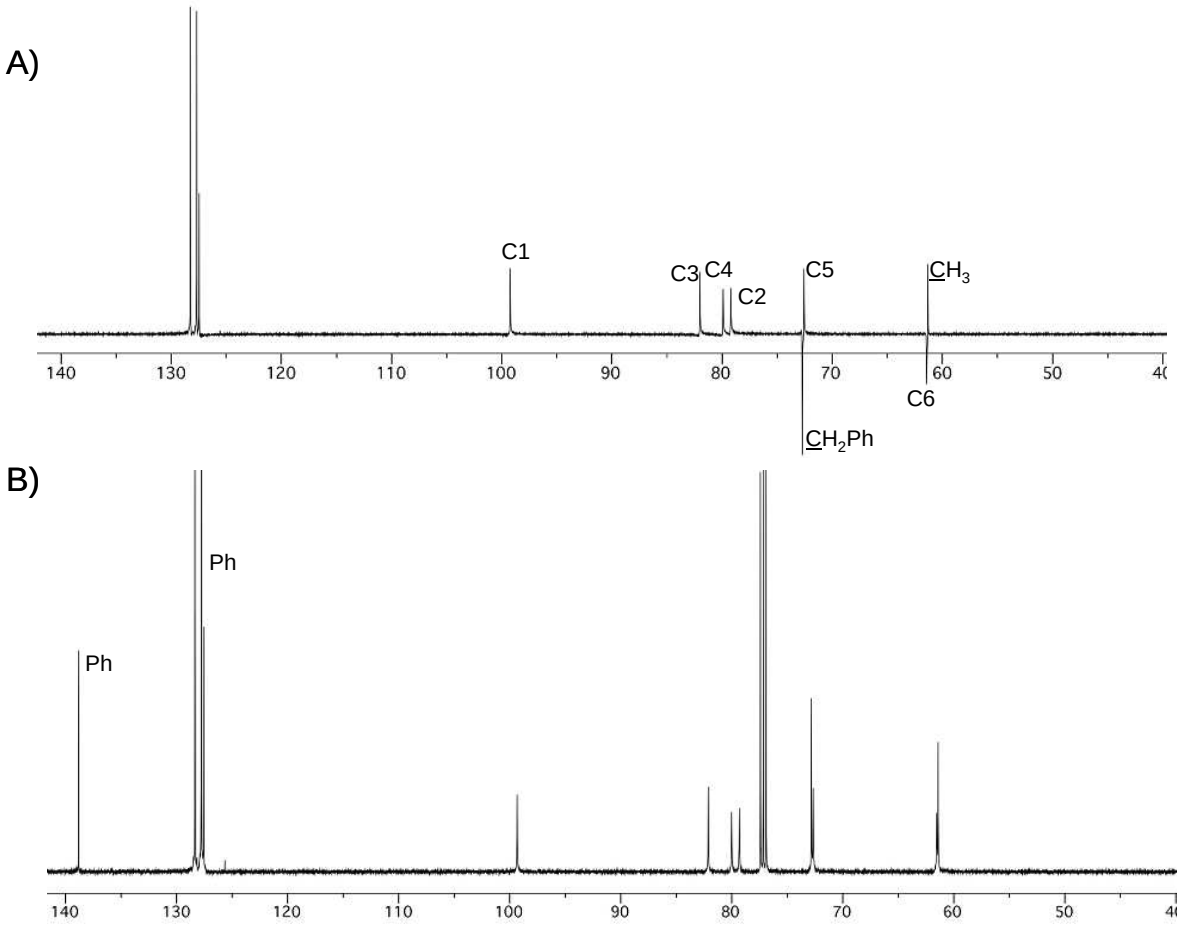

Figure 24. A) DEPT and B) ^{13}C NMR spectra of intermediate (**4**) in $CDCl_3$

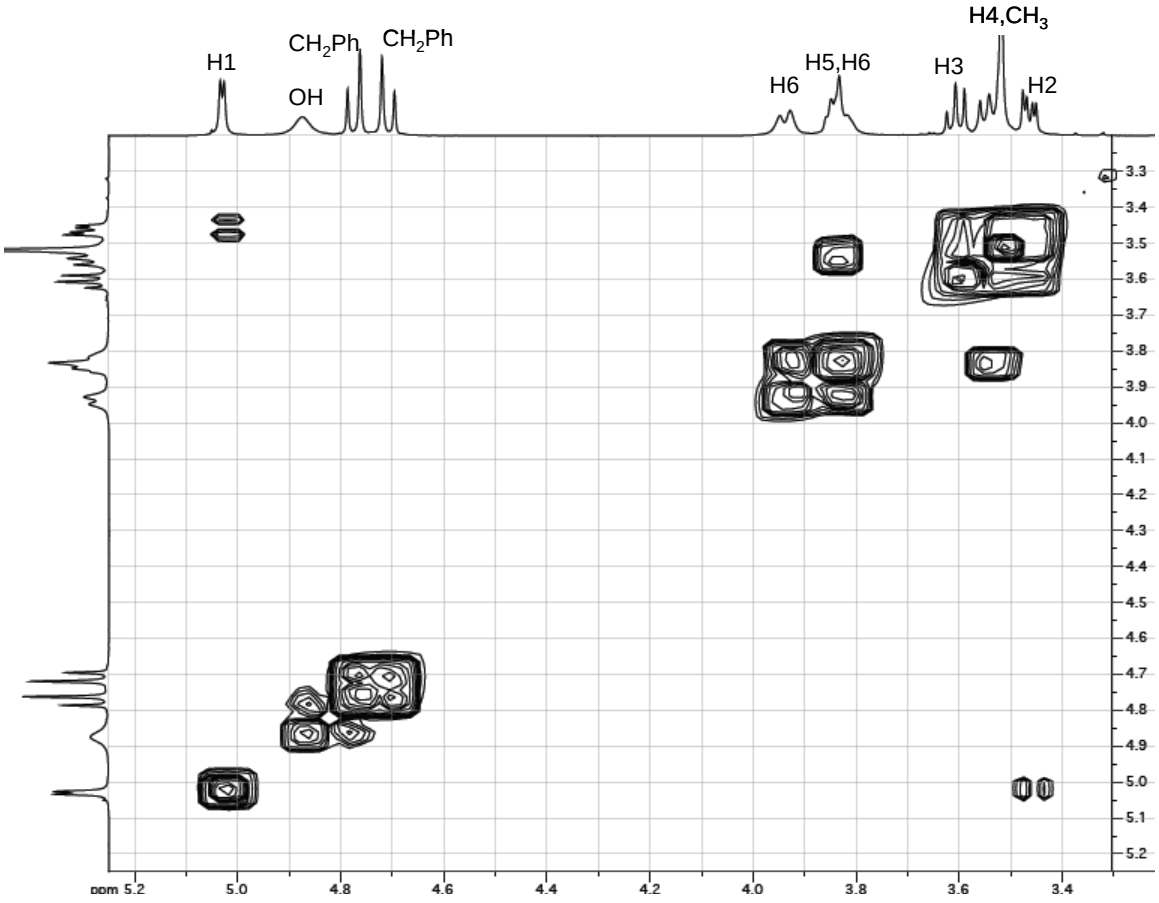

Figure 25. 2D COSY NMR spectrum of intermediate (**4**) in $CDCl_3$

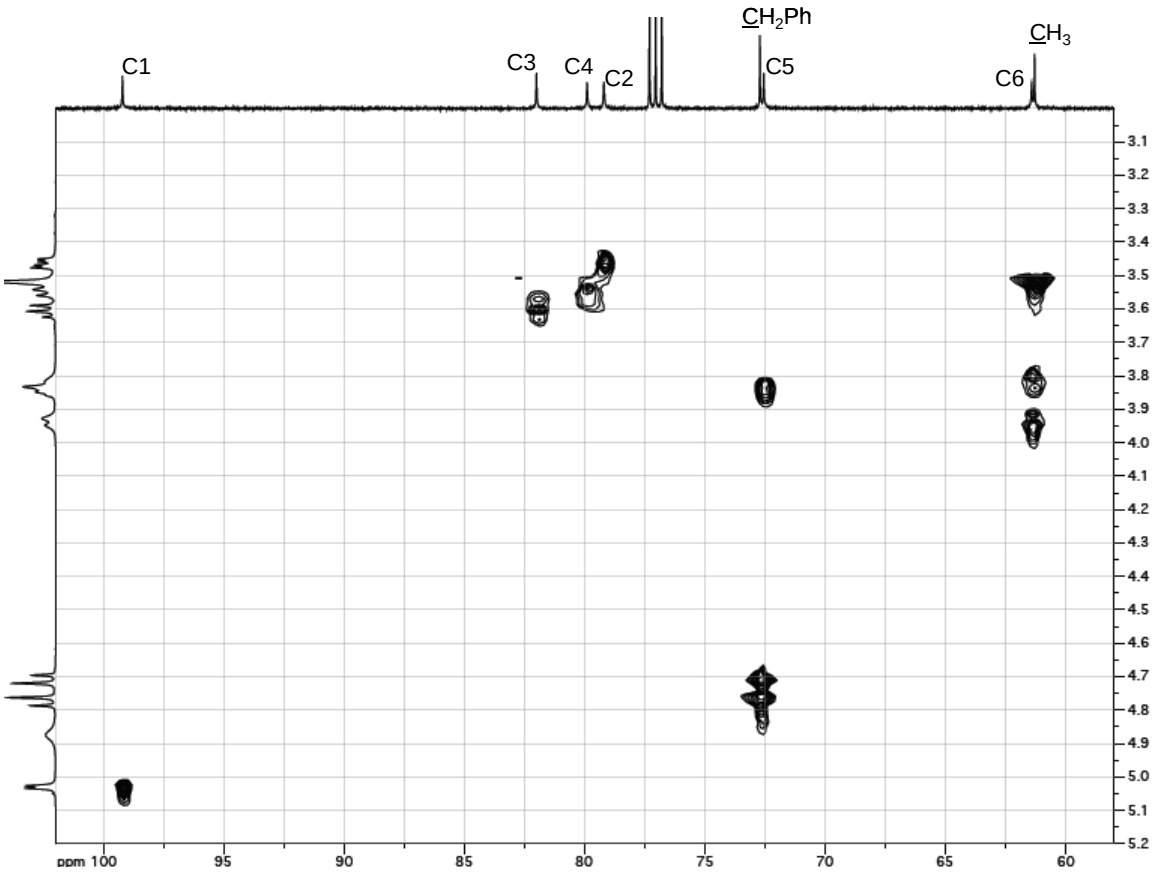

Figure 26. ^{1}H-^{13}C HMQC NMR spectrum of intermediate (**4**) in $CDCl_3$

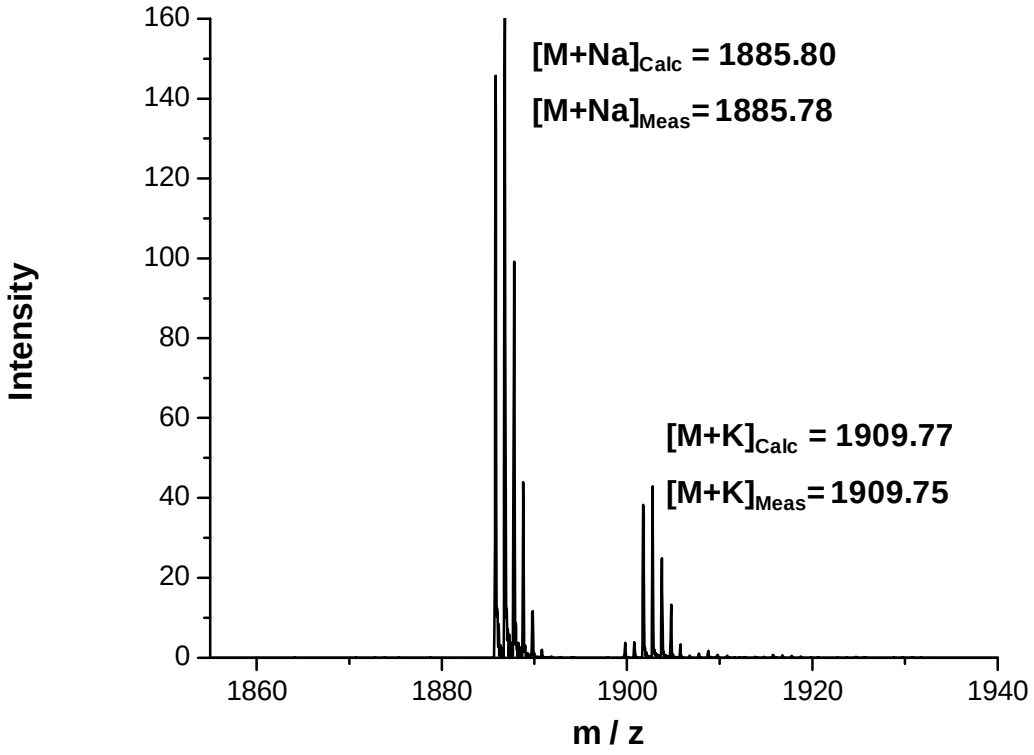

Figure 27. The Na^+ and K^+ion-adduct portion of the MALDI-TOF mass spectrum of intermediate (**4**)

2.2.5 Heptakis(2-*O*-benzyl-3-*O*-methyl-6-*O*-acetyl)cyclomaltoheptaose, Intermediate (5)

Acetylation of intermediate (**4**) was carried out in pyridine at 50ºC for 2.5 h, in the presence of excess acetic anhydride following a modified procedure reported by Vincent et al.[59] Reaction progress was monitored by isocratic RP-HPLC using a 5µm Luna, C18 column and a 95 : 5 MeOH : H_2O mobile phase at a flow rate of 2 ml/min, at ambient temperature. Upon completion, the reaction solvent and acetic acid were removed under vacuum. The crude product was dissolved in CH_2Cl_2 and the target was precipitated with hexanes. The product was dried in vacuo to yield intermediate (**5**) as a white powder at 99 % isomeric purity. Figure 28 shows a chromatogram of the recrystallized product.

The structure of intermediate (**5**) was confirmed by high-resolution ^1H and ^{13}C NMR spectroscopy. Peak assignments for the ^1H and ^{13}C NMR spectra shown in Figures 29 and 30 respectively were determined by DEPT and 2-dimensional ^1H-^1H COSY and ^1H-^{13}C HMQC NMR spectroscopy (spectra shown in Figures 30, 31 and 32, respectively). ^1H NMR data in $CDCl_3$: δ 7.46-7.29 (multiplet, 35 H, Ph); δ 4.93 (doublet, 7 H, $J_{1\text{-}2}$ = 3.5 Hz, H-1); δ 4.77 (singlet, 14 H, CH_2Ph); δ 4.45 (doublet, 7 H, $J_{6\text{-}6'}$ = 8.5 Hz, H-6);

δ 3.61 (doublet of doublets, 7 H, $J_{6'-5}$ = 4.5 Hz, $J_{6'-6}$ = 8.5 Hz, H-6′6); δ 3.55 (doublet of doublets, 7 H, $J_{5-6'}$ = 4.5 Hz, J_{5-4} = 9.5 Hz, H-5); δ 4.01 (triplet, 7 H, J_{3-4} = 9.0 Hz, J_{3-2} = 9.5 Hz, H-3); δ 3.57 (singlet, 21 H, CH_3,); δ 3.51 (triplet, 7 H, J_{4-3} = 9.0 Hz, J_{4-5} = 9.5 Hz, H-4); δ 3.33 (doublet of doublets, 7 H, J_{2-1} = 3.5 Hz, J_{2-3} = 9.5 Hz, H-2); δ 2.06 (singlet, 21 H, CH_3CO). ^{13}C NMR data in $CDCl_3$: δ 170.63 ($CH_3\underline{C}O$); δ 138.76 (C_{Ph}); δ 128.39 (C_{Ph}); δ 127.93 (C_{Ph}); δ 127.71 (C_{Ph}); δ 99.75 (C-1); δ 81.88 (C-3); δ 80.89 (C-4); δ 79.40 (C-2); δ 73.05 (**C**H_2Ph); δ 69.87 (C-5); δ 63.49 (C-6); δ 61.64 (CH_3); δ 20.92 ($\underline{C}H_3CO$).

The ^1H-^1H COSY and ^1H-^{13}C HMQC NMR spectra (Figures 29 and 30), show only the signals corresponding to the glucopyranose subunits and indicate the presence of acetyl groups connected to the C-6 positions.

High resolution MALDI-TOF mass spectrometry was used to determine the molecular mass of intermediate (**5**). The Na^+ and K^+ ion-adduct portion of the mass spectrum of intermediate (**5**) is shown in Figure 33. The calculated monoisotopic m/z values of the Na^+ and K^+ ion-adducts are 2179.87 and 2195.84, which agree well with the values obtained using MALDI-TOF-MS, 2179.89 and 2195.90, respectively, indicating the presence of seven acetyl groups on intermediate (**5**).

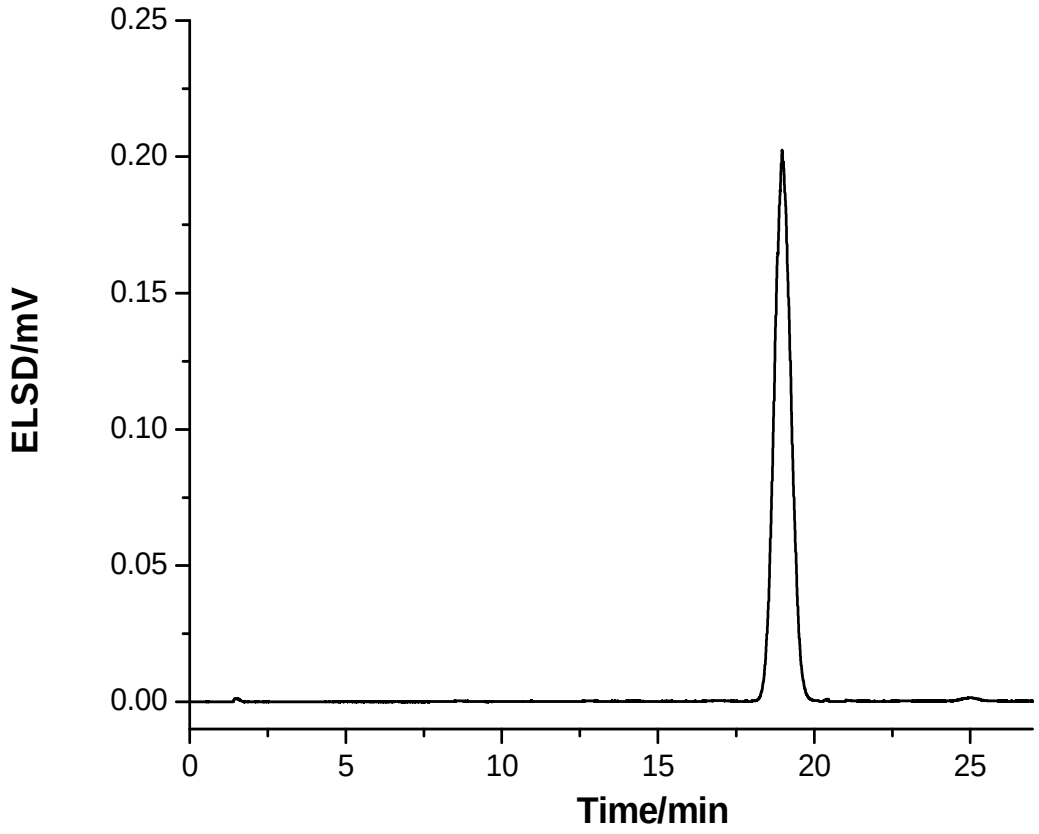

Figure 28. HPLC-ELSD chromatogram of recrystallized intermediate (**5**)

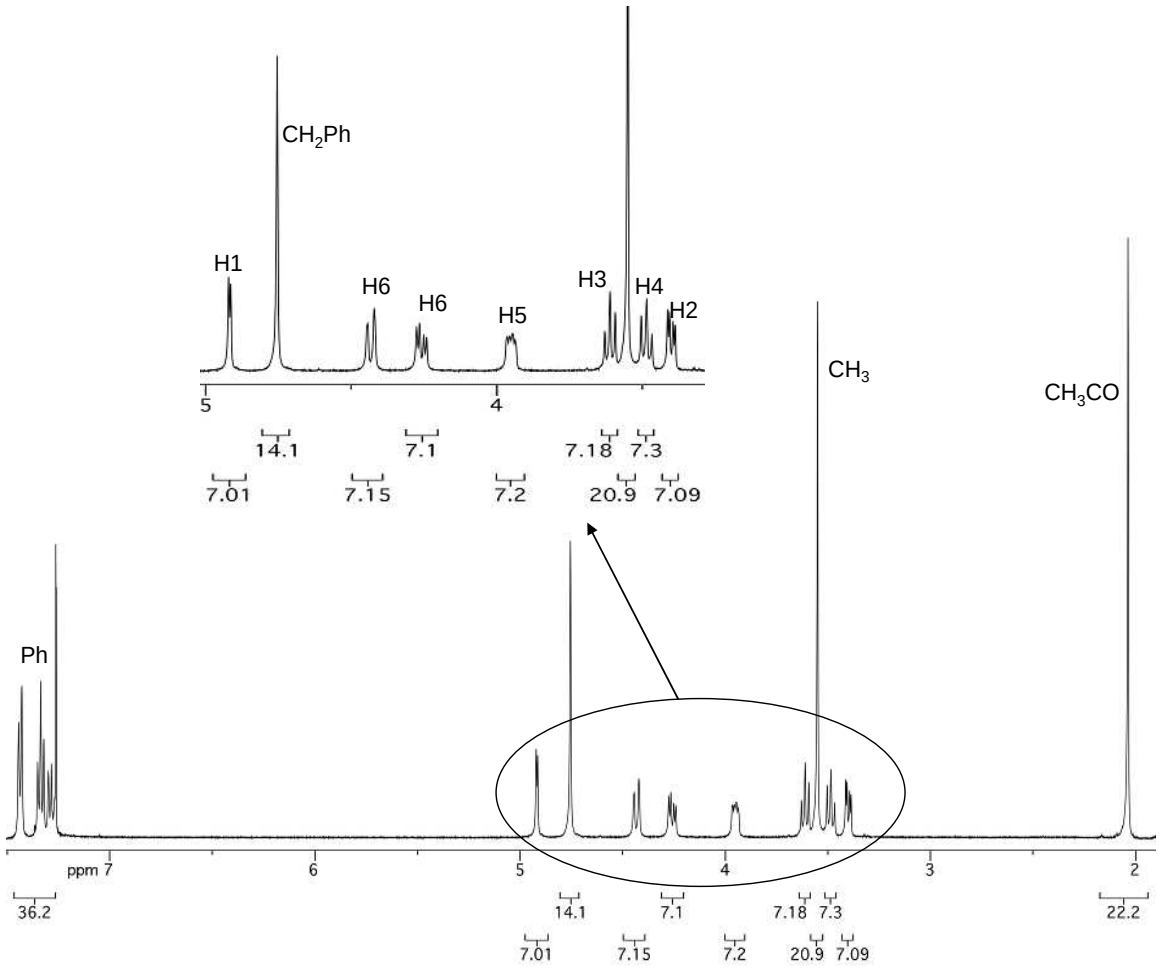

Figure 29. ^{1}H NMR spectrum of intermediate (**5**) in $CDCl_3$

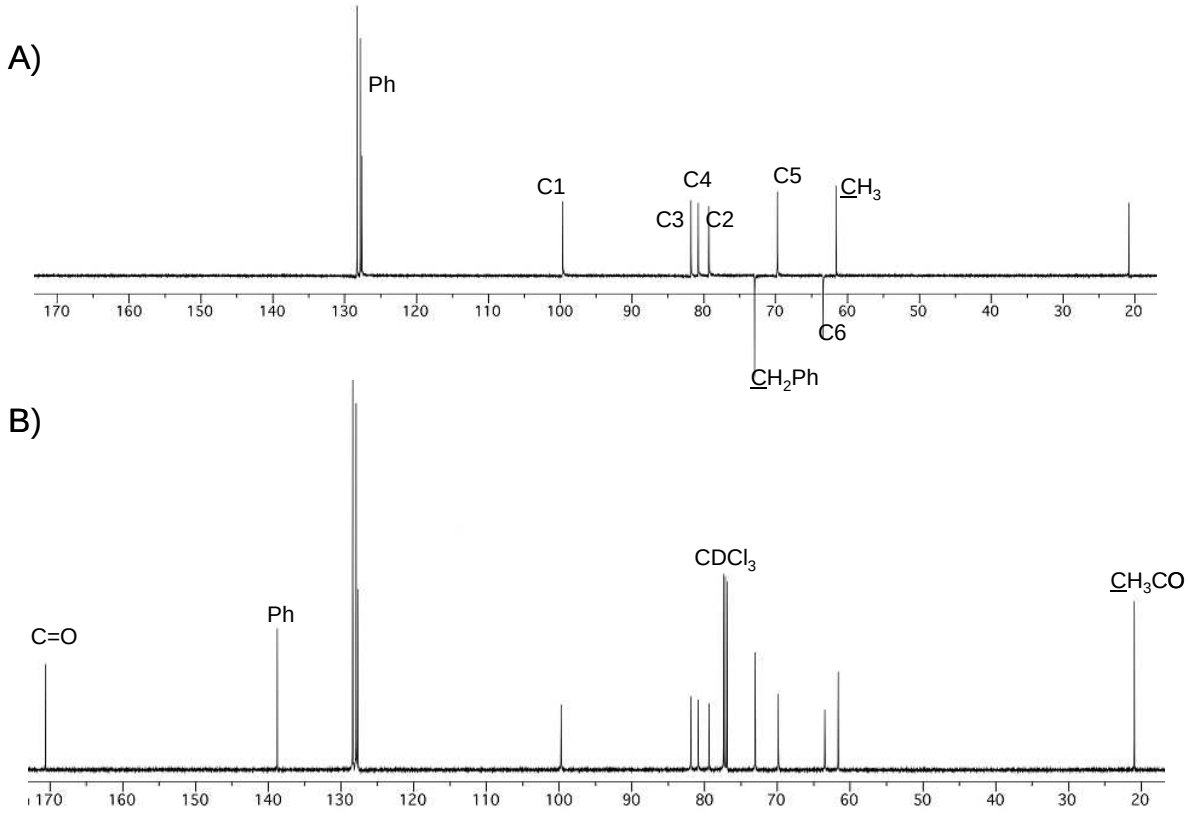

Figure 30. A) DEPT and B) ^{13}C NMR spectra of intermediate (**5**) in $CDCl_3$

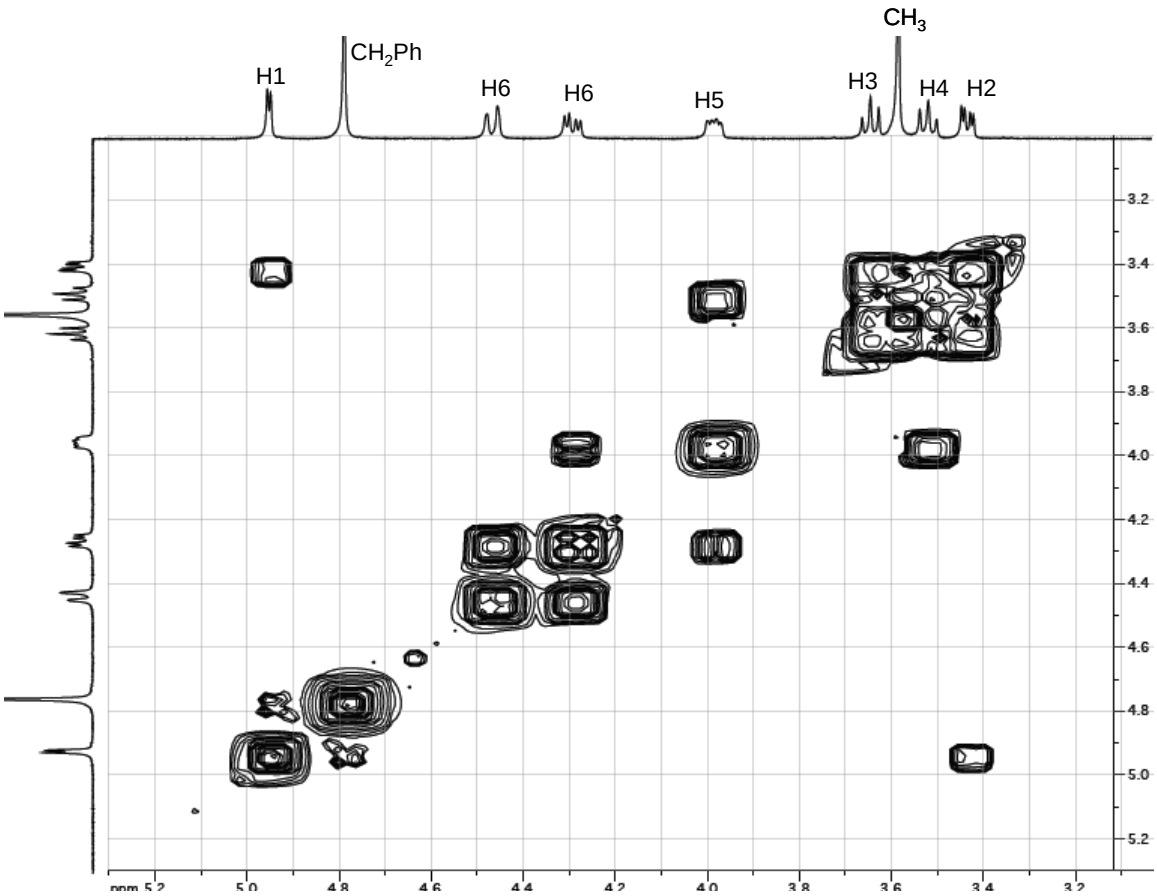

Figure 31. 2D COSY NMR spectrum of intermediate (**5**) in $CDCl_3$

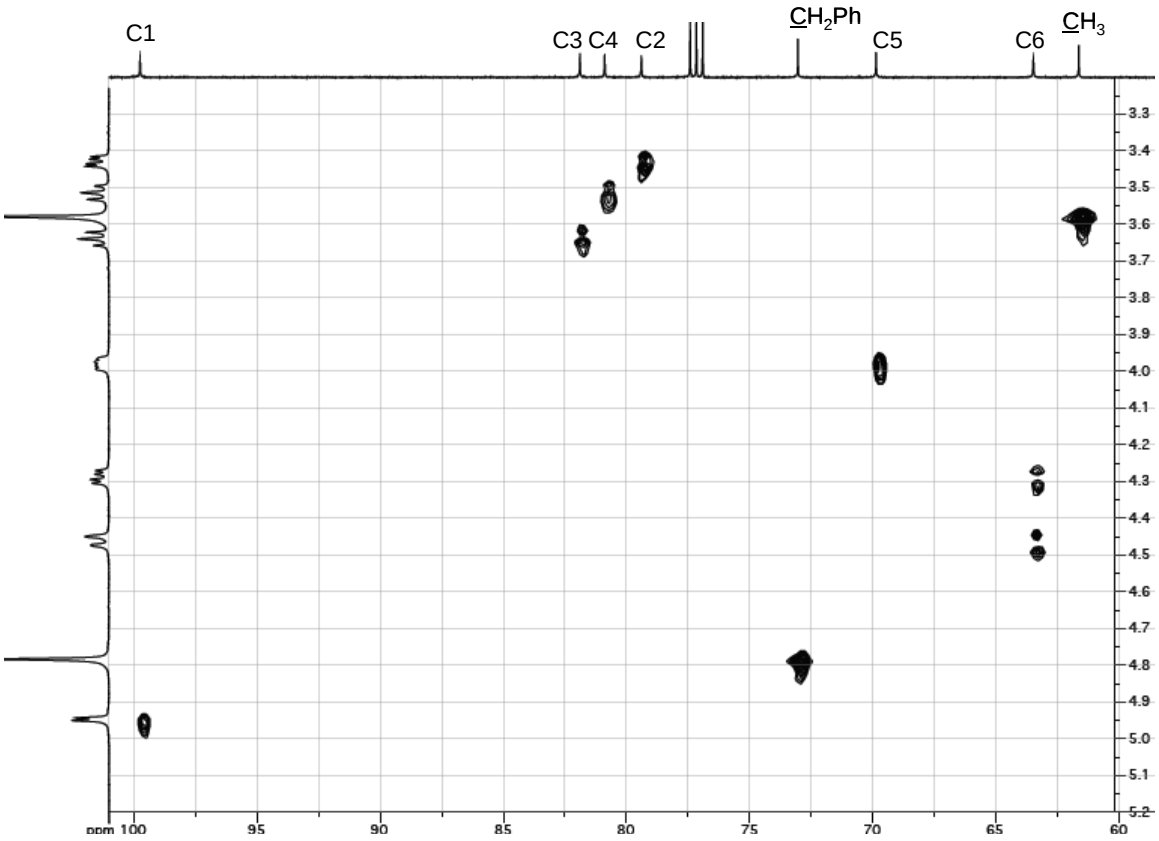

Figure 32. ^{1}H-^{13}C HMQC NMR spectrum of intermediate (**5**) in $CDCl_3$

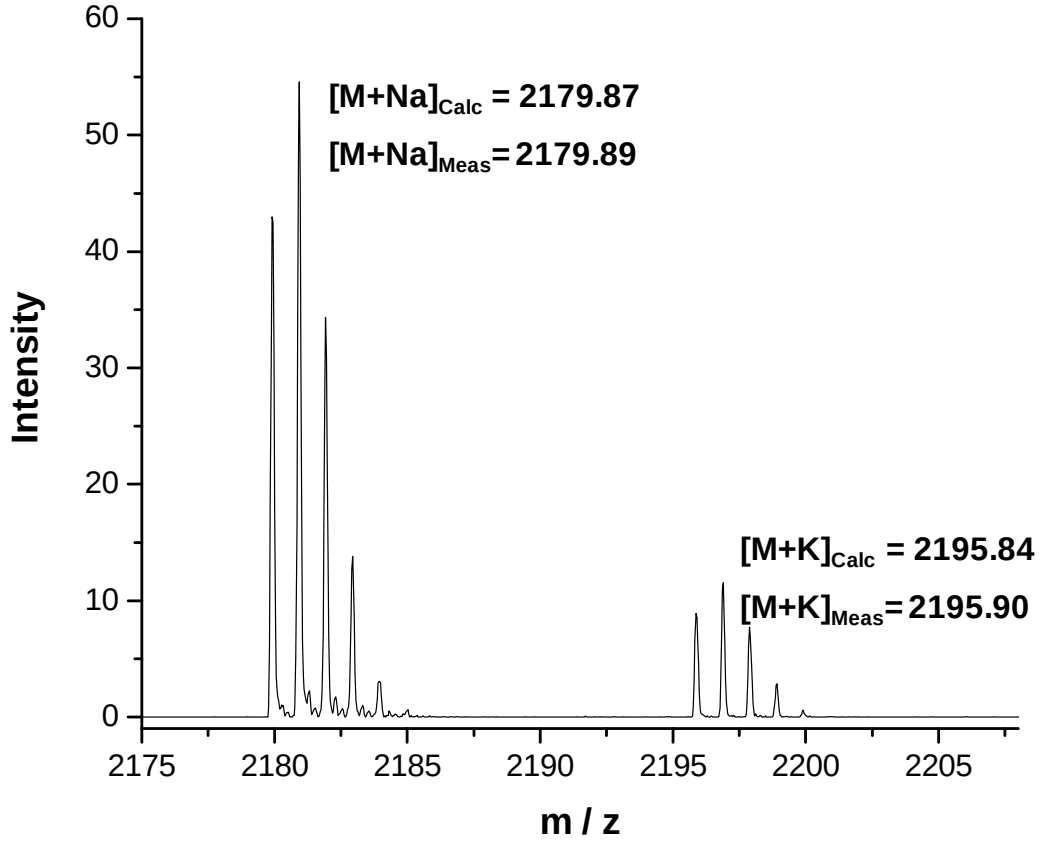

Figure 33. The Na^+ and K^+ ion-adduct portion of the MALDI-TOF mass spectrum of intermediate (**5**)

2.2.6 Heptakis(3-*O*-methyl-6-*O*-acetyl)cyclomaltoheptaose, Intermediate (6)

Debenzylation of intermediate (**5**) was accomplished following a modified version of the procedure reported by Angibeaud et al.[78] The reaction was carried out in a 1:1 mixture of anhydrous MeOH and dioxane, using 10% Pd on activated charcoal as a catalyst, in an atmosphere of H_2. Reaction progress was monitored by RP-HPLC using a 5µm Luna, C18 column and gradient elution at a flow rate of 1 ml/min. The initial mobile phase composition was 80 : 20 H_2O : ACN that was changed to 2 : 98 H_2O : ACN in 15 min, at 40ºC. Upon completion of the reaction, the catalyst was filtered and the reaction solvent was removed under reduced pressure. The crude product was dissolved in CH_2Cl_2 and precipitated with hexanes to yield intermediate (**6**) as a white powder of 98% isomeric purity. Figure 34 shows a chromatogram of the recrystallized product.

The structure of intermediate (**6**) was confirmed by high-resolution ^1H and ^{13}C NMR spectroscopy. Peak assignments for the ^1H and ^{13}C NMR spectra shown in Figures 35 and 36, respectively, were determined by DEPT and 2-dimensional ^1H-^1H COSY and ^1H-^{13}C HMQC NMR spectroscopy (spectra shown in Figures 36, 37 and 38, respectively). ^1H NMR data in $CDCl_3$: δ 4.93 (doublet, 7 H, $J_{1\text{-}2}$ = 3.5 Hz, H-1); δ 4.63 (doublet, 7 H, $J_{6\text{-}6'}$ = 10.5 Hz, H-6); δ 4.50 (doublet, 7 H, J = 9.5 Hz, OH-2); δ 4.06 (doublet of doublets, 7 H, $J_{6'\text{-}5}$ = 5.5 Hz, $J_{6'\text{-}6}$ = 10.5 Hz, H-6′6); δ 4.01 (doublet of doublets, 7 H, $J_{5\text{-}6'}$ = 5.5 Hz, $J_{5\text{-}4}$ = 9.5 Hz, H-5); δ 3.73 (singlet, 21 H, CH_3); δ 3.66 (doublet of triplets, 7 H, $J_{2\text{-}1}$ = 3.5 Hz, $J_{2\text{-}3}$ = 9.5 Hz, H-2); δ 3.52 (triplet, 7 H, $J_{3\text{-}4}$ = 9.5 Hz, $J_{3\text{-}2}$ = 9.5 Hz, H-3); δ 3.45 (triplet, 7 H, $J_{4\text{-}3}$ = 9.5 Hz, $J_{4\text{-}5}$ = 9.5 Hz, H-4); δ 2.06

(singlet, 21 H, CH_3CO). ^{13}C NMR data in $CDCl_3$: δ 170.69 ($CH_3\underline{C}O$); δ 103.37 (C-1); δ 83.09 (C-3); δ 80.21 (C-4); δ 73.76 (C-2); δ 70.41 (C-5); δ 62.89 (C-6); δ 59.69 (CH_3); δ 20.84 ($\underline{C}H_3CO$).

The ^1H-^1H COSY and ^1H-^{13}C HMQC NMR spectra (Figures 37 and 38) show only the signals that correspond to the glucopyranose subunits. The ^1H and ^{13}C NMR spectra, Figures 35 and 36, respectively, show that all the benzyl groups at the C-2 positions were removed from intermediate (**5**) while the acetyl and methyl groups remained intact. A significant upfield shift was seen for the C-2 carbon atoms, from 79.40 ppm in intermediate (**5**) to 73.76 ppm in intermediate (**6**), confirming that the change occurred at the C-2 carbon atoms.

High resolution MALDI-TOF mass spectrometry was used to determine the molecular mass of intermediate (**6**). The Na^+ and K^+ion-adduct portion of the mass spectrum of intermediate (**6**) is shown in Figure 39. The calculated monoisotopic m/z values of the Na^+ and K^+ ion-adducts, 1549.54 and 1565.52, agree well with the values obtained using MALDI-TOF-MS, 1549.53 and 1565.50, respectively, confirming the complete removal of the benzyl groups from intermediate (**5**).

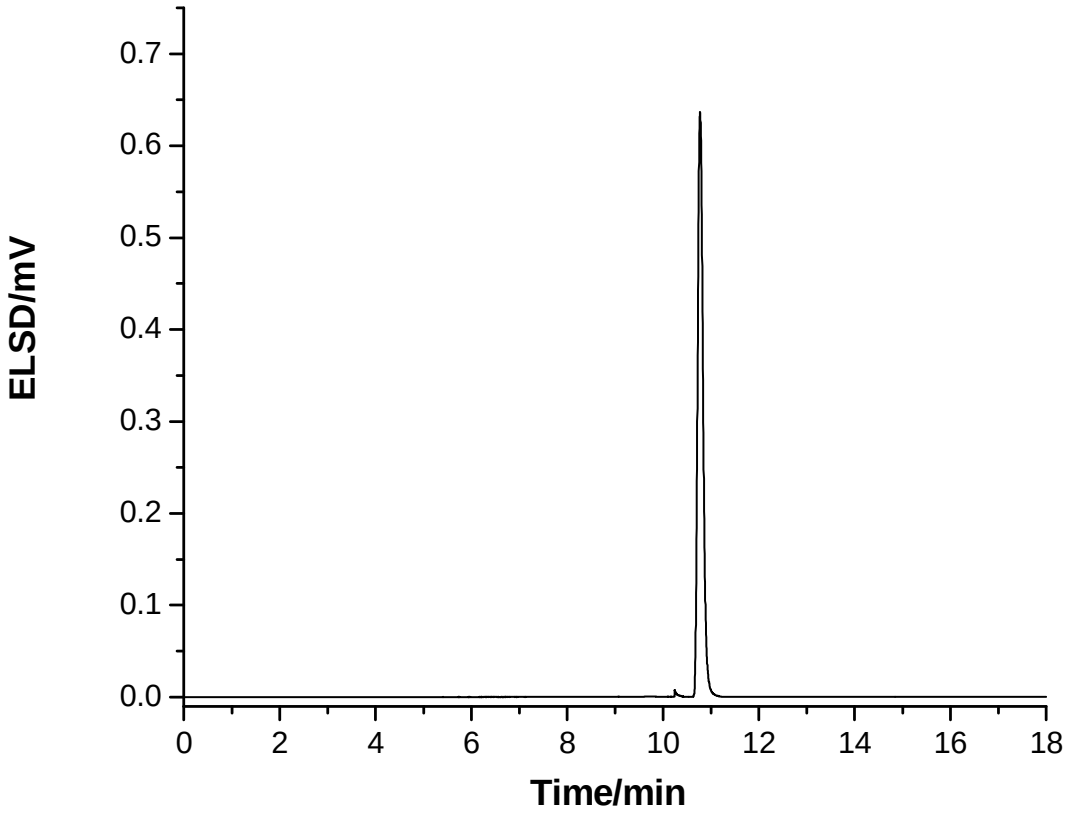

Figure 34. HPLC-ELSD chromatogram of recrystallized intermediate (**6**)

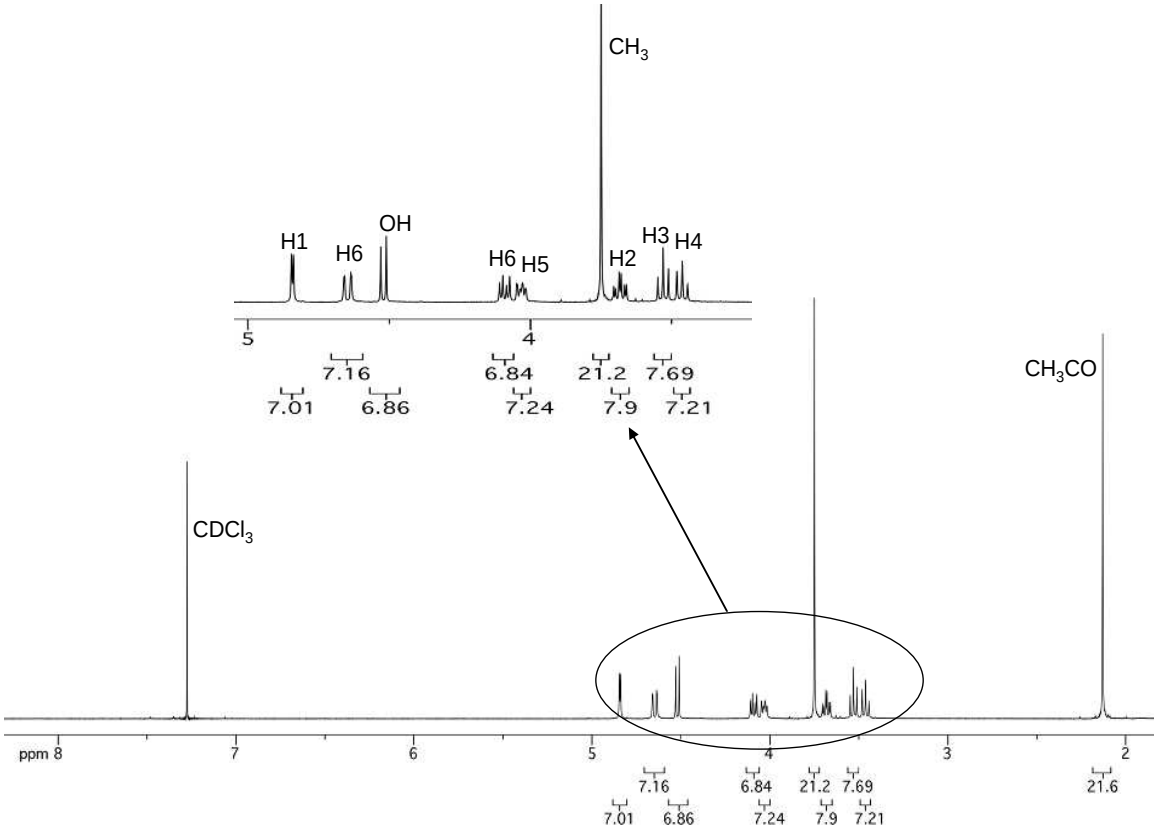

Figure 35. ^{1}H NMR spectrum of intermediate (**6**) in $CDCl_3$

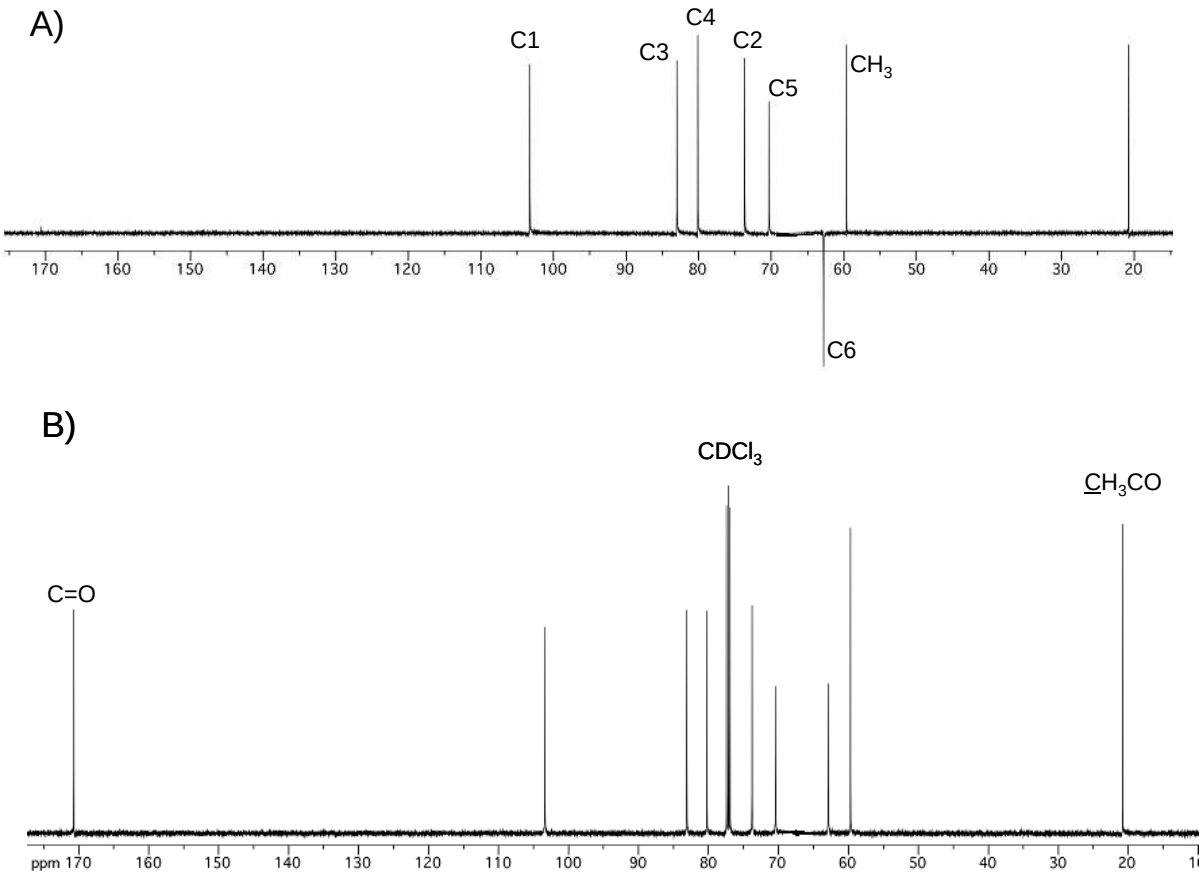

Figure 36. A) DEPT and B) ^{13}C NMR spectra of intermediate (**6**) in $CDCl_3$

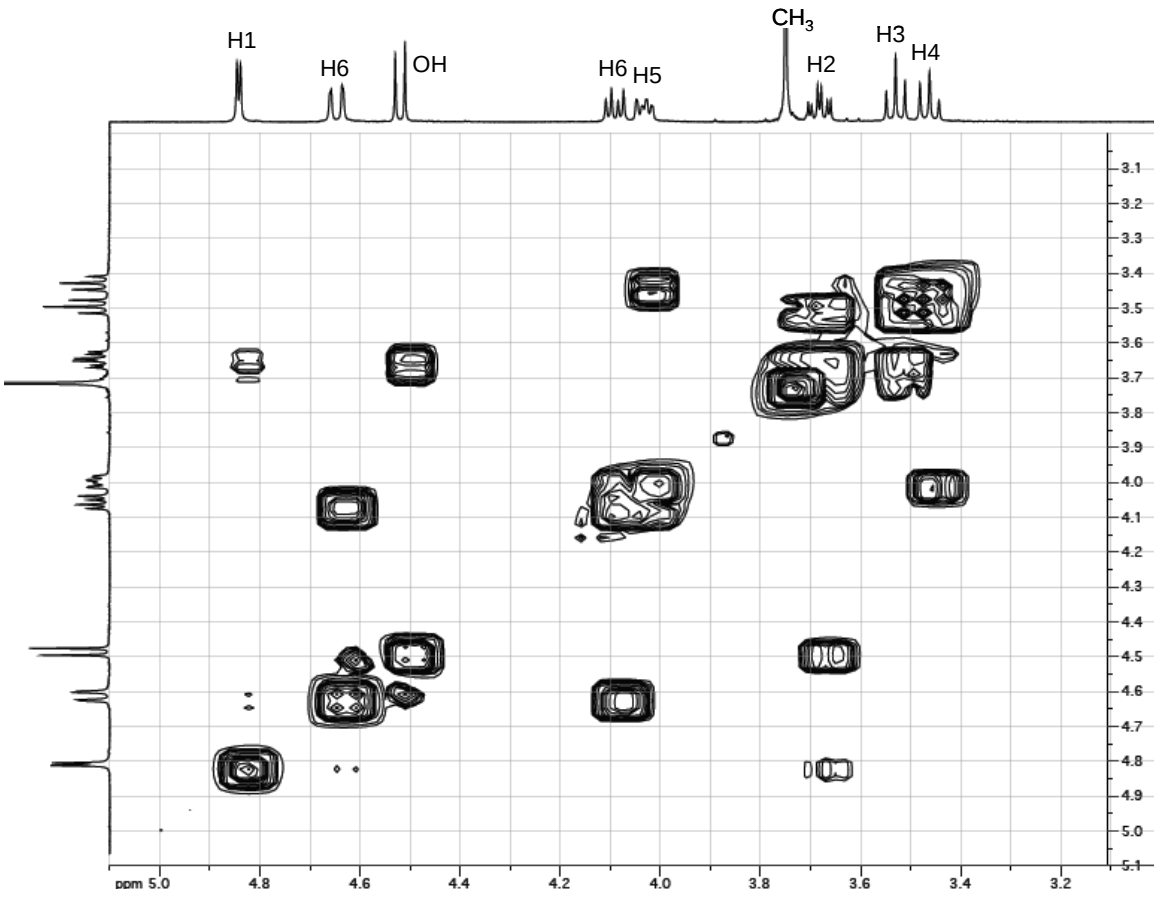

Figure 37. 2D COSY NMR spectrum of intermediate (**6**) in $CDCl_3$

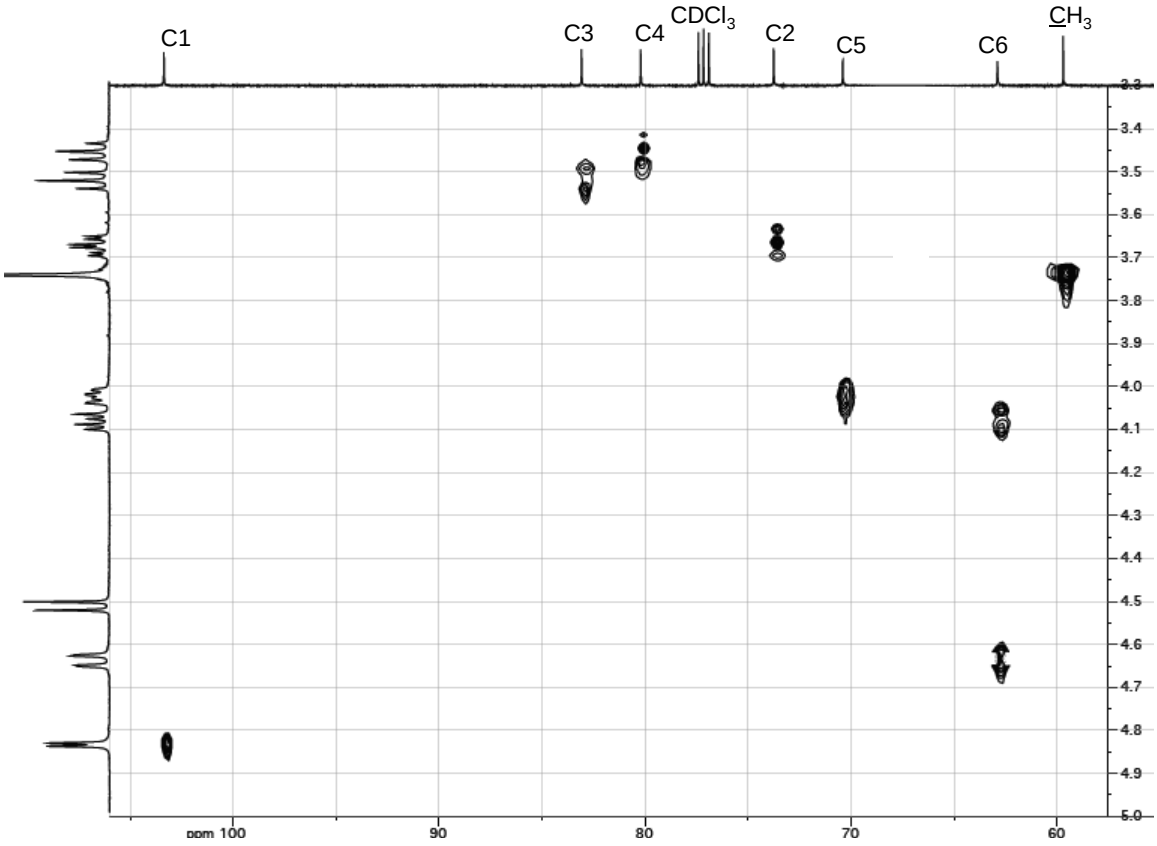

Figure 38. ^{1}H-^{13}C HMQC NMR spectrum of intermediate (**6**) in $CDCl_3$

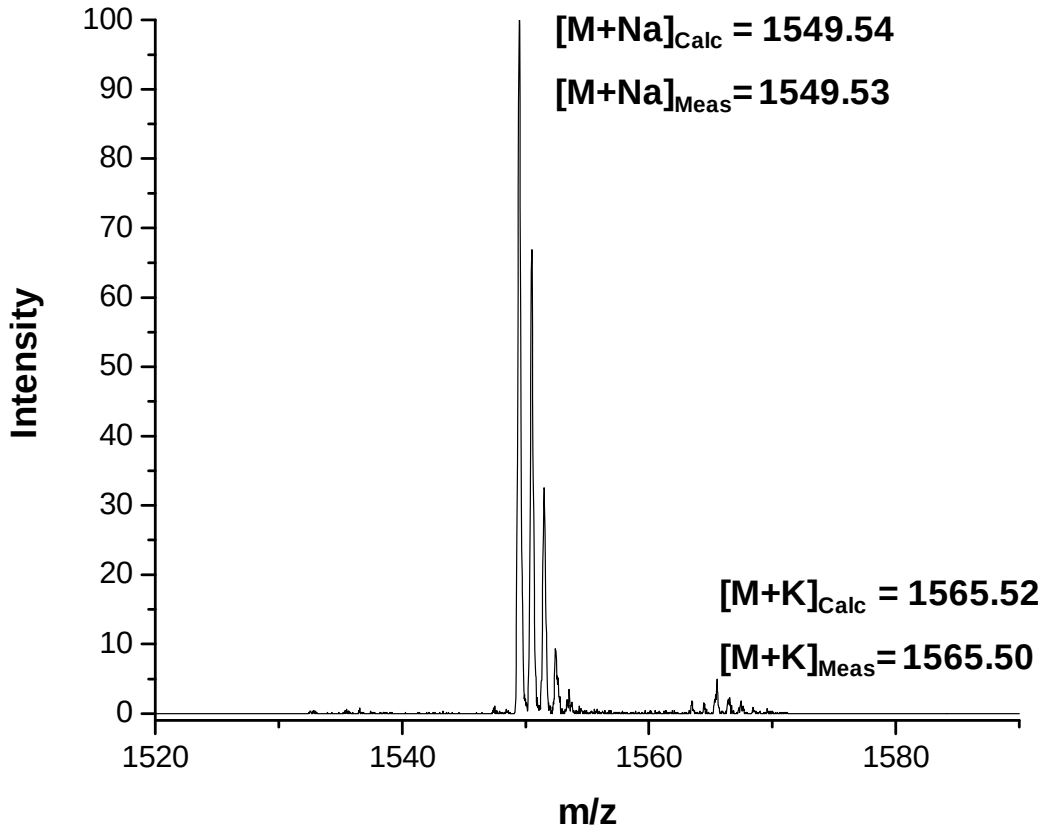

Figure 39. The Na^+ and K^+ion-adduct portion of the MALDI-TOF mass spectrum of intermediate (**6**)

2.2.7 Heptakis(2-*O*-sulfo-3-*O*-methyl-6-*O*-acetyl)cyclomaltoheptaose (HAMS)

Following a modified procedure of Vincent et al.[59], sulfation of intermediate (**6**) was conducted in DMF at 50ºC with an excess of sulfur trioxide pyridine complex using pyridine as the base. Reaction progress was monitored by HPLC using a 3µm Luna, HILIC column and gradient elution at a flow rate of 1 ml/min. The initial mobile phase composition was 100% A that was changed to 50% A : 50% B in 30 min (A: 5 mM $HCOONH_4$ in 95% ACN, B: 5mM $HCOONH_4$ in H_2O) at room temperature. Upon completion of the reaction, sodium bicarbonate was added to the reaction mixture and the sodium sulfate precipitate produced was filtered. The reaction solvents were removed under reduced pressure. The crude product was dissolved in a minimum amount of MeOH and the product was precipitated by pouring the solution into diethyl ether to yield the final product, **HAMS**, as a white powder of 97% isomeric purity. Figure 40 shows a chromatogram of the recrystallized product.

The structure of **HAMS** was confirmed by high-resolution ^{1}H and ^{13}C NMR spectroscopy. Peak assignments for the ^{1}H and ^{13}C NMR spectra shown in Figures 41 and 42, respectively, were determined by DEPT and 2-dimensional ^{1}H-^{1}H COSY and ^{1}H-^{13}C HMQC NMR spectroscopy (spectra shown in Figures 42, 43 and 44, respectively).

^{1}H NMR data in D_2O: δ 5.33 (doublet, 7 H, $J_{1\text{-}2}$ = 3.5 Hz, H-1); δ 4.38 (doublet, 7 H, $J_{6\text{-}6'}$ = 10.5 Hz, H-6); δ 4.26 (doublet of doublets, 7 H, $J_{6'\text{-}5}$ = 5.5 Hz, $J_{6'\text{-}6}$ = 10.5 Hz, H-6′6); δ 3.66 (doublet of doublets, 7 H, $J_{2\text{-}1}$ = 3.5 Hz, $J_{2\text{-}3}$ = 9.5 Hz, H-2); δ 4.01 (doublet of doublets, 7 H, $J_{5\text{-}6'}$ = 5.5 Hz, $J_{5\text{-}4}$ = 9.5 Hz, H-5); δ 3.79-3.72 (multiplet, 14 H, H-3, H-4); δ 3.58 (singlet, 21 H, CH_3); δ 2.07 (singlet, 21 H, CH_3CO). ^{13}C NMR data in D_2O: δ 173.27 ($CH_3\underline{C}O$); δ 97.14 (C-1); δ 79.32 (C-3); δ 77.07 (C-2) δ 76.62 (C-4); δ 69.08 (C-5); δ 63.51 (C-6); δ 60.67 (CH_3); δ 20.22 ($\underline{C}H_3CO$).

The ^{1}H-^{1}H COSY and ^{1}H-^{13}C HMQC NMR spectra (Figures 43 and 44) show only the signals that correspond to the glucopyranose subunits. The ^{1}H and ^{13}C NMR spectra, Figures 41 and 42, respectively, show that the acetyl groups at the C-6 position remained intact during sulfation of intermediate (**6**). A significant downfield shift was seen for the C-2 carbon atoms; from 73.75 ppm in intermediate (**6**) to 77.07 ppm in the final product, **HAMS**, confirming that the change occurred at the C-2 carbon atoms.

High resolution MALDI-TOF mass spectrometry was used to confirm the molecular mass of **HAMS**. The Na^+ ion-adduct portion of the mass spectrum of **HAMS** is shown in Figure 45. The calculated monoisotopic m/z value of the Na^+ ion-adduct, 2263.11, agrees well with the value obtained using MALDI-TOF-MS, 2263.11.

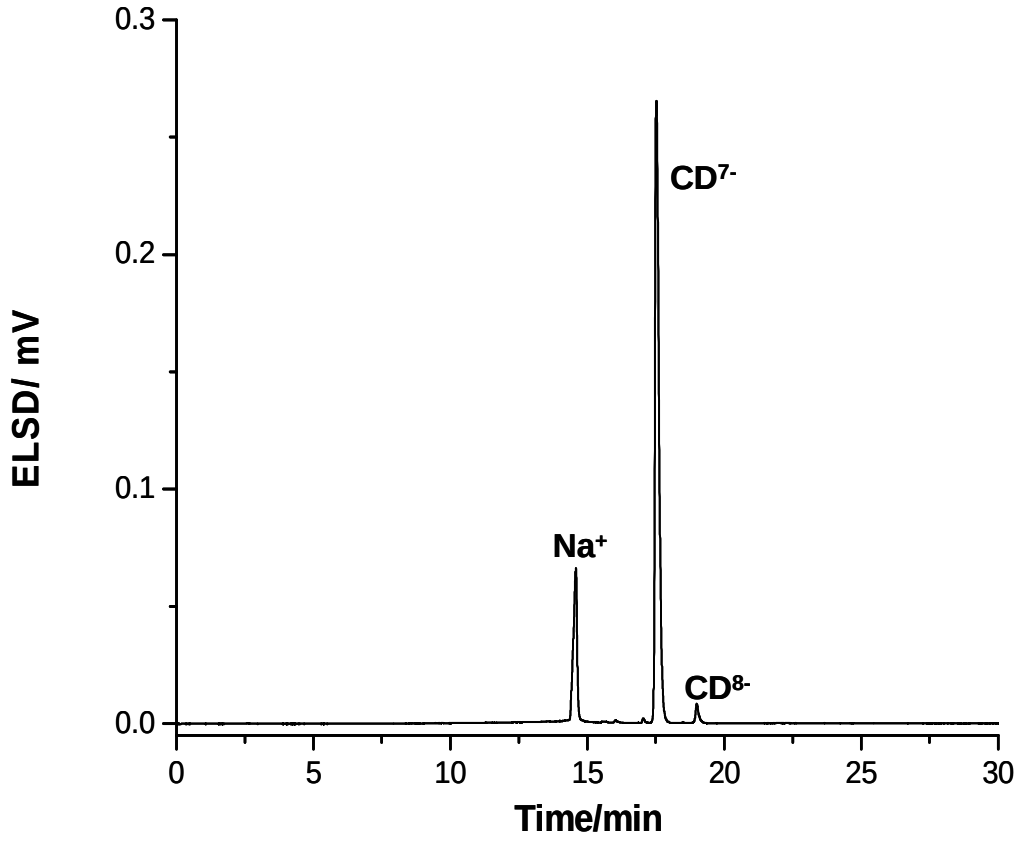

Figure 40. HPLC-ELSD chromatogram of recrystallized final product (**HAMS**)

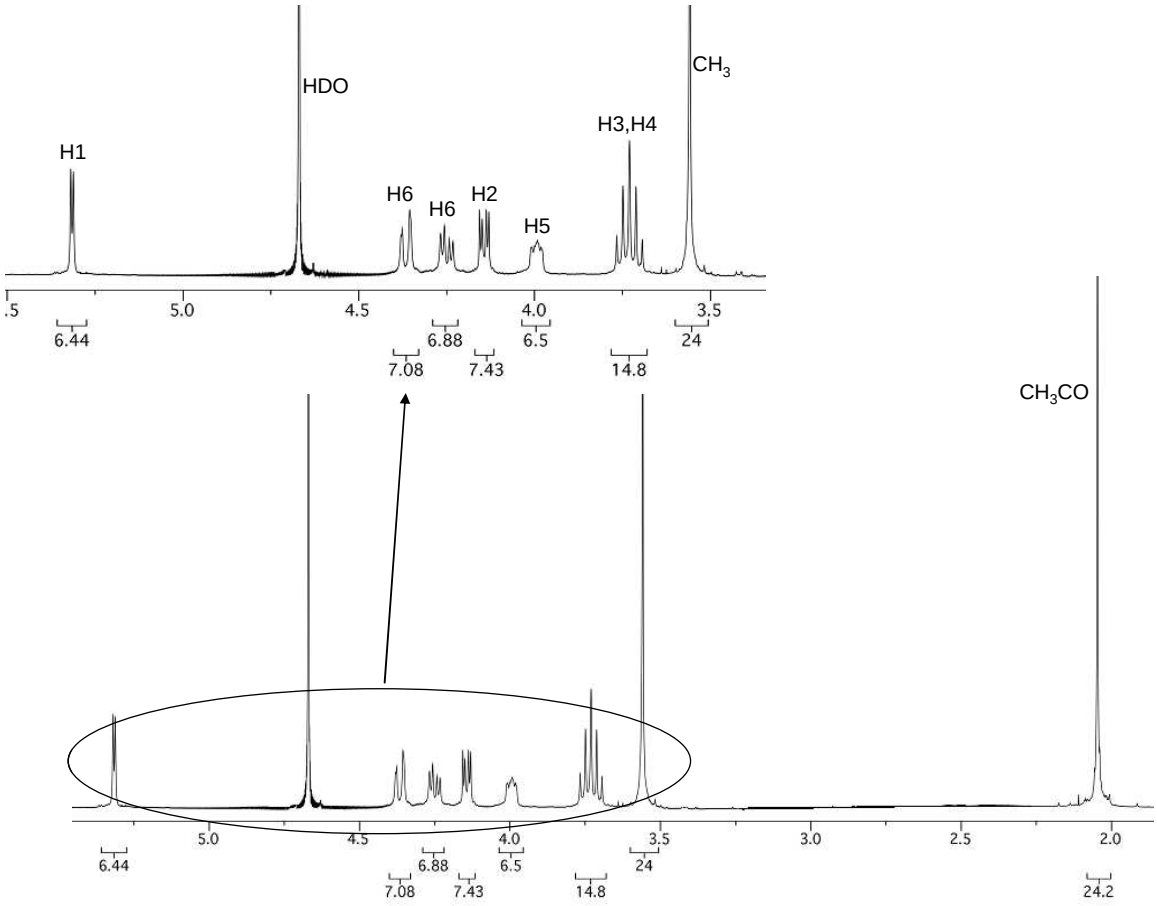

Figure 41. ^{1}H NMR spectrum of final product (**HAMS)** in D_2O

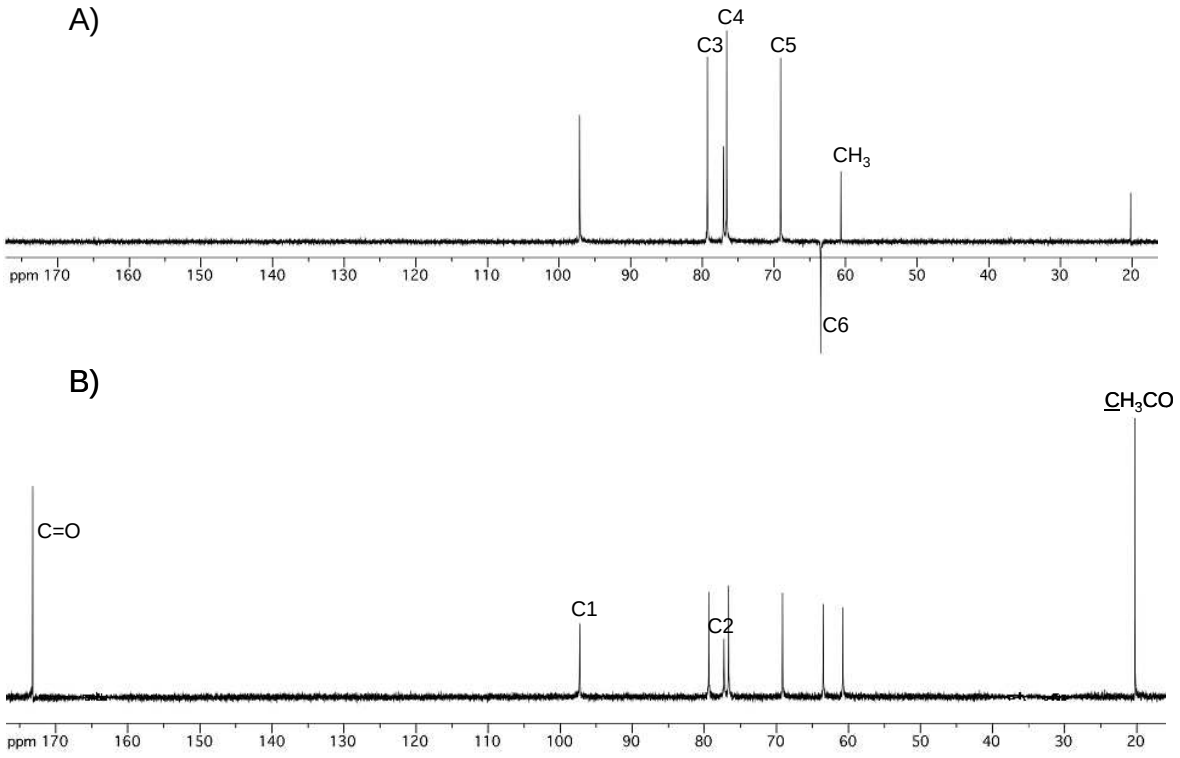

Figure 42. A) DEPT and B) ^{13}C NMR spectra of final product (**HAMS**) in D_2O

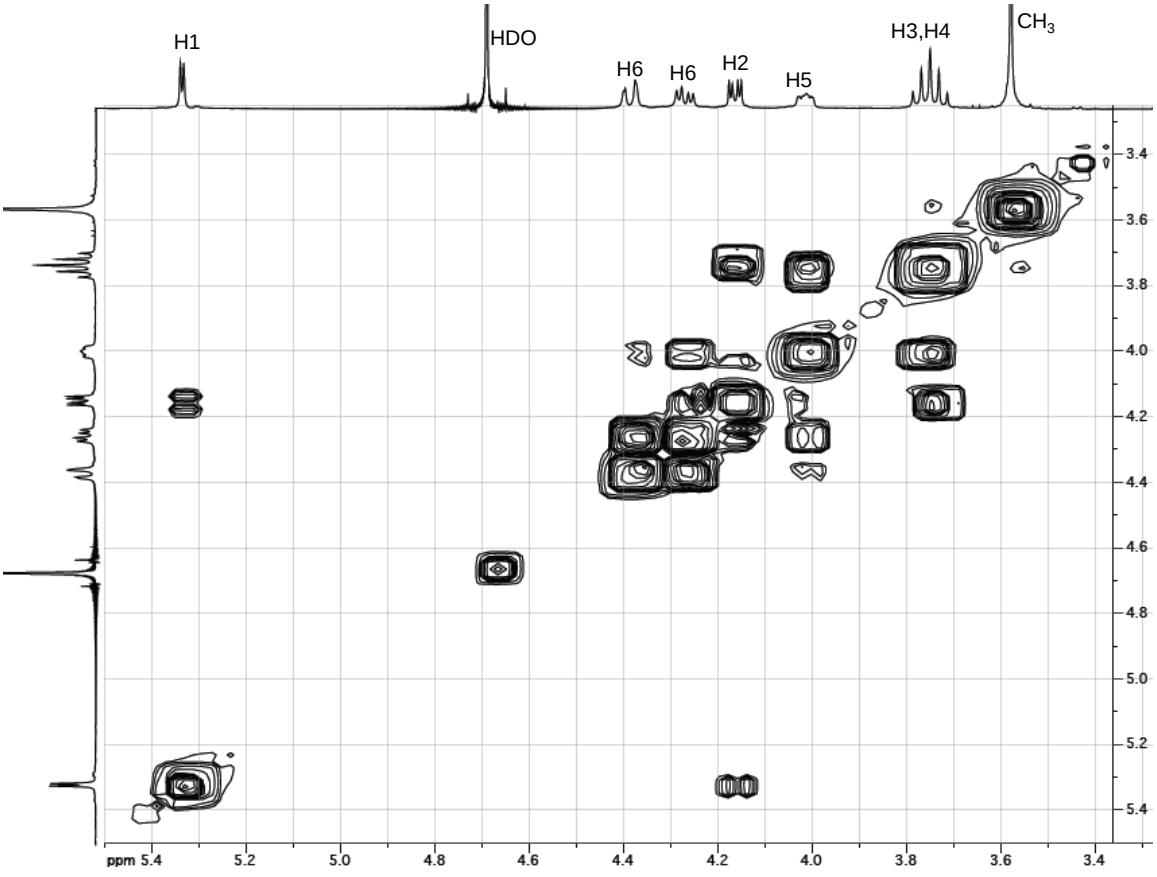

Figure 43. 2D COSY NMR spectrum of final product **(HAMS)** in D_2O

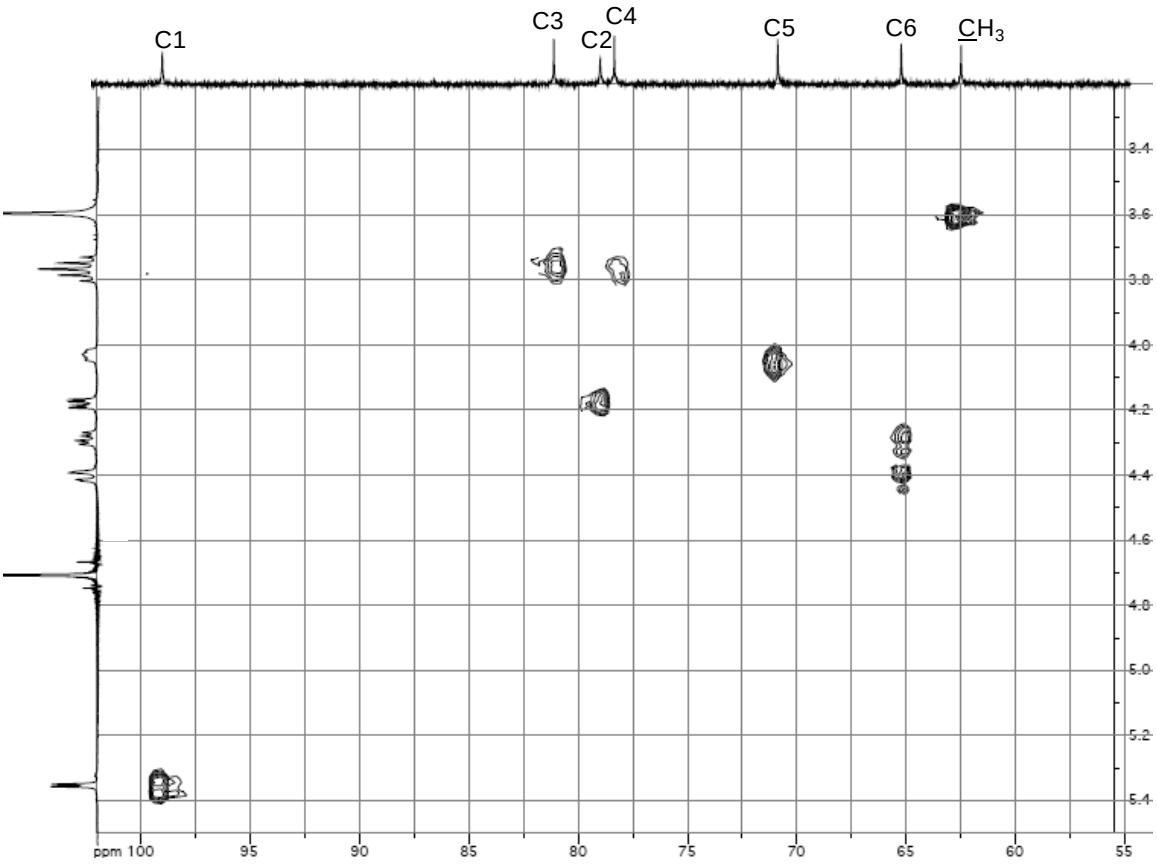

Figure 44. ^{1}H-^{13}C HMQC NMR spectrum of final product (**HAMS**) in D_2O

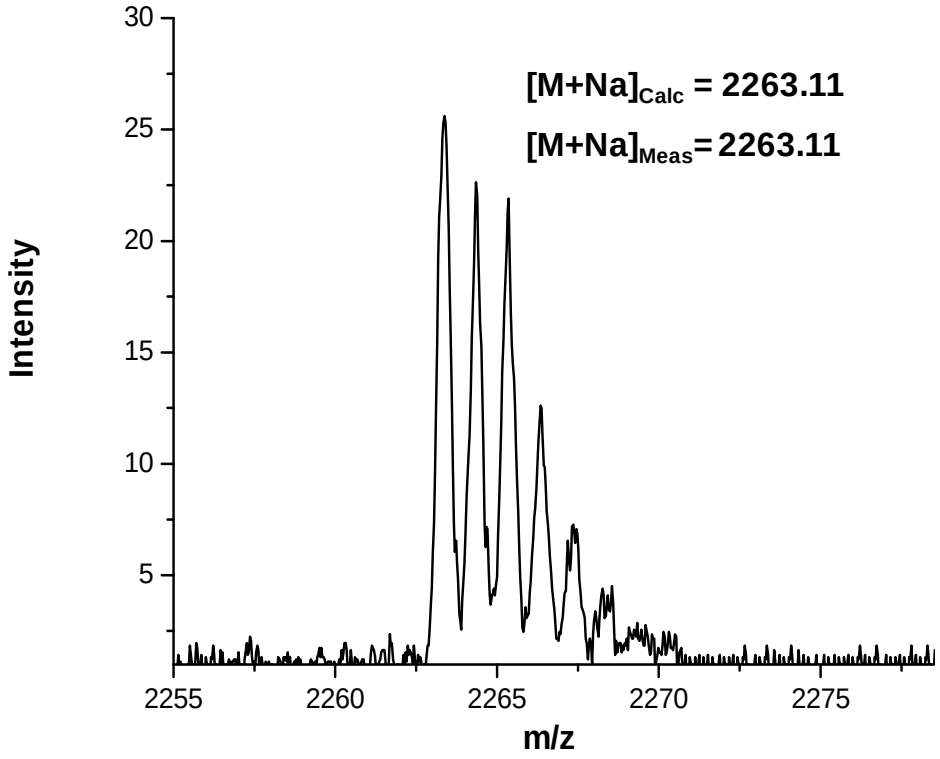

Figure 45. The Na^+ ion-adduct portion of the MALDI-TOF mass spectrum of final product (**HAMS**)

2.3 Summary

The synthesis of the sodium salt of HAMS for use as a chiral resolving agent in capillary electrophoretic separation of enantiomers has been accomplished via a seven-step synthetic methodology. Key to the successful synthesis of this product lies in the regioselective protection and deprotection steps outlined in the synthetic scheme. Although the use of each of these procedures alone, along with extensive chromatographic purification steps, has been reported in the literature, the modifications and their combination reported here permitted the making of large quantities of the intermediates at high purity, facilitating the synthesis of the final product. The structural identity of each intermediate and final product was ascertained by ^{1}H NMR and ^{13}C NMR, 2D NMR and MALDI- and ESI-TOF-MS analysis. Both gradient and isocratic HILIC and reversed-phased HPLC methods were developed for the determination of the respective isomeric purities, which were in excess of 97 % mol/mol.

CHAPTER III

CE SEPARATION OF ENANTIOMERS

Several single-isomer sulfated CD derivatives, carrying the sulfate groups on either the C3 or C6 positions of the glucopyranose units, have been used as chiral resolving agents in CE. Previous work has shown that the cavity size of the cyclodextrins, and the type of the substituents (hydroxyl, acetyl or methyl groups) play significant roles in the chiral recognition processes. However, the effect of the attachment position of the sulfate group on the enantiorecognition capabilities of CDs has not been fully investigated since a single-isomer sulfated CD carrying the sulfate groups on C2 positions had not been synthesized. This chapter describes the chiral recognition behavior of HAMS, a single-isomer CD carrying the sulfate moiety on the chiral face at the C2 position. Whenever possible, qualitative comparison was made between the separations achieved with HAMS and other β-functionalized SISCD.

3.1 Materials

All chiral analytes were obtained either from Aldrich Chemical Co. (Milwaukee, WI), Sigma (St. Louis, MO), Wiley Organics (Coshocton, OH) or Research Diagnostic (Rockdale, MD). Dimethylsulfoxide (DMSO) was purchased from EM Science (Gibbstown, NJ). All aqueous solutions used in these experiments were prepared from deionized water obtained from a Milli-Q unit (Millipore, Milford, MA). 0.45 μm Nalgene nylon membrane filters were purchased from VWR (South Plainfield, NJ).

Phosphoric acid and lithium hydroxide were purchased from Aldrich Chemical Co. HAMS was prepared as described in Chapter II. The stock buffer was prepared by titration of a 25 mM aqueous solution of H_3PO_4 (pK_{a1}, 2.1) to pH 2.5 with LiOH. The chiral resolving agent-containing BGEs were prepared immediately prior to use by weighing out the required amount of the sodium salt of HAMS into 25 ml volumetric flasks and bringing the volume to mark with the stock buffer solution.

3.2 CE Conditions and Methods

All enantiomer separations were performed on either a P/ACE 5010 or a P/ACE 2010 capillary electrophoresis instruments with their UV detectors set to 214 nm. A 26.4 cm total length (19.6 cm to detector), 27 µm i.d., fused silica capillary (Polymicro Technologies, Phoenix, AZ, USA) was used for CE measurements. A UV detection window was prepared by removing a section of the polyimide coating by burning off with an electric coil heater. The exposed capillary section was then wiped clean with methanol-soaked Kimwipe. All separations were obtained between 7 and 20 kV applied potential and 20 ºC cartridge coolant temperature. Between runs, the capillary was flushed with deionized water for 3 min, followed by the running buffer for 3 min. Dimethylsulfoxide (DMSO), which has been reported to have zero effective mobility with SISCDs,[57] was selected as the electroosmotic flow (EOF) mobility marker for HAMS. Its suitability as a mobility maker has been experimentally verified.[79] The enantiomers were dissolved in the cyclodextrin-containing BGE and either co-injected with the EOF marker by pressure for 1 s or the marker was injected separately followed

by electrokinetic injection of the enantiomers at 10 kV for 5s. The effective mobilities were measured against DMSO and these measurements were carried out within the linear region of Ohm's law. All solutions were filtered prior to use with a 0.45 µm Nalgene nylon membrane filter.

Separation selectivity (α) was determined as a function of the concentration of the chiral resolving agent in aqueous low pH BGEs. The effective mobilities (μ^{eff}) and the normalized electroosmotic mobilities (β) were calculated per equations 7 and 13 (see Chapter I), respectively. Peak resolution was calculated from peak half-height widths (w^h) as:

$$Rs = \frac{2(t_2 - t_1)}{1.699(w_2^h + w_1^h)}$$

Migration time (t) values used were taken at the estimated point of infinite dilution for peaks suffering electromigration dispersion (EMD). Effective mobilities and separation selectivities were plotted as a function of the resolving agent concentration to evaluate the optimum chiral resolving agent concentration for the highest available separation selectivity.

3.3 Separations of Enantiomers of Weak Base Analytes Using HAMS in Low pH BGEs

According to the CHARM model, when a strong electrolyte resolving agent, such as HAMS is used for enantioseparations, only two stock BGEs, one at low pH and another at high pH are required.[47] Previous work has shown that a low pH BGE will provide good resolution values because more favorable β values can be obtained than in high pH BGEs. For ionoselective separation of weak base enantiomers, peak resolution is high at low pH.[47] Thus, chiral recognition can be maximized by taking advantage of the electrostatic interaction between the SISCD and the protonated enantiomers, in addition to other intermolecular interactions that may also be present. Effective mobilities for singly-charged, weakly basic compounds usually lie between +10 and +35 mobility units (10^{-5} $cm^2V^{-1}s^{-1}$). Generally, at low pH, μ^{eo} values are between +10 to +25 mobility units in fused silica capillaries. Previous work has shown that complexation of weak bases with SISCDs leads to anionic effective mobilities as high as -30 mobility units. This effect makes it possibility to adjust the SISCD concentration to bring about an effective mobility that is nearly equal in magnitude but opposite in direction to the EOF mobility in order to achieve resolution. It is therefore reasonable to evaluate the potential of a new SISCD for enantioseparation by beginning with weak base enantiomers in low pH BGEs.

3.3.1 Results and Discussion

The structures of the thirty-three, structurally diverse, weakly basic enantiomers (mostly pharmaceuticals) selected to evaluate the utility of HAMS as a chiral resolving agent for use in CE enantiomer separations are shown in Figure 46. All thirty-three weakly basic compounds have been shown to have cationic effective mobilities under the selected conditions at 0 mM HAMS concentration. Shown in Table 1 are the effective mobilities of the less mobile enantiomer, μ, the separation selectivities, α, the calculated peak resolution, Rs, the corresponding dimensionless, normalized EOF mobility values, β, and the injector-to-detector potential drop values, U, obtained in the low pH aqueous BGEs for the weakly basic enantiomers. An entry of N/A indicates that a value could not be calculated due to overlap with either a non-comigrating system peak or overlap with the neutral marker peak. The applied potential was 20 kV in 0.5 mM HAMS-containing BGE and decreased with increasing HAMS concentration to 11 kV in the 20 mM HAMS-containing BGE. The mobility of the cathodic EOF (μ^{EOF}) was between 10 to 20 mobility units over the 0.5 to 20 mM HAMS concentration range, indicating that HAMS was adsorbed on the walls of the capillary. No studies were conducted to quantify the contribution of chromatographic retention of the effective migration of the analytes.

There was at least some separation selectivity for the enantiomers of 27 of the 33 weakly basic compounds tested within the HAMS concentration range studied. Of these, 18 were baseline resolved (i.e., Rs > 1.5) under the conditions used. For six analytes, including atenolol, ketamine, mepenzolate bromide, metoprolol, tolperisone and

chlorpheniramine, there was no resolution. Atenolol and ketamine were weakly complexing at all HAMS concentrations. Mepenzolate bromide and chlorpheniramine have chiral centers sterically crowded by two aromatic rings. Even though metoprolol and tolperisone complex strongly with HAMS, lack of resolution may be due to unfavorable β-values provided by the separation conditions used. Although these explanations seem reasonable, NMR and X-ray crystallographic experiments are needed to aid our understanding of the enantiorecogntion process.

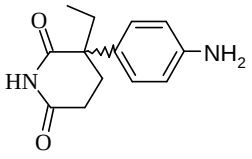

B03: Aminoglutethimide

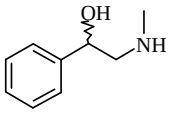

B04: Halostachine

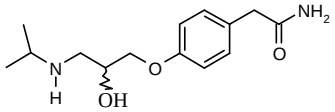

B08: Atenolol

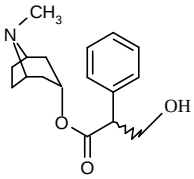

B09: Atropine

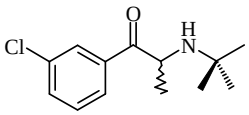

B11:Bupropion

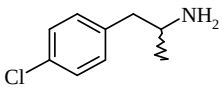

B13: 4-Chloroamphetamine

Figure 46. Names and structures of weakly basic analytes

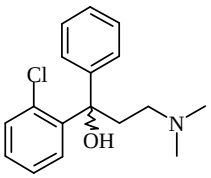

B14: Chlophedianol

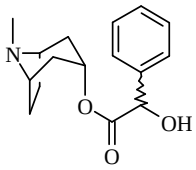

B19: Homatropine

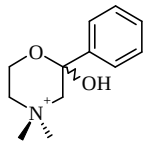

B20: Hemicholinium-15

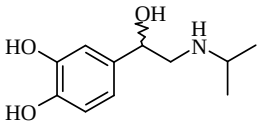

B21: Isoproterenol

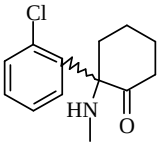

B22: Ketamine

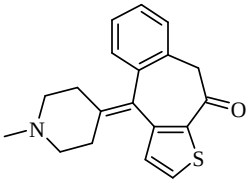

B23:Ketotifen

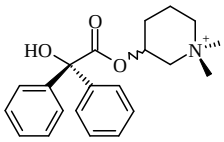

B25: Mepenzolate Bromide

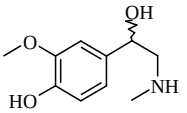

B26: Metanephrine

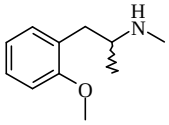

B28: Methoxyphenamine

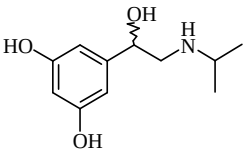

B30 Metaproterenol

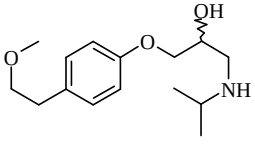

B31: Metoprolol

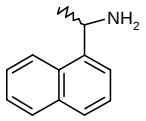

B33: (1-Napthyl)ethylamine

Figure 46. Continued

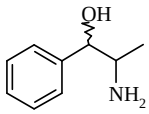

B34: Norephedrine

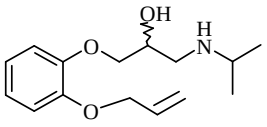

B37:Oxprenolol

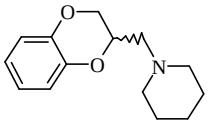

B38: Piperoxan

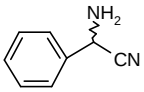

B39: Phenylglycinonitrile

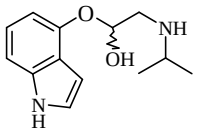

B41: Pindolol

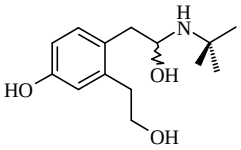

B45: Salbutamol

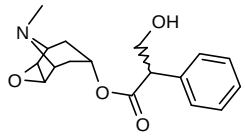

B46: Scopolomine

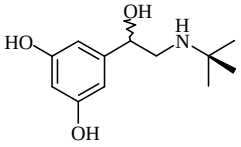

B47: Terbutaline

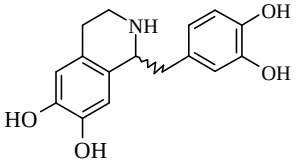

B49: Tetrahydropapaveroline

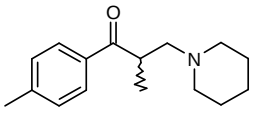

B51: Tolperisone

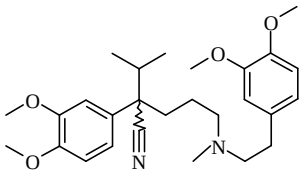

B54: Verapamil

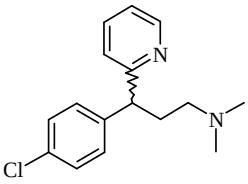

B56: Chlorpheniramine

Figure 46. Continued

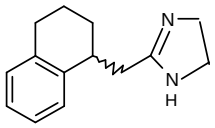

B58: Tetrahydrozoline

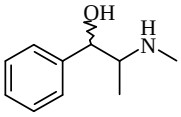

B60: Ephedrine

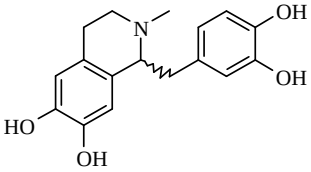

B75: Laudanosoline

Figure 46. Continued

Table 1. Separation data for the weak base analytes in pH 2.5 aqueous HAMS BGEs. (μ, in 10^{-5} cm^2/Vs units)

[CD]	0 mM		0.5mM			0.75mM			
U (KV)	20		20			20			
Analyte	μ	μ	α	β	Rs	μ	α	β	Rs
B03	19.73	15.44	1.00	0.27	0.00	14.01	1.02	0.42	0.15
B04	23.65	20.32	1.00	0.27	0.00	19.30	1.00	0.33	0.00
B08	16.67	14.24	1.00	0.43	0.00	13.54	1.00	0.41	0.00
B09	25.57	10.75	1.17	0.54	1.27	8.88	1.24	0.73	1.73
B11	34.90	16.05	1.13	0.47	1.26	8.45	1.27	0.80	2.67
B13	23.28	2.61	<1.01	2.09	0.10		N/A		
B14	17.62	4.91	1.82	1.11	3.80	1.58	3.64	4.88	4.35
B19	18.67	14.01	1.13	0.36	1.24	12.28	1.18	0.51	1.69
B20	30.80	22.81	1.00	0.24	0.00	18.05	1.00	0.46	0.00
B21	25.89	20.01	1.00	0.32	0.00	17.10	1.00	0.56	0.00
B22	28.90	21.50	1.00	0.26	0.00	18.02	1.00	0.39	0.00
B23	18.04	-3.96	-0.37	-2.02	3.64	-8.01	0.80	-1.31	4.67
B25	16.91	10.50	1.00	1.12	0.00	8.30	1.00	0.86	0.00
B26	20.36	17.67	1.00	0.33	0.00	16.75	1.00	0.48	0.00
B28	22.11	12.89	1.15	0.43	1.04	10.35	1.23	0.73	1.24
B30	17.92	14.90	1.03	0.39	0.43	13.45	1.06	0.52	0.60
B31	16.35	11.29	1.00	0.38	0.00	9.34	1.00	0.88	0.00
B33	19.70	9.95	1.03	1.07	0.18	6.10	1.07	2.45	0.41

Table1.Continued

[CD]			1.0mM				2.0mM	
U (KV)			20				19	
Analyte	μ	α	β	Rs	μ	α	β	Rs
B03	12.66	1.04	0.62	0.78	8.45	1.10	1.70	0.95
B04	18.40	1.00	0.44	0.00	15.05	1.00	0.97	0.00
B08	12.80	1.00	0.61	0.00	10.39	1.00	0.70	0.00
B09	7.21	1.31	1.14	2.20	1.27	2.79	8.16	3.14
B11	5.51	1.41	1.48	2.81	-1.11	0.37	-6.22	3.31
B13	-5.03	0.88	-1.62	1.04		N/A		
B14		N/A			-7.01	0.45	-1.53	4.51
B19	10.63	1.22	0.83	2.19	5.67	1.56	1.37	2.77
B20	19.04	1.00	0.52	0.00	13.12	<1.01	0.49	<0.1
B21	14.98	1.00	0.69	0.00	11.55	1.00	0.59	0.00
B22	16.18	1.00	0.55	0.00	12.49	1.00	0.56	0.00
B23	-9.74	0.97	-1.35	0.37		N/A		
B25	6.08	1.00	1.51	0.00		N/A		
B26	15.90	1.00	0.66	0.00	12.89	1.00	0.65	<0.1
B28	7.96	1.33	1.21	1.75	1.54	2.10	9.17	1.89
B30	12.17	1.11	0.78	1.18	8.23	1.20	1.04	1.42
B31	7.75	1.00	1.23	0.00	2.48	1.00	4.55	0.00
B33	3.37	1.15	3.12	0.95	-3.30	0.79	-3.16	1.45

Table1.Continued

[CD]		2.5mM				3.5mM		
U (KV)		19				15		
Analyte	μ	α	β	Rs	μ	α	β	Rs
B03	6.73	1.14	1.77	1.13	4.31	1.21	3.95	1.30
B04	13.47	1.00	1.05	0.00		N/A		
B08	9.39	1.00	1.35	0.00		N/A		
B09	-1.02	-2.15	-11.78	N/A	-3.94	0.10	-4.31	3.81
B11	-3.49	N/A	-4.04	N/A	-6.57	0.59	-2.59	3.25
B13	-12.77	0.95	-1.06	1.21		N/A		
B14	-9.78	0.55	-1.38	6.71	-13.50	0.72	-1.23	5.09
B19	3.83	1.92	4.14	3.10	1.08	2.81	10.41	5.03
B20	12.00	<1.02	1.27	0.28	9.99	1.03	1.69	0.39
B21	10.28	1.00	1.21	0.00		N/A		
B22	11.31	1.00	1.62	0.00		N/A		
B23		N/A				N/A		
B25	-2.21	1.00	-6.32	0.00		N/A		
B26	11.80	<1.01	1.18	<0.1	9.96	1.02	1.70	0.35
B28	-1.24	-1.33	-10.14	4.08	-4.39	0.32	-3.87	3.50
B30	6.71	1.26	1.87	2.37	4.25	1.55	4.33	2.51
B31		N/A				N/A		
B33	-5.68	0.87	-1.97	1.65	-9.46	0.92	-1.80	1.48

Table 1. Continued

[CD]		5mM				10mM		
U (KV)		15				11		
Analyte	μ	α	β	Rs	μ	α	β	Rs
B03	2.45	1.41	4.43	1.88	-1.20	0.29	-7.05	4.62
B04	9.50	1.02	1.25	0.20	6.04	1.04	1.50	0.45
B08	6.46	1.00	2.02	0.00	3.78	1.00	2.47	0.00
B09	-6.14	0.66	-3.06	3.20		N/A		
B11	-9.07	0.70	-2.08	3.14		N/A		
B13		N/A				N/A		
B14	-15.76	0.80	-1.25	4.00		N/A		
B19	-1.06	-2.71	-16.50	6.16	-3.98	0.46	-10.51	5.10
B20	8.18	1.05	1.70	0.44	4.87	1.10	1.97	0.70
B21	7.70	1.00	2.24	0.00	5.06	1.03	1.86	0.27
B22	8.32	1.00	1.68	0.00	4.50	1.00	1.82	0.00
B23		N/A				N/A		
B25	-8.17	1.00	-2.39	0.00	-12.20	1.00	-1.05	0.00
B26	8.23	1.04	2.26	0.43	5.33	1.11	1.80	0.98
B28	-7.15	0.59	-2.67	3.35		N/A		
B30	2.31	2.06	6.43	2.95	-1.21	-1.25	-8.17	6.77
B31	-4.17	1.00	-4.68	0.00	-6.03	1.00	-2.23	0.00
B33	-12.35	0.94	-1.57	1.43		N/A		

Table 1. Continued

[CD]		15mM				20mM		
U (KV)		11				11		
Analyte	μ	α	β	Rs	μ	α	β	Rs
B03	-4.01	0.79	-3.05	3.51	-5.65	0.85	-2.25	4.38
B30	-3.98	0.41	-3.16	7.83	-5.54	0.55	-2.32	11.22

Table 1. Continued

[CD]	0 mM		0.5mM			0.75mM			
U (KV)	20		20			20			
Analyte	μ	μ	α	β	Rs	μ	α	β	Rs
B34	31.95	23.10	1.00	0.33	0.00	19.02	1.00	0.46	0.00
B37	17.09	5.55	1.37	1.04	1.25	3.07	1.70	2.70	1.48
B38	28.67	13.02	1.00	0.50	0.00	5.80	<1.01	2.31	<0.1
B39	33.85	26.50	1.00	0.25	0.00	23.10	1.00	0.42	0.00
B41	18.05	13.58	1.03	0.42	0.46	11.57	1.06	0.80	0.63
B45	17.09	15.20	1.00	0.41	0.00	14.46	1.00	0.55	0.00
B46	18.49	13.70	1.04	0.78	0.46	11.72	1.08	1.07	1.10
B47	17.56	14.66	1.03	0.39	0.47	13.14	1.07	0.63	1.10
B49	16.72	11.65	1.06	0.36	0.94	9.30	1.11	0.84	1.12
B51	19.10	13.49	1.00	0.32	0.00	11.05	1.00	0.70	0.00
B54	13.45	-1.81	-0.87	-2.65	5.72	-6.02	0.51	-1.35	6.20
B56	31.82	-32.90	1.00	-0.18	0.00	-32.38	1.00	-0.24	0.00
B58	22.21	17.35	1.03	0.24	0.30	14.91	1.09	0.58	0.91
B60	21.70	18.01	1.00	0.57	0.00	16.09	1.03	1.06	0.32
B75	16.61	13.05	1.01	0.31	0.18	11.43	1.03	0.74	0.30

Table 1. Continued

[CD]			1.0mM				2.0mM	
U (KV)			20				19	
Analyte	μ	α	β	Rs	μ	α	β	Rs
B34	16.52	1.02	0.59	0.25	11.96	1.06	0.76	0.45
B37		N/A			-6.73	0.70	-1.72	2.40
B38		N/A			-7.18	0.91	-1.66	0.80
B39	20.63	1.00	0.51	0.00	17.21	<1.01	0.51	<0.1
B41	10.02	1.08	1.03	0.73	4.38	1.13	1.74	0.85
B45	13.80	1.00	0.73	0.00	11.58	1.00	0.78	0.00
B46	10.31	1.12	1.01	1.28	6.28	1.25	1.84	1.68
B47	12.13	1.09	0.87	1.11	8.51	1.16	1.14	1.45
B49	7.65	1.15	1.40	1.22	2.42	1.45	5.14	1.81
B51	8.80	1.00	1.21	0.00	1.14	1.00	11.87	0.00
B54	-6.83	0.99	-1.56	<0.05		N/A		
B56	-32.04	1.00	-0.33	0.00		N/A		
B58	12.64	1.13	0.86	1.06	7.02	1.23	1.48	1.42
B60	14.70	1.05	0.71	0.55	10.93	1.08	1.05	1.03
B75	9.91	1.05	1.08	0.57	5.84	1.10	1.86	1.09

Table 1. Continued

[CD]		2.5mM				3.5mM		
U (KV)		19				15		
Analyte	μ	α	β	Rs	μ	α	β	Rs
B34	10.45	1.08	1.63	0.78		N/A		
B37	-9.40	0.76	-1.91	2.64	-11.91	0.83	-1.51	2.81
B38	-10.04	0.94	-1.79	0.87	-12.52	0.96	-1.35	0.81
B39	16.04	1.01	1.17	0.32		N/A		
B41	2.39	1.18	8.05	1.14		N/A		
B45	10.76	1.00	1.21	0.00		N/A		
B46	4.64	1.36	2.14	1.71	1.77	2.02	10.37	2.45
B47	7.27	1.22	1.78	1.47		N/A		
B49		N/A			-1.40	0.08	-10.04	3.09
B51		N/A				N/A		
B54		N/A				N/A		
B56	-31.10	1.00	-0.49	0.00		N/A		
B58	4.80	1.30	2.54	1.46	1.33	2.33	12.73	1.72
B60	9.48	1.10	1.13	1.11		N/A		
B75	4.20	1.14	2.89	1.13	1.38	1.61	13.35	1.33

Table 1. Continued

[CD]		5mM				10mM		
U (KV)		15				11		
Analyte	μ	α	β	Rs	μ	α	β	Rs
B34	6.33	1.22	2.40	1.40	2.46	1.66	3.33	2.66
B37	-13.93	0.86	-1.41	3.01		N/A		
B38		N/A				N/A		
B39	12.68	1.04	1.23	1.16	8.20	1.09	1.84	1.19
B41	-1.88	0.46	-9.39	N/A	-4.63	0.80	-1.76	6.69
B45	8.11	1.00	1.96	0.00	5.94	1.02	1.72	0.32
B46		N/A			-1.75	0.61	-2.50	5.16
B47	3.41	1.54	4.75	2.98		N/A		
B49	-3.76	0.65	-4.98	3.21		N/A		
B51	-5.41	1.00	-3.58	0.00	-9.02	1.00	-2.01	0.00
B54		N/A				N/A		
B56		N/A				N/A		
B58		N/A			-2.74	0.33	-3.23	6.81
B60	4.86	1.26	3.39	1.42		N/A		
B75		N/A			-2.89	0.73	-2.93	5.44

In reference to Maynard's classification of SISCD-mediated separations of weakly basic enantiomers,[70] four categories of compounds were identified: weakly binding, moderately strongly binding, strongly binding and very strongly binding. Categorization of the separations in this way provides some insight into the separation selectivity patterns observed. It also allows qualitative comparison of the utility of HAMS to various SISCDs for a given enantiomer separation.

For weakly binding analytes, the effective mobilities do not become anionic over the HAMS concentration ranged studied. Figure 47 shows the effective mobilities (top panels) and separation selectivities (bottom panels) as a function of the HAMS concentration for two weakly binding analytes, terbutaline, B47 and ephedrine, B60. In each case, the initial cationic effective mobility of the weak base is 17.5 mobility units (B47) and 21.7 mobility units (B60), respectively. As the HAMS concentration is increased, their effective mobilities begin to decrease toward zero, but do not become anionic. This is due to an increase in the mole fraction of the HAMS-analyte complex and to ionic strength-related depression of the effective mobilities of both the free and the complexed forms of the weak base. The separation selectivity values increase without approaching a limiting value over the HAMS concentration range tested.

The effective mobilities of moderately strongly binding base analytes are, like the weakly binding bases, initially cationic but become anionic at some intermediate HAMS concentration. The panels of Figure 48 show the effective mobilities (top panels) and the separation selectivities (bottom panels) for two moderately strongly binding weak base analytes, aminoglutethimide, B03, and metaproterenol, B30. In both cases,

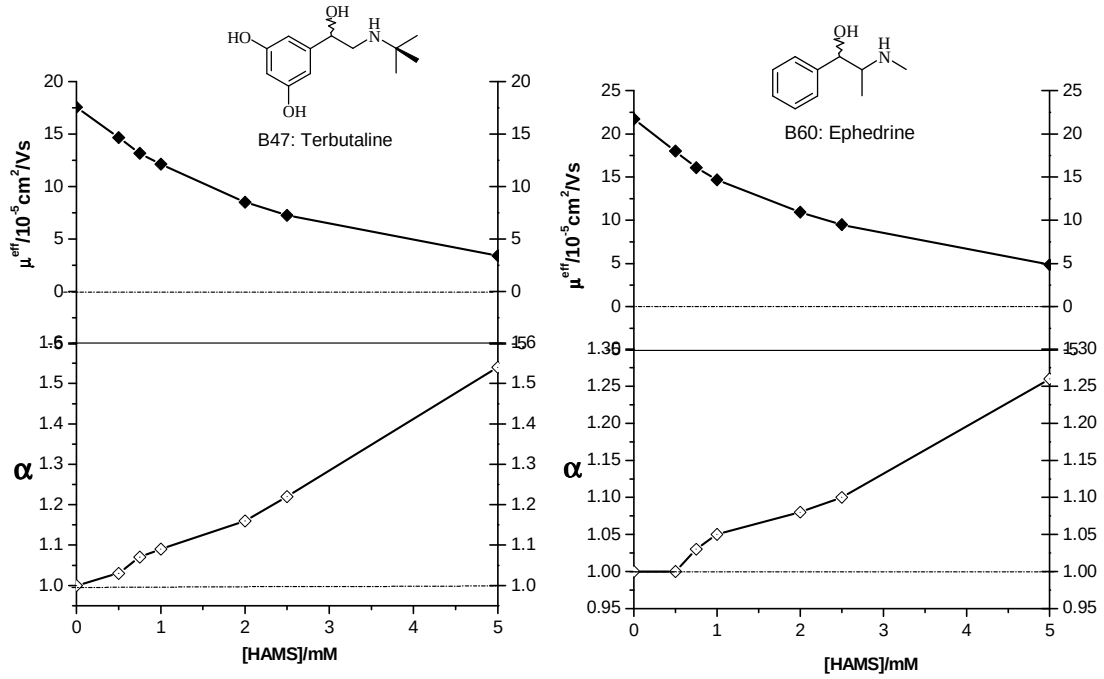

Figure 47. Effective mobilities (top panels) and separation selectivities (bottom panels) of weakly binding weak base analytes as a function of HAMS concentration

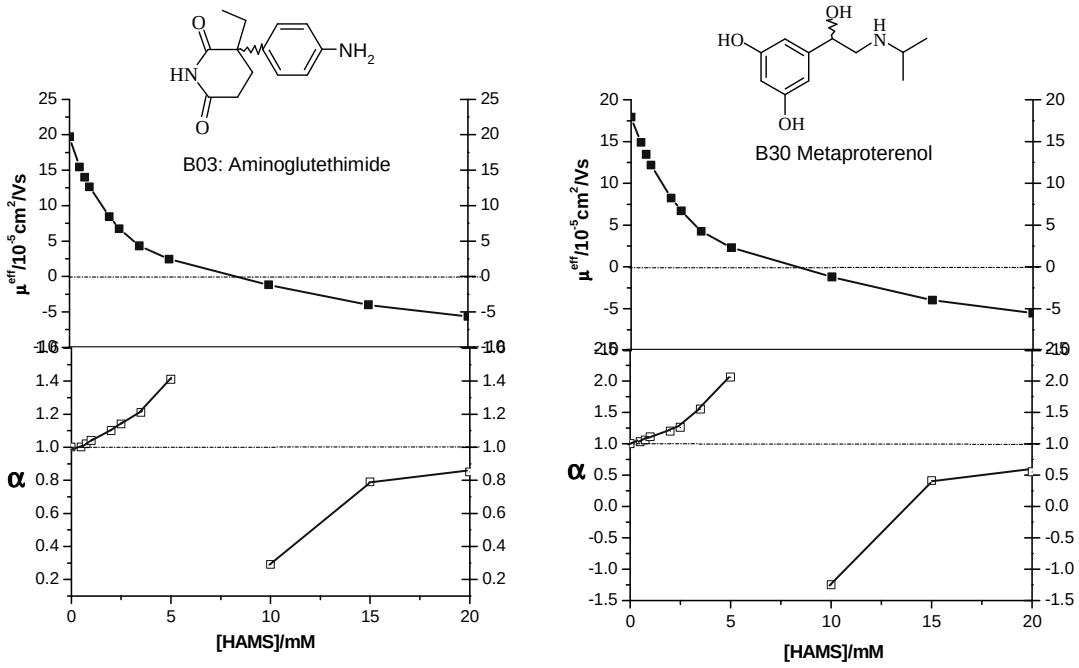

Figure 48. Effective mobilities (top panels) and separation selectivities (bottom panels) of moderately strongly binding weak base analytes as a function of HAMS concentration

the effective mobilities are cationic at zero and low HAMS concentrations but become anionic at an intermediate HAMS concentration ([HAMS]>7.5mM). At HAMS concentrations where the effective mobilities of both enantiomers are cationic, separation selectivity values are positive and approach infinitely high values as the effective mobility of the faster enantiomer approaches zero. As the HAMS concentration increases towards an intermediate value, the separation selectivity values become negative as the effective mobility of one of the enantiomers becomes anionic and that of the other enantiomer remains cationic. At higher HAMS concentrations, the separation selectivity values become positive again and approach unity as the effective mobilities of both enantiomers remain anionic. Separation selectivities become more favorable as the HAMS concentration approaches the point where the effective mobility of one of the enantiomers changes from cationic to anionic, as predicted by CHARM model.[47]

Strongly binding analytes include those whose effective mobilities have become anionic at low HAMS concentrations. Figure 49 shows the effective mobility curves (top panels) and the separation selectivity curves (bottom panels) for two strongly binding analytes, (1-napthyl)ethylamine, B33 and oxprenolol, B37. Their effective mobilities become anionic at HAMS concentrations as low as 1.5 mM and remain anionic over the entire concentration range used. Although the separation selectivities follow the trend observed for moderately strongly binding analytes, they approach a limiting value of $\alpha < 1$ at much lower HAMS concentrations.

For this discussion, we consider a weak base to be a very strongly binding analyte when the effective mobilities of the enantiomers become anionic at a very low

HAMS concentration. 4-Chloroamphetamine, B13, and ketotifen, B23, shown in Figure 50 are examples of weak base analytes that bind very strongly to HAMS. Their effective mobilities (top panels) are anionic at HAMS concentrations lower than 0.6 mM. The separation selectivities (bottom panels) follow the classical trends depicted by moderately strongly binding and strongly binding weak base analytes. However, their separation selectivities approach unity at very low HAMS concentrations (≤ 2.5 mM) compared with strongly binding analytes (≤ 5.0 mM) and moderately strongly binding analytes (≤ 20.0 mM).

The effective mobility and separation selectivity trends so far observed for the weak base enantiomers follow the predictions of the CHARM model.[47]

Typical electropherograms for the enantiomers of the weak base analytes, obtained with HAMS in pH 2.5 BGEs are shown in Figure 51. Each electropherogram includes the analyte identifier (see Figure 46), the actual applied potential in kV (between the point of injection and the detector) and the HAMS concentration (in mM) used for the separation. Baseline resolution was achieved for most of the analytes using low concentrations of HAMS. Run time for most of the weak bases was reasonably short, except for pindolol, B41 with a time of 23 min.

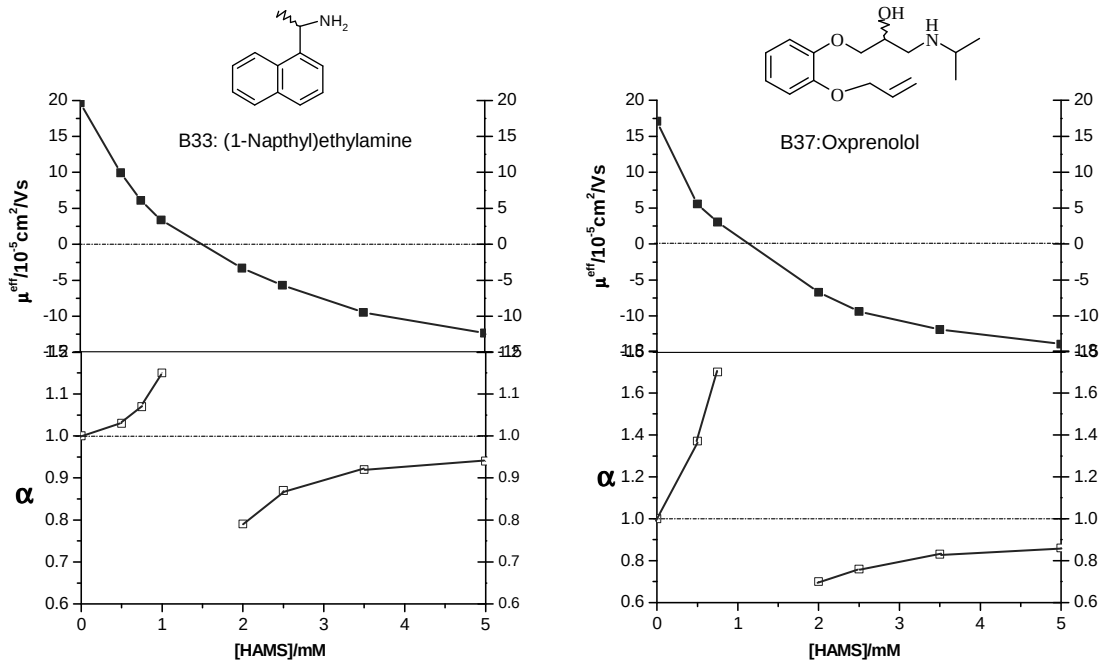

Figure 49. Effective mobilities (top panels) and separation selectivities (bottom panels) of strongly binding weak base analytes as a function of HAMS concentration

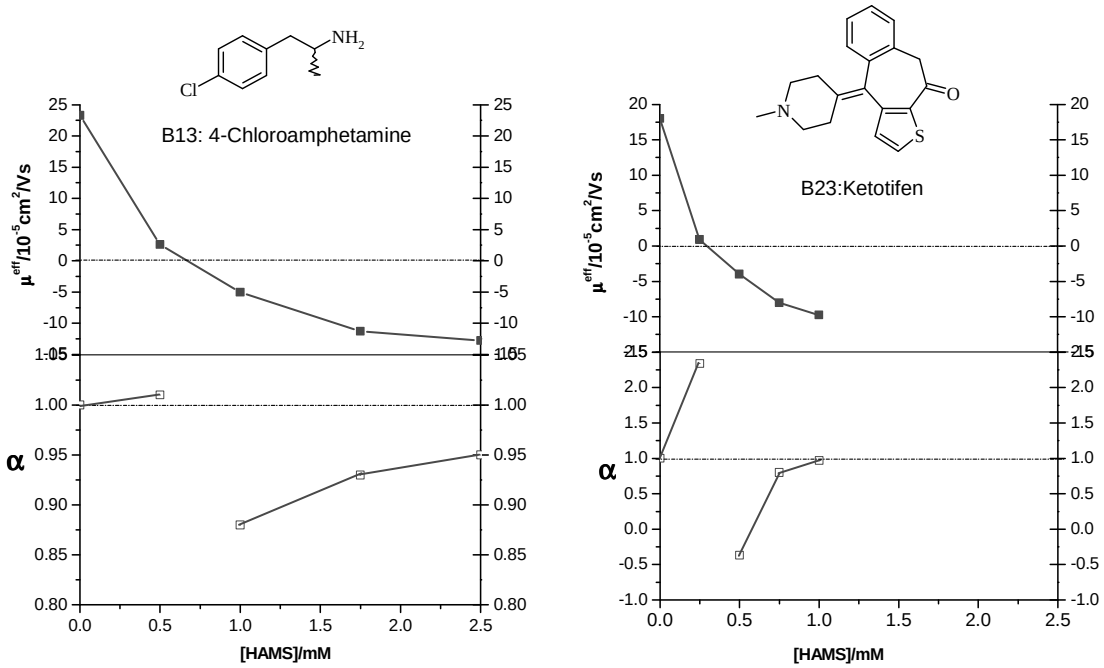

Figure 50. Effective mobilities (top panels) and separation selectivities (bottom panels) of very strongly binding weak base analytes as a function of HAMS concentration

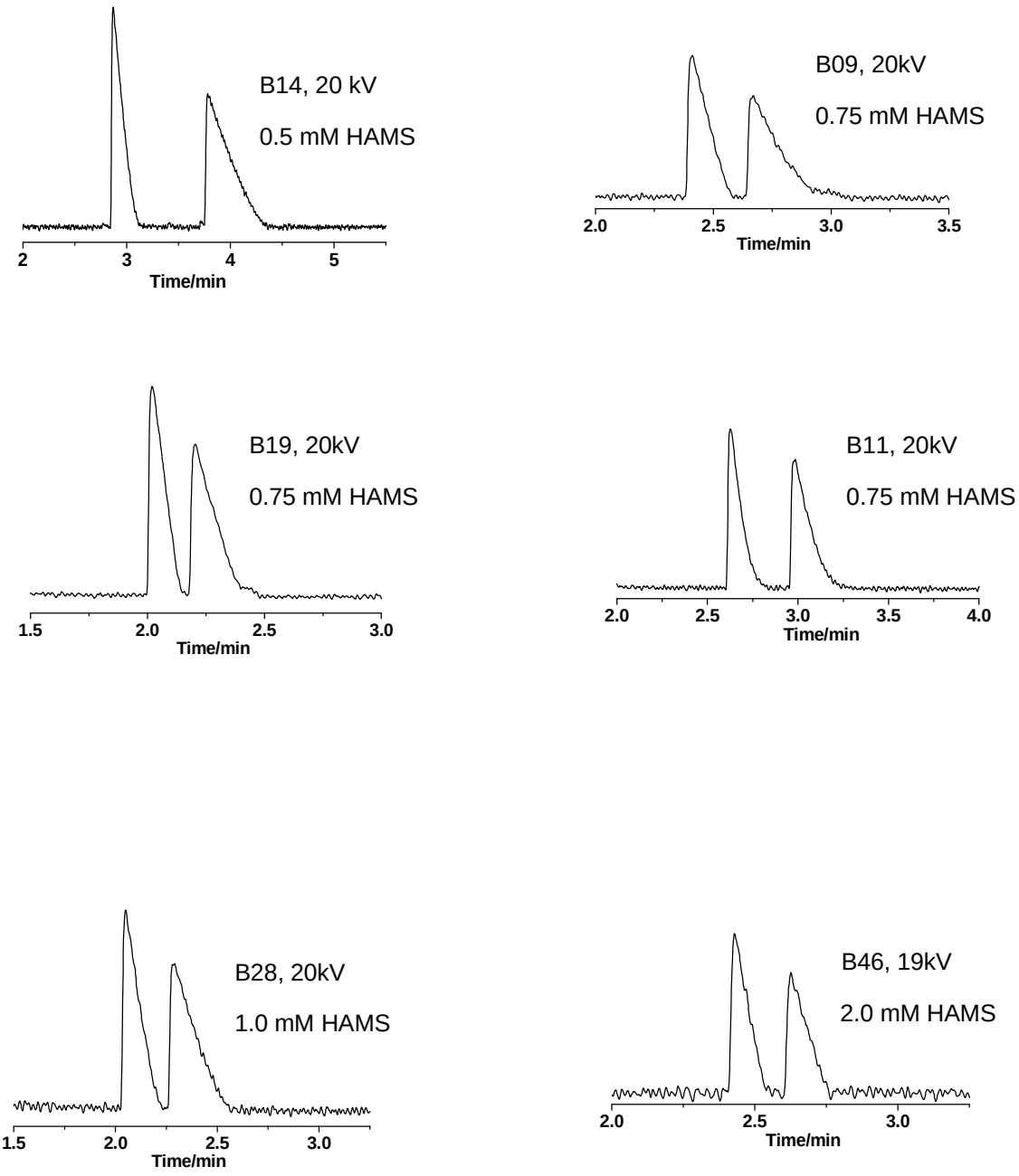

Figure 51. Typical electropherograms of weak base analytes in pH 2.5 BGE with HAMS

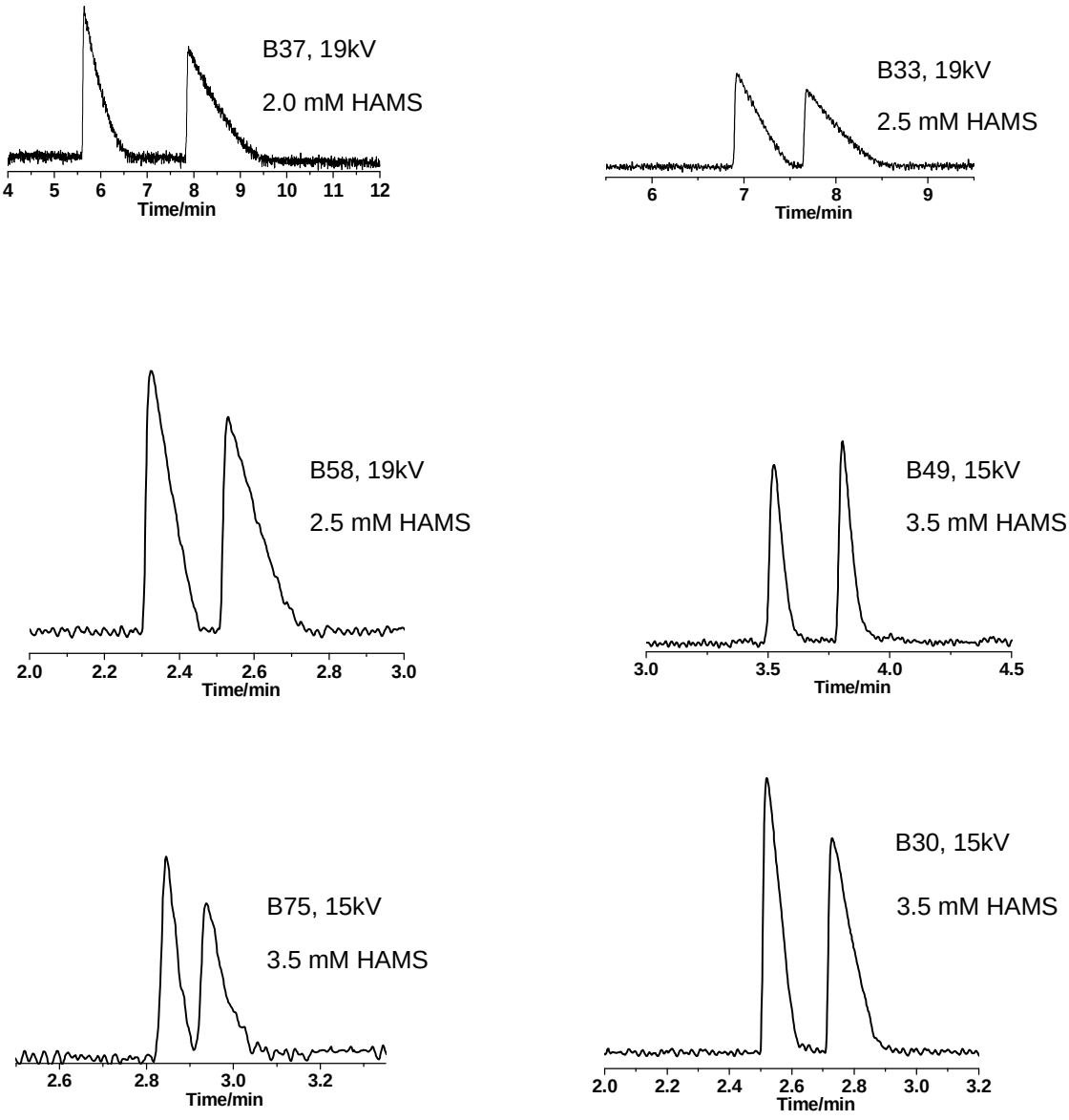

Figure 51. Continued

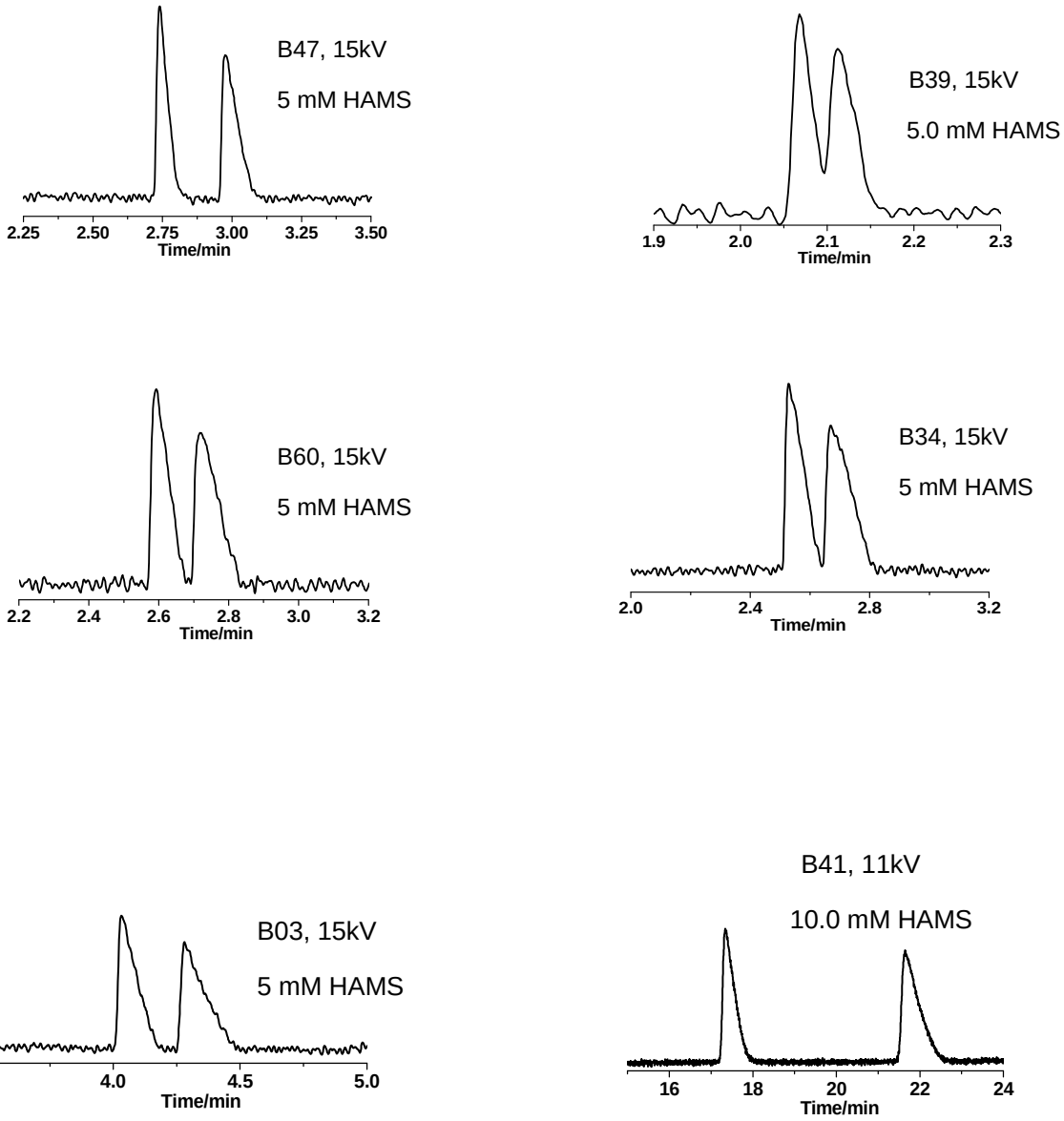

Figure 51. Continued

3.3.2 Effects of Weak Base Structure on Separation Selectivity

The binding strength of an enantiomer is highly dependent on its structure and the structure of the chiral resolving agent. Small changes in the analytes structure can lead to significant changes in the separations. Figure 52 shows the effective mobility (top panel) and separation selectivity (bottom panel) curves for four structurally related weak bases including B26, B30, B47 and B60. Effective mobilities vary from 8.2 mobility units for B26 to 2.3 mobility units for B30 at 5 mM HAMS. In order of increasing binding strength, they are B30 ≈ B47 > B60 >B26. It is observed that the size and the type of substituents about the aromatic ring have some influence on the binding strength. The ortho- and meta-catecholamine enantiomers show strong intermolecular interaction with HAMS. The weakest binder is metanephrine, B26, with one methyl and one OH group on the aromatic ring. The trend observed for the separation selectivities is a mirror image of the trend shown by their effective mobilities. Metaproterenol, B30 the strongest binding analyte among them exhibits the best separation selectivity while separation selectivity is very low for metanephrine, B26, over the concentration range tested. These observations, while valid, provide little insight into the enantiorecognition mechanism. NMR experiments need to be performed to get mechanistic information.

Another group of compounds which are structurally related: atropine, B09 and homatropine, B19 (shown in Figure 53) differ from each other by a methylene group. However, these two compounds show significant difference in their binding strengths with HAMS.

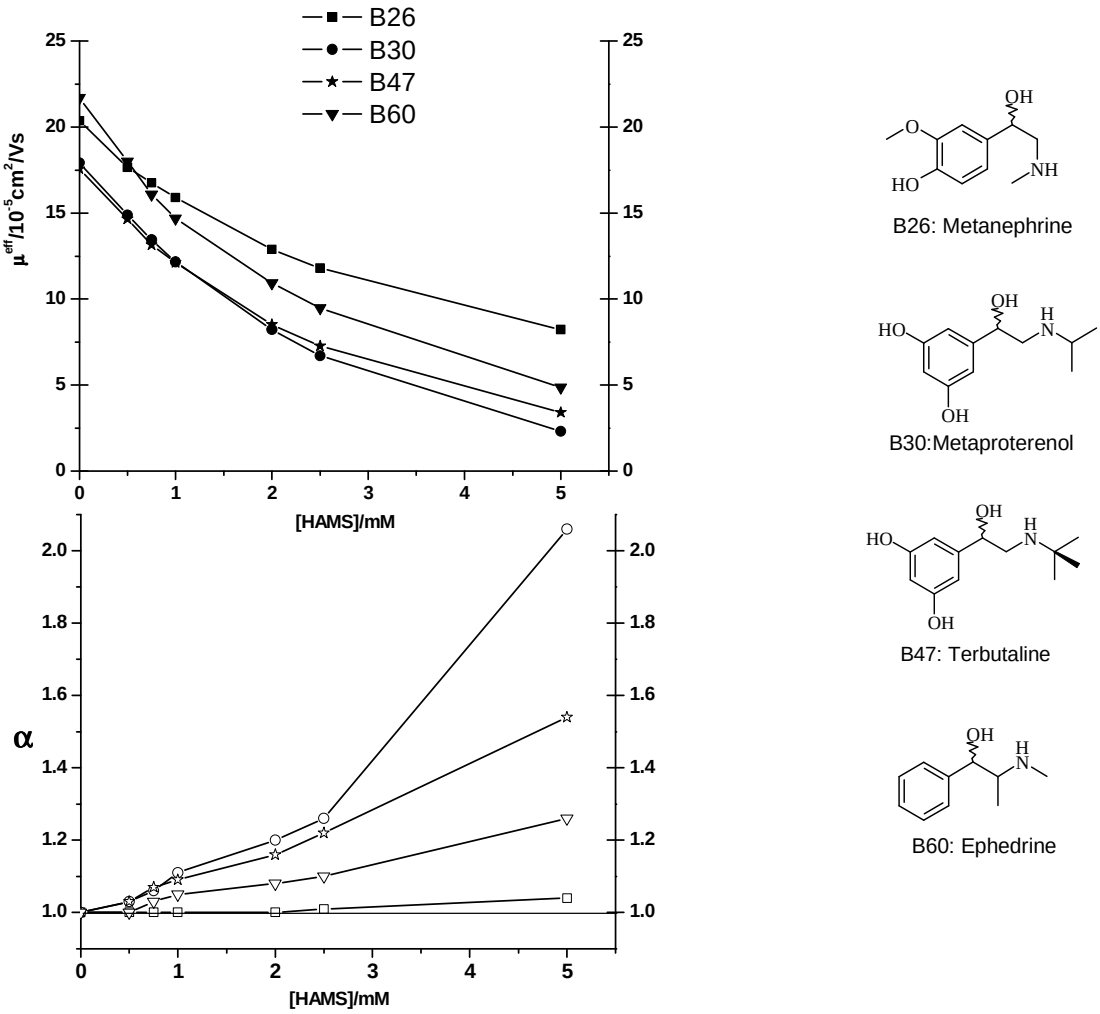

Figure 52. Effects of analyte structure on effective mobilities (top panel) and separation selectivities (bottom panel) for weak bases B26, B30, B47 and B60 obtained in pH 2.5 BGE using HAMS

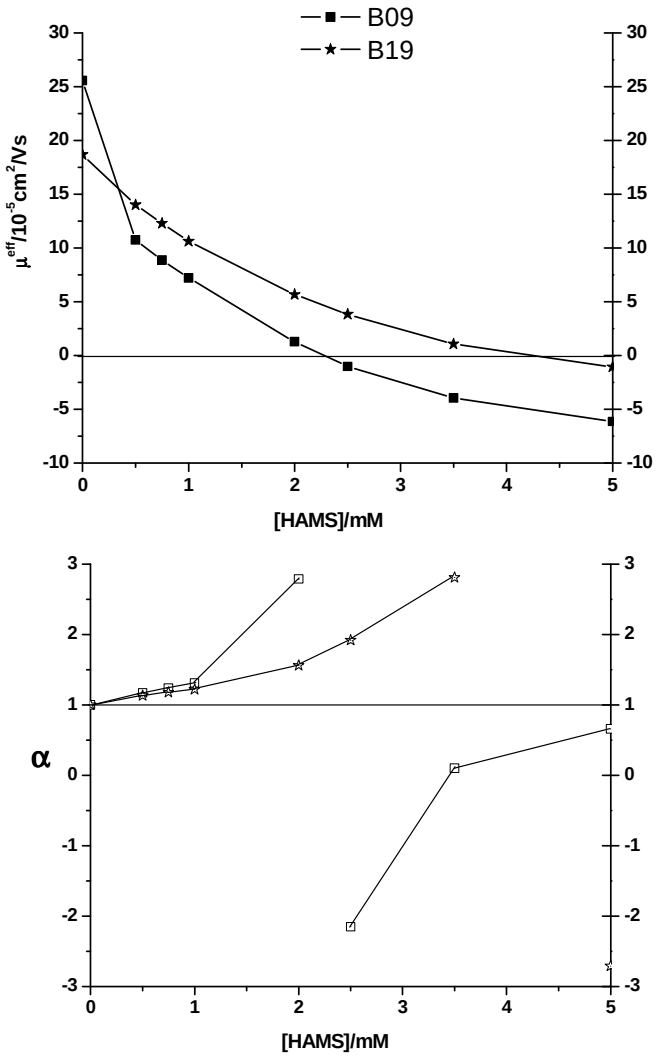

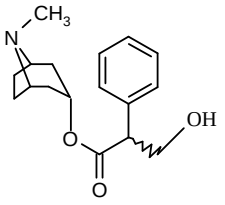

B09: Atropine

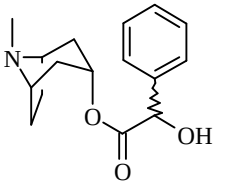

B19: Homatropine

Figure 53. Effects of analyte structure on effective mobilities (top panel) and separation selectivities (bottom panel) for weak bases B09 and B19 obtained in pH 2.5 BGE using HAMS

3.4 Effects of the Attachment Position of the Sulfate Group on Enantiorecognition

SISCDs as chiral resolving agents in CE enantioseparations can carry the sulfate group either at C2, C3 or C6 positions of the glucopyranose subunits. In order to investigate the influence of the position of the sulfate group on enantiorecognition, the sodium salt of heptakis(2-*O*-methyl-3-*O*-acetyl-6-*O*-sulfo)cyclomaltoheptaose[80] (HMAS) which carries the sulfate group at the C6 position, and heptakis(2-*O*-methyl-3,6-di-*O*-sulfo)cyclomaltoheptaose[81] (HMdiSu) which carries the sulfate group at both the C3 and C6 positions are compared to HAMS for the separation of the enantiomers of weak bases. These SISCDs, including HAMS, carry non-identical substituents at the C2 and C3 positions. The changes in the binding strength for homatropine, B19, chlophedianol, B14, and metoprolol, B31 are represented in the effective mobility (top panel) and separation selectivity (bottom panel) curves shown in Figures 54, 55 and 56, respectively. The binding strength for B19 (homatropine) follows the order HMdiSu > HAMS > HMAS while for B14 (chlophedianol), the order is HAMS > HMdiSu > HMAS. HAMS offers the best separation selectivity (Figures 54 and 55, bottom panel) for B19 and B14 at low SISCD concentration where the effective mobilities of the enantiomers remain cationic. No separation was observed for the enantiomers of B19 using HMAS. Interestingly, HAMS does not offer any separation selectivity for the enantiomers of B31 over the concentration range studied compared to HMdiSu which offered excellent separation selectivity. It is worth noting that although changes in the position of the sulfate group on the glucopyranose subunits influence separation selectivity, the presence of other substituents including acetyl and methyl groups also

play a significant role in the chiral recognition mechanism. X-ray crystallographic and NMR spectroscopic measurements are needed for better understanding of the enantiorecognition process.

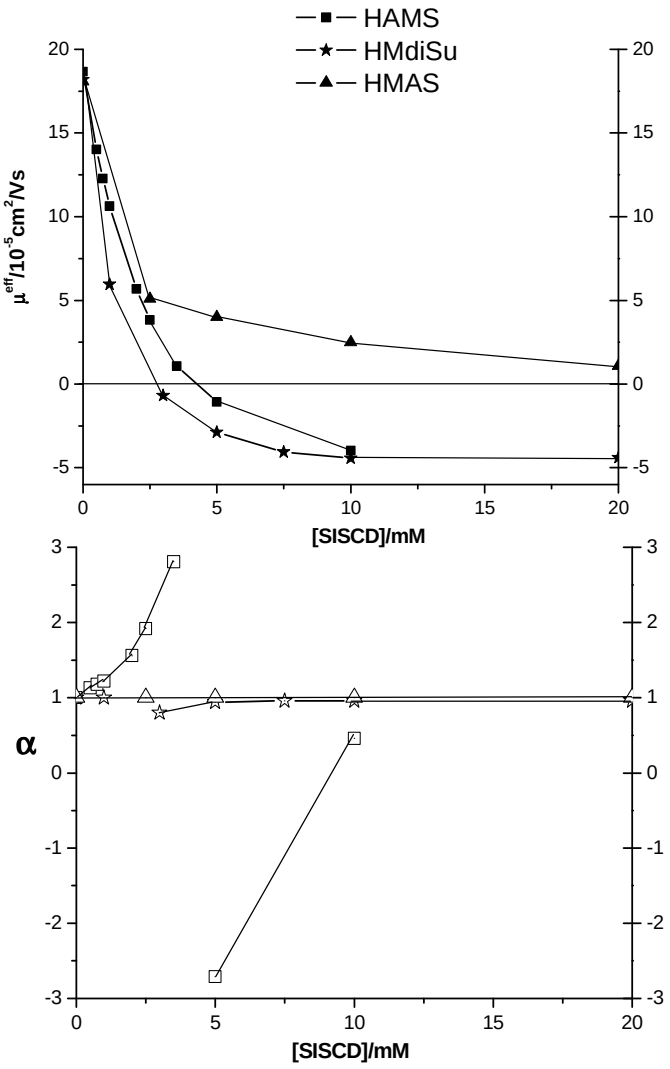

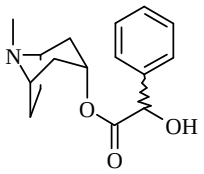

B19: Homatropine

Figure 54. Effective mobilities (top panel) and separation selectivites (bottom panel) for the enantiomers of B19 in pH 2.5 aqueous BGEs with HAMS, HMdiSu and HMAS

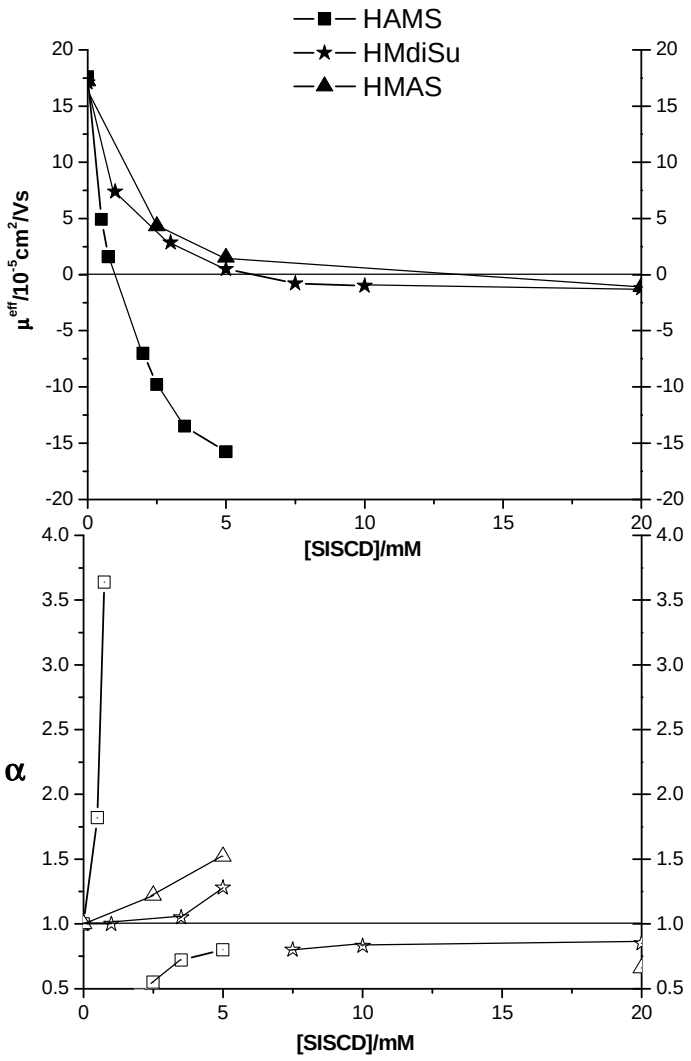

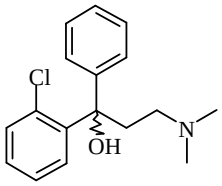

B14: Chlophedianol

Figure 55. Effective mobilities (top panel) and separation selectivites (bottom panel) for the enantiomers of B14 in pH 2.5 aqueous BGEs with HAMS, HMdiSu and HMAS

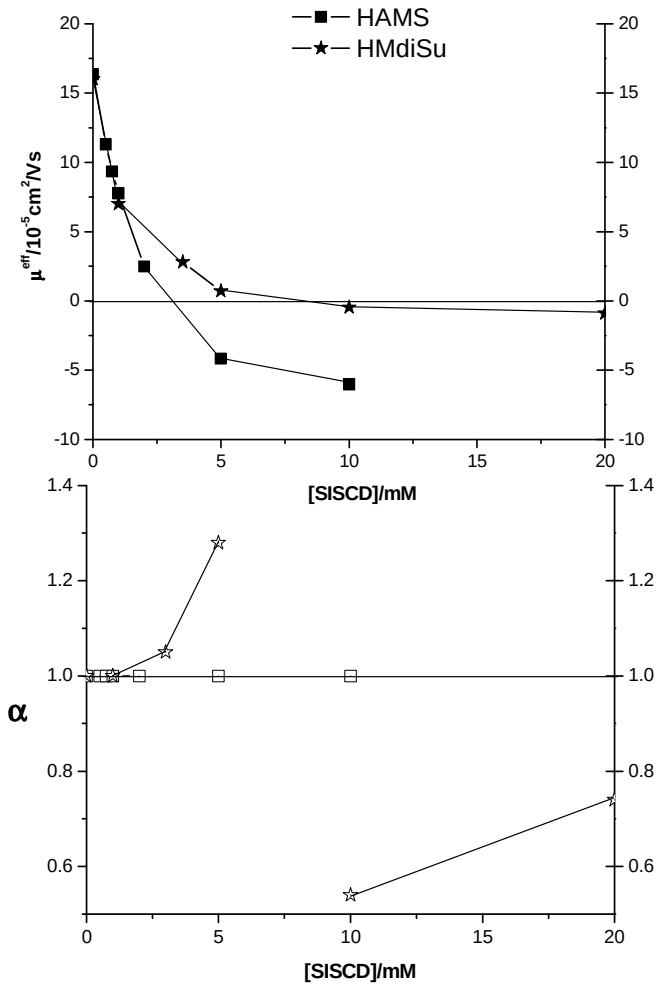

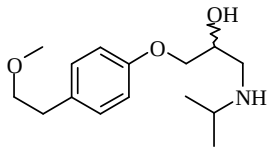

B31: Metoprolol

Figure 56. Effective mobilities (top panel) and separation selectivites (bottom panel) for the enantiomers of B31 in pH 2.5 aqueous BGEs with HAMS, HMdiSu

3.5 Separations of the Enantiomers of Nonionic Analytes Using HAMS in Low pH BGEs

According to Williams[47], peak resolution values for the enantiomers of nonionic analytes are similar at all pH values when SISCDs are used as resolving agents. Therefore, it is reasonable to evaluate the utility of HAMS using nonionic analytes at low pH. The structures of the fourteen, structurally diverse, nonionic analytes tested are shown in Figure 57. Table 2 shows the effective mobilities of the less mobile enantiomer, μ, the separation selectivities, α, the calculated peak resolution, Rs, the corresponding dimensionless, normalized EOF mobility values, β, and the injector-to-detector potential drop values, U, obtained in the low pH aqueous BGEs for the nonionic enantiomers. An entry of N/A indicates that a value could not be calculated due to overlap with either a non-comigrating system peak or overlap with the neutral marker peak.

Enantiomer separations were observed for all of the fourteen nonionic analytes tested. All the nonionic analytes were baseline resolved (i.e., Rs > 1.5), except 2-phenylbutanol, N02. This group of analytes could be assigned to three distinctive categories: weakly binding, moderately strongly binding and strongly binding.

For weakly binding analytes, the effective anionic mobilities (Figure 58, top panel) increased as the concentration of HAMS was increased, but remained low, only reaching -3.5×10^{-5} cm^2/Vs. Increased effective anionic mobility indicates that complexation of the nonionic analytes with HAMS overrides the mobility-reducing effects of both higher ionic strength and higher viscosity. The corresponding separation

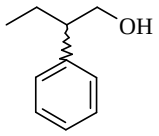

N02: 2-Phenylbutanol

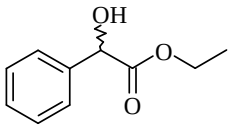

N10: Ethylmandelate

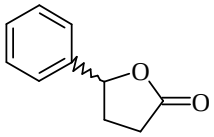

N13: γ-(Phenyl)-γ-butyrolactone

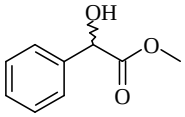

N15: Methylmandelate

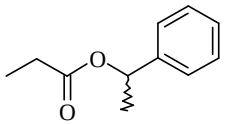

N20: 1-Phenylethylpropionate

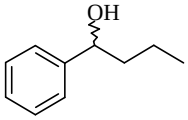

N21: 1-Phenybutanol

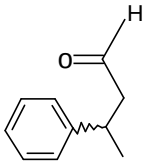

N22: 3-Phenylbutyraldehyde

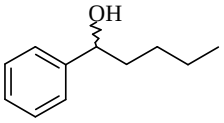

N25: 1-Phenylpentanol

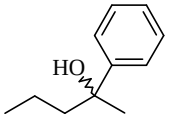

N26: 2-Phenyl-2-pentanol

Figure 57. Names and structures of nonionic analytes

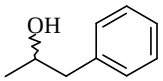

N27: 1-Phenyl-2-propanol

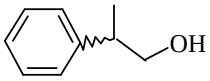

N28: 2-Phenyl-1-propanol

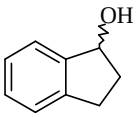

N36:1-Indanol

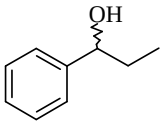

N34: 1-Phenylpropanol

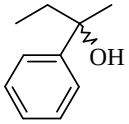

N38: 2-Phenyl-2-butanol

Figure 57. Continued

selectivities increased to a maximum and then slowly decreased as the concentration of HAMS was increased (Figure 58, bottom panel), in agreement with the prediction of the CHARM model.[47]

In the case of moderately strongly binding nonionic analytes, their effective anionic mobilities (Figure 59, top panel) increased with increasing HAMS concentration approaching -10×10^{-5} cm^2/Vs. The separation selectivities (Figure 59, bottom panel) for this class of nonionic analytes followed the trend depicted by the weakly binding analytes.

Effective anionic mobilities, (Figure 60, top panel) for the strongly binding analytes, increased beyond -10×10^{-5} cm^2/Vs with increasing HAMS concentration. The separation selectivity (Figure 60, bottom panel) patterns resembled those of the moderately strongly binding and weakly binding analytes.

A small change in the structure of the nonionic analytes not only affected whether or not a separation was obtained, but it also affected the separation behavior. For example, 2-phenylbutanol, N02, 1-phenylbutanol, N21, and 2-phenyl-2-butanol, N38 all have the same number of carbon atoms, however, the environments around their chiral carbon atoms differ from one to the other. This subtle structural difference still leads to significant complexation differences as shown in Figure 61. The order of binding strength is N38 > N02 ≈ N21. Interestingly, 1-phenylbutanol, N21 with the lowest binding strength exhibits the best separation selectivity (Figure 61, bottom panel). In addition to the example describe above, it is also observed that increasing the carbon number in the long hydrophobic chain without changing the chiral center can affect the

enantiorecogntion processes. Two sets of nonionic analytes which form homologous series are depicted in Figures 62 and 63. The first set includes 1-phenylpropanol, N34, 1-phenylbutanol, N21, and 1-phenylpentanol, N25 (Figure 62). Ethylmandelate, N10, and methylmandelate, N15 (Figure 63) constitute the second set. Their effective anionic mobilities (top panels) are shown in their respective figures. The order of increasing binding strength for the aromatic alcohols is N25 > N21 ≈ N38 and N10 ≈ N15 for the mandelates. The separation selectivity (Figures 62 and 63, bottom panels) trends indicate that the hydrophobic chain significantly influences the enantiorecogntion process. Again, detailed NMR spectroscopic studies are needed to provide insight into the chiral recognition mechanism.

Typical electropherograms for the nonionic analytes obtained by using HAMS as chiral resolving agent are shown in Figure 64. Each electropherogram includes the analyte identifier (see Figure 57), the actual applied potential in kV (between the point of injection and the detector) and the HAMS concentration (in mM) used for the separation.

Table 2. Separation data for the nonionic analytes in pH 2.5 aqueous HAMS BGE. (μ in 10^{-5} cm^2/Vs units)

[CD]	0 mM		0.5mM			0.75mM			
U (KV)			20.0			20.0			
Analyte	μ	μ	α	β	Rs	μ	α	β	Rs
N02	0.00	-1.61	1.00	-12.07	0.00	-2.18	1.00	-8.53	0.00
N10	0.00	-0.45	1.06	-43.06	0.64	-0.65	1.17	-26.49	1.32
N13	0.00	-1.32	1.00	-15.01	0.00	-1.70	1.00	-10.73	0.00
N15	0.00	-0.55	1.00	-33.42	0.00	-0.72	1.04	-24.14	0.60
N20	0.00	-4.01	1.04	-4.49	0.80	-4.90	1.08	-3.47	0.87
N21	0.00	-1.43	1.09	-13.84	0.77	-2.01	1.18	-8.87	1.31
N22	0.00	-1.95	<1.01	-10.16	<0.1	-2.67	1.05	-6.83	0.34
N25	0.00	-2.78	1.09	-7.15	0.97	-3.55	1.20	-5.15	1.56
N26	0.00	-2.92	1.04	-6.79	0.55	-4.02	1.09	-4.53	1.14
N27	0.00	-1.13	1.00	-15.10	0.00	-1.48	1.07	-13.48	0.53
N28	0.00	-1.30	1.00	-15.20	0.00	-1.76	1.00	-10.58	0.00
N34	0.00	-1.32	1.00	-14.94	0.00	-1.81	1.00	-10.27	0.00
N36	0.00	-0.85	1.00	-22.97	0.00	-1.09	1.04	-16.64	0.60
N38	0.00	-2.12	1.06	-10.10	0.65	-3.13	1.10	-5.65	1.40

Table 2. Continued

[CD]	1.5mM				2.5mM			
U (KV)	20				19			
Analyte	μ	α	β	Rs	μ	α	β	Rs
N02	-3.35	1.04	-6.15	0.36	-4.71	1.08	-3.16	0.63
N10	-1.02	1.40	-17.28	2.22	-1.45	1.46	-9.71	3.57
N13	-2.69	1.08	-7.63	0.44	-3.82	1.10	-3.92	1.40
N15	-1.16	1.16	-21.02	1.16	-1.41	1.25	-11.54	2.52
N20	-6.50	1.21	-3.22	2.32	-7.80	1.26	-2.24	6.45
N21	-3.10	1.29	-6.04	2.03	-4.27	1.34	-2.13	4.22
N22	-4.39	1.10	-4.15	0.87	-6.31	1.14	-1.86	2.26
N25	-4.86	1.29	-3.84	3.22	-6.42	1.31	-2.58	3.98
N26	-6.29	1.19	-2.75	1.85	-9.08	1.19	-2.03	1.97
N27	-2.50	1.16	-7.41	1.35	-3.69	1.18	-4.02	1.80
N28	-2.75	1.04	-7.16	0.45	-3.98	1.08	-3.81	0.73
N34	-2.88	1.08	-6.97	0.45	-4.11	1.11	-3.55	1.33
N36	-1.59	1.18	-12.09	1.44	-2.22	1.30	-4.71	3.71
N38	-5.31	1.20	-3.37	1.49	-7.74	1.19	-2.21	1.63

Table 2. Continued

[CD]			3.5mM				5.0mM	
U (KV)			15				15	
Analyte	μ	α	β	Rs	μ	α	β	Rs
N02	-5.92	1.10	-2.31	1.38	-7.16	1.08	-2.01	0.91
N10	-1.84	1.51	-7.99	5.47	-2.31	1.49	-6.58	5.22
N13	-4.88	1.11	-3.05	1.50	-6.21	1.10	-2.60	1.49
N15	-1.73	1.27	-9.66	2.96	-2.02	1.29	-8.05	3.47
N20	-8.70	1.24	-1.82	8.25	-9.67	1.21	-1.49	9.76
N21	-5.45	1.32	-2.07	4.10	-6.97	1.29	-1.65	4.61
N22	-8.02	1.13	-1.91	2.03	-10.17	1.11	-1.74	2.03
N25	-7.78	1.31	-1.73	6.71	-9.54	1.25	-1.57	7.35
N26	-11.44	1.16	-1.59	2.59	-13.81	1.12	-1.31	4.51
N27	-4.79	1.17	-3.13	1.86	-6.17	1.16	-2.37	2.55
N28	-5.11	1.10	-2.91	1.62	-6.57	1.09	-2.44	1.31
N34	-5.28	1.11	-2.80	1.83	-6.76	1.10	-1.97	2.05
N36	-2.78	1.30	-4.19	3.29	-3.38	1.29	-2.48	6.49
N38	-9.87	1.16	-1.81	2.36	-12.11	1.12	-1.31	3.57

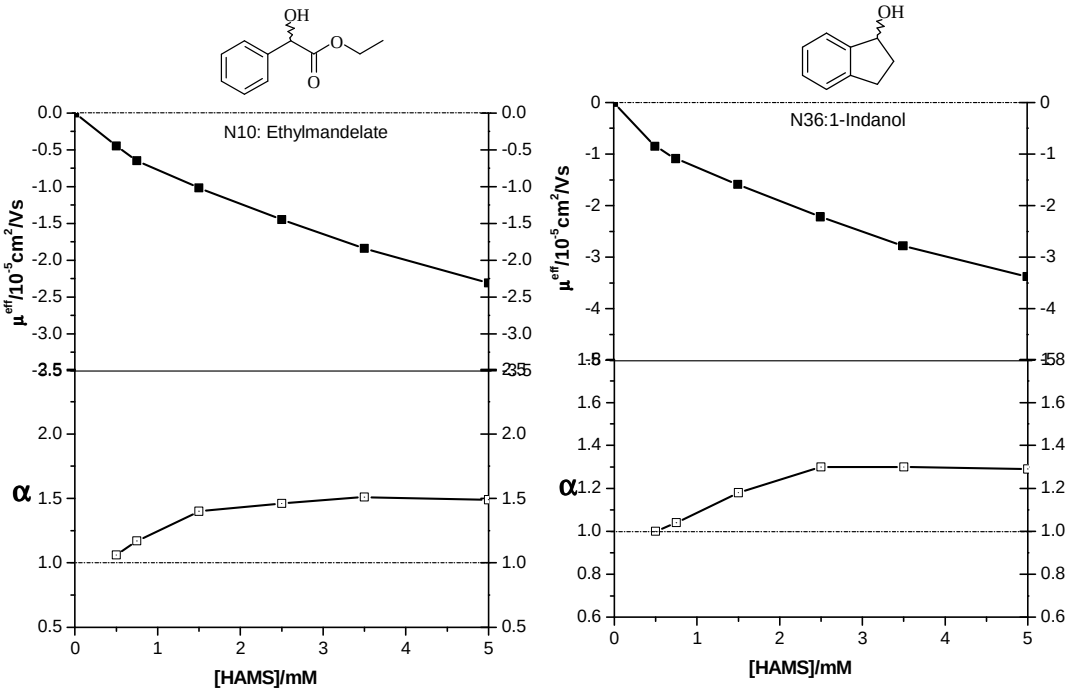

Figure 58. Effective mobilities (top panels) and separation selectivities (bottom panels) of weakly binding nonionic analytes as a function of the HAMS concentration

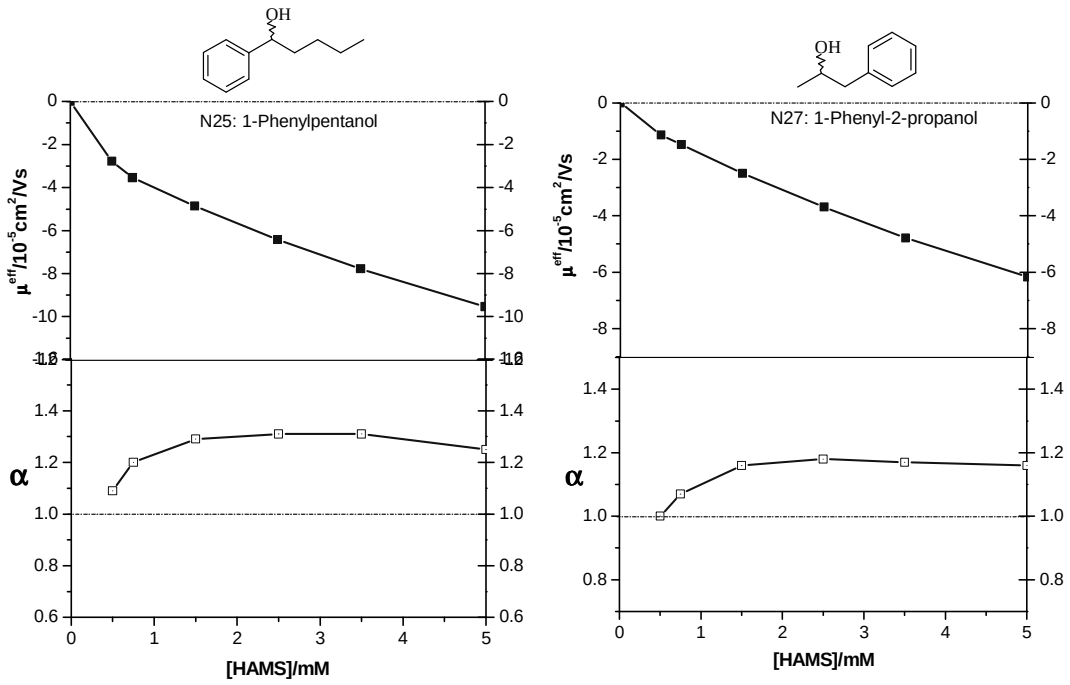

Figure 59. Effective mobilities (top panels) and separation selectivities (bottom panels) of moderately strongly binding nonionic analytes as a function of HAMS concentration

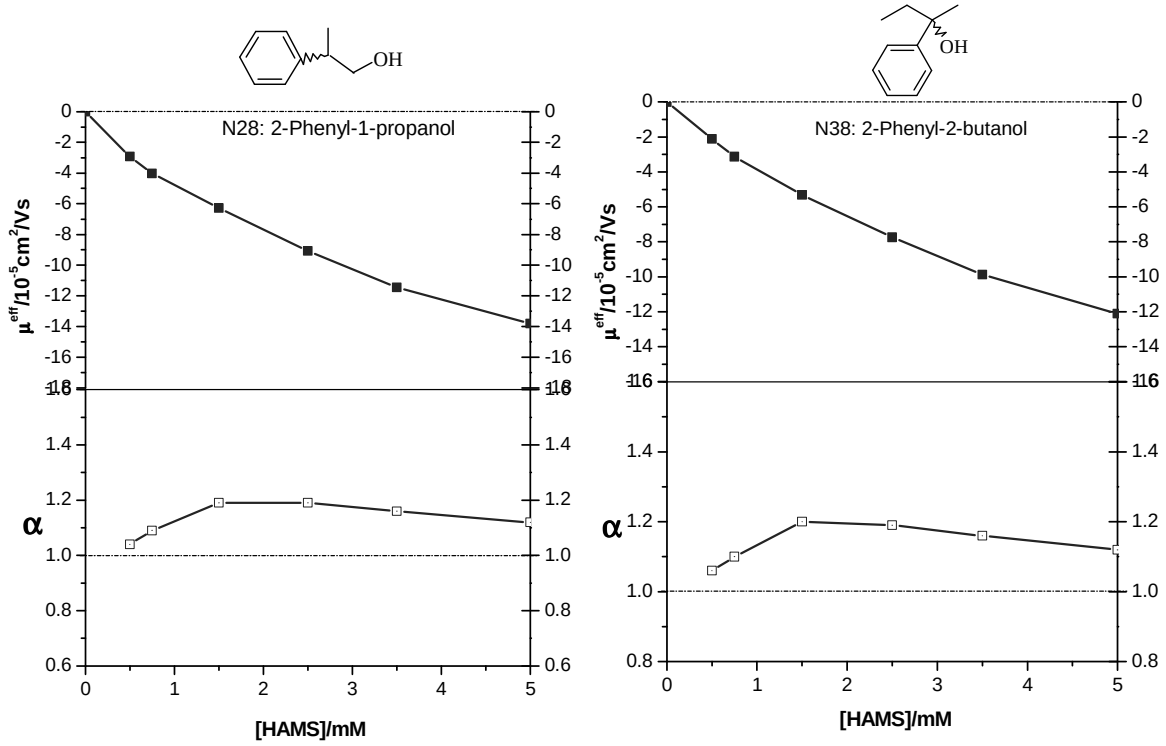

Figure 60. Effective mobilities (top panels) and separation selectivities (bottom panels) of strongly binding nonionic analytes as a function of the HAMS concentration

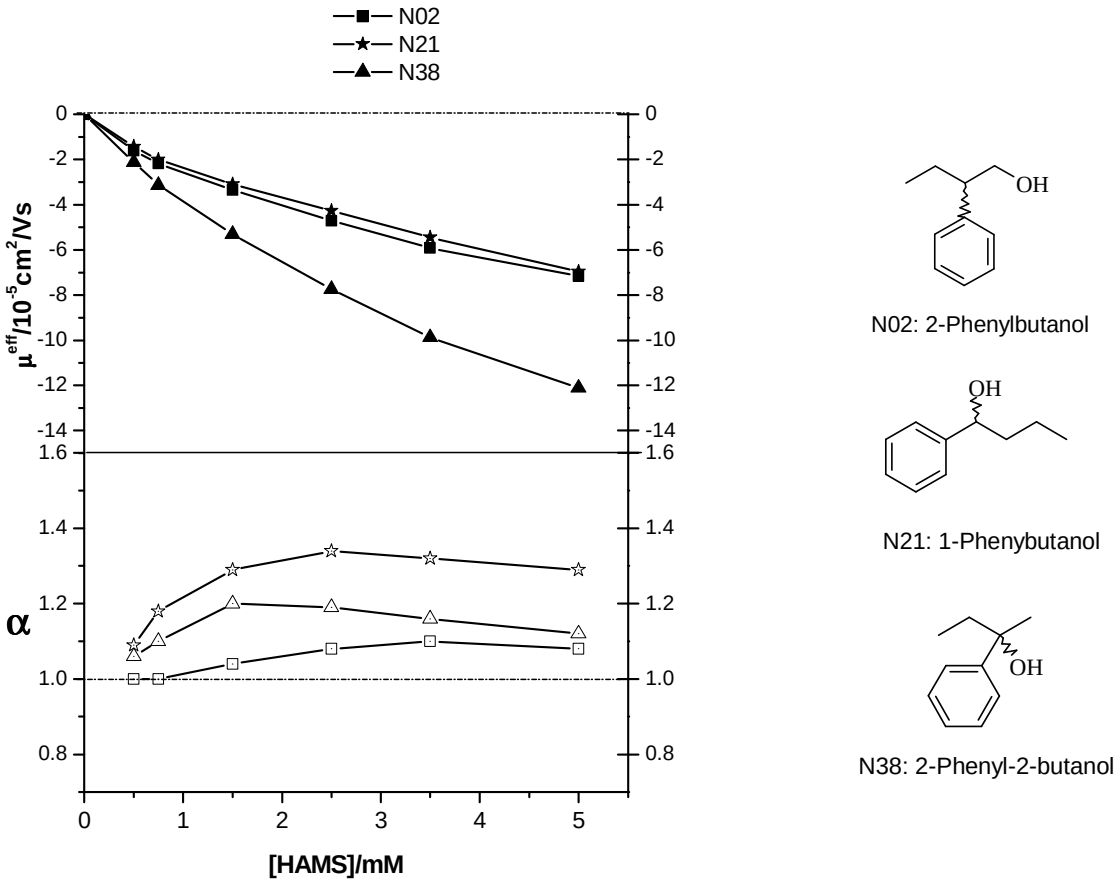

Figure 61. Effects of analytes structure on effective mobilities (top panel) and separation selectivities (bottom panel) for nonionic analytes N02, N21 and N38 obtained in pH 2.5 BGE using HAMS

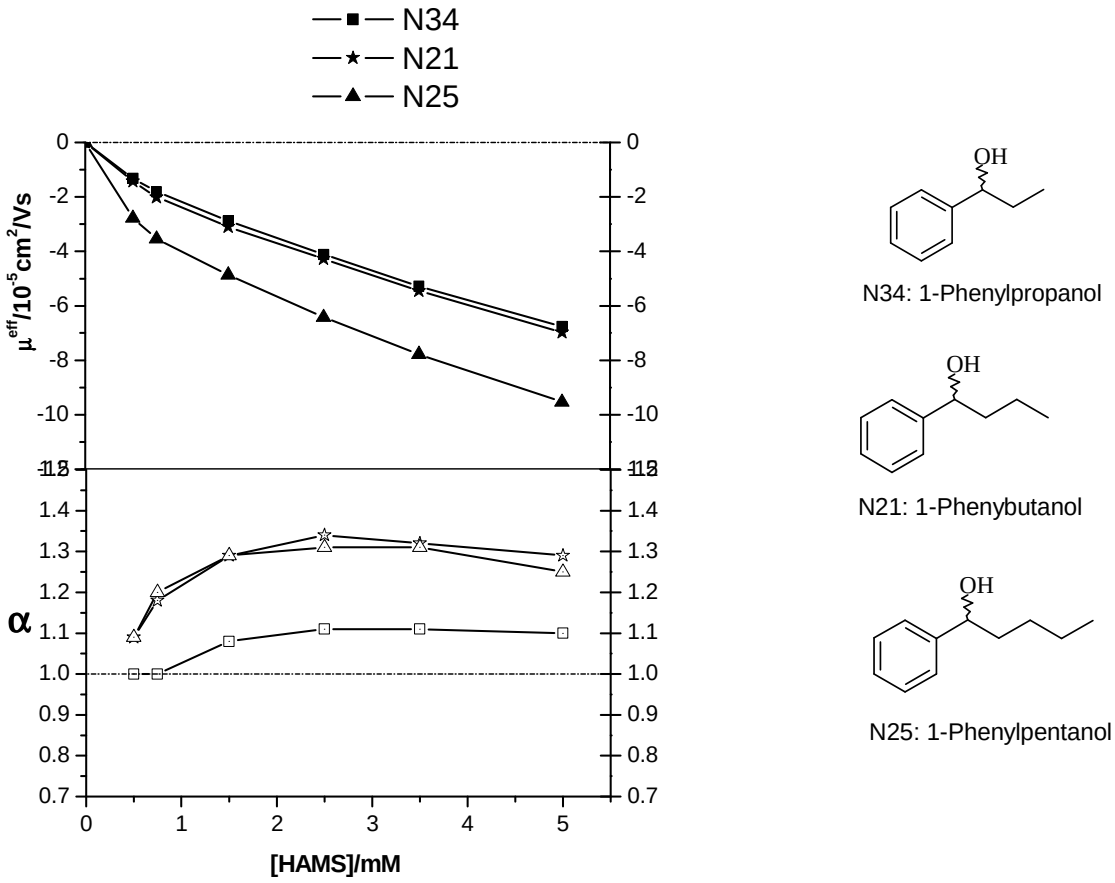

Figure 62. Effects of the analyte structures on effective mobilities (top panel) and separation selectivities (bottom panel) for nonionic analytes N34, N21 and N25 obtained in pH 2.5 BGE using HAMS

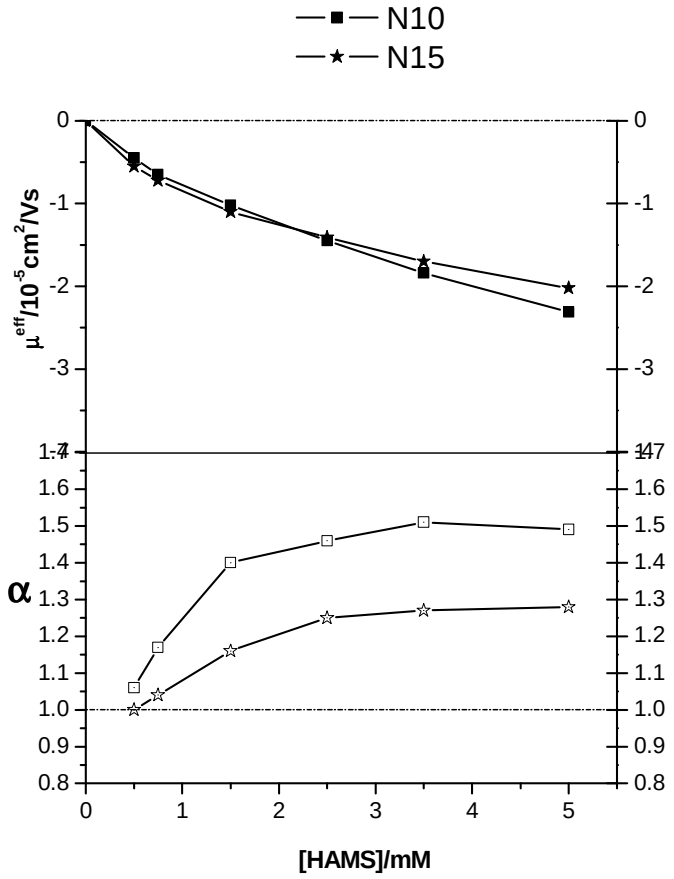

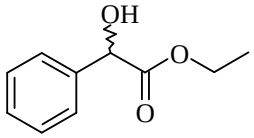

N10: Ethylmandelate

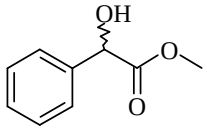

N15: Methylmandelate

Figure 63. Effects of analyte structure on the effective mobilities (top panel) and separation selectivities (bottom panel) for nonionic analytes N10 and N15 obtained in pH 2.5 BGE using HAMS

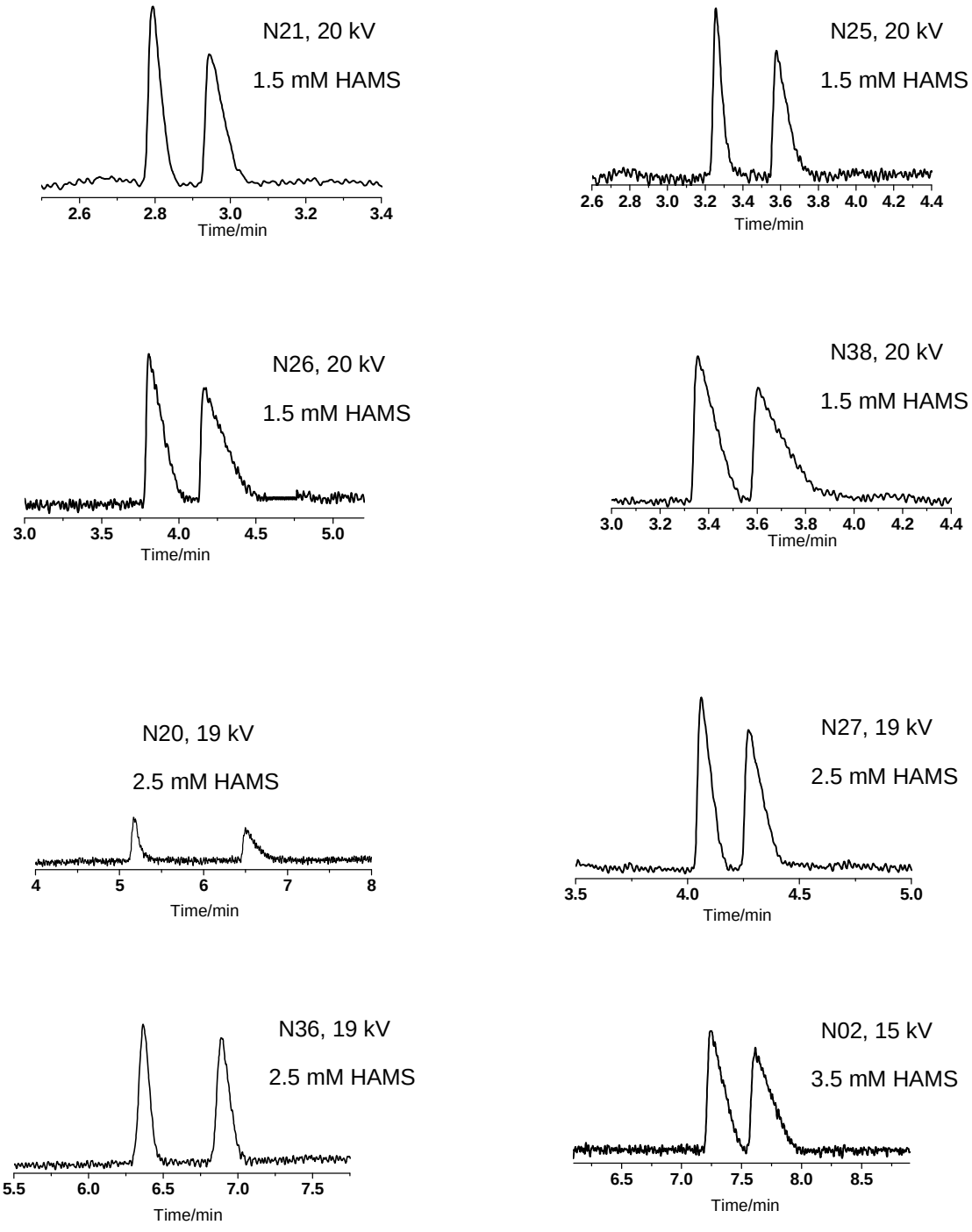

Figure 64. Typical electropherograms of nonionic analytes in pH 2.5 BGE with HAMS

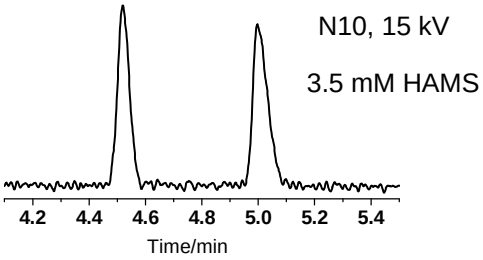

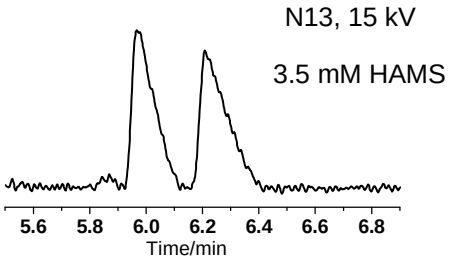

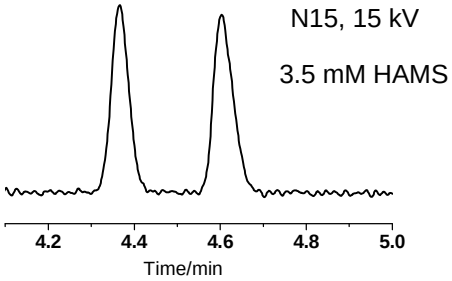

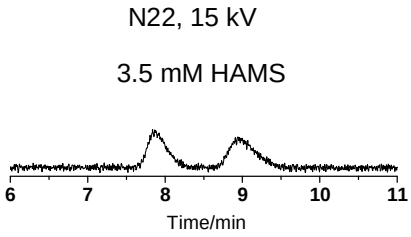

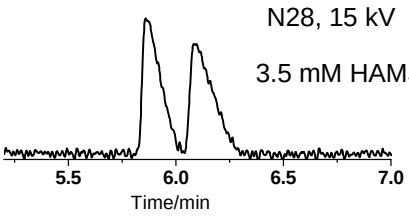

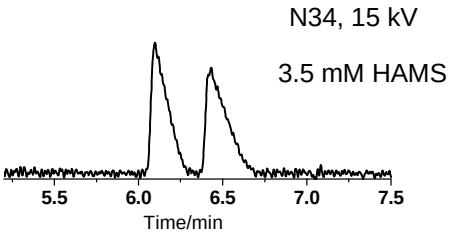

Figure 64. Continued

The changes in the binding strength for some selected nonionic analytes due to differences in the functionalization at the C2, C3 and C6 positions are represented in the effective mobility (left panel) and separation selectivity (right panel) curves for HAMS, HDMS[82] (heptakis(2,3-di-*O*-methyl-6-*O*-sulfo)cyclomaltoheptaose) and HDAS[83] (heptakis(2,3-di-*O*-acetyl-6-*O*-sulfo)cyclomaltoheptaose) shown in Figure 65. HDMS and HDAS both carry the sulfate group at the C6 positions. While HDMS carries methyl groups at the C2 and C3 positions, HDAS carries acetyl groups at those two positions. From the effective mobility values it is observed that the effective anionic mobilities increase with increasing SISCDs concentration. Separation selectivity increases to a maximum at a low SISCDs concentration and then decreases as SISCDs concentration is increased. These trends are in agreement with the predictions of the CHARM model. The binding strength of 2-phenyl-2-pentanol, N26, 1-phenylpentanol, N27, and 2-phenyl-1-propanol, N28 to HAMS (N27 and N28, moderately strongly binding; N26, strongly binding) is much higher compared to HDMS (N26, N27 and N28, weakly binding). While separation selectivity is higher for N26 and N28 with HAMS as the chiral selector compared to HDMS, the opposite is true for N27. HDAS shows similar trends in the binding strength of methyl mandelate, N15, 1-phenylpentanol, N27, and 2-phenyl-1-propanol, N28 compared to HAMS. However, HDAS offers much higher separation selectivities for N15 and N28 compared to HAMS. It is very clear that different substituents at the C2, C3 and C6 positions of the glucopyranose subunits offer different separation selectivities for the same enantiomer pair. However, NMR experiments are needed to aid our understanding of the chiral recognition mechanism.

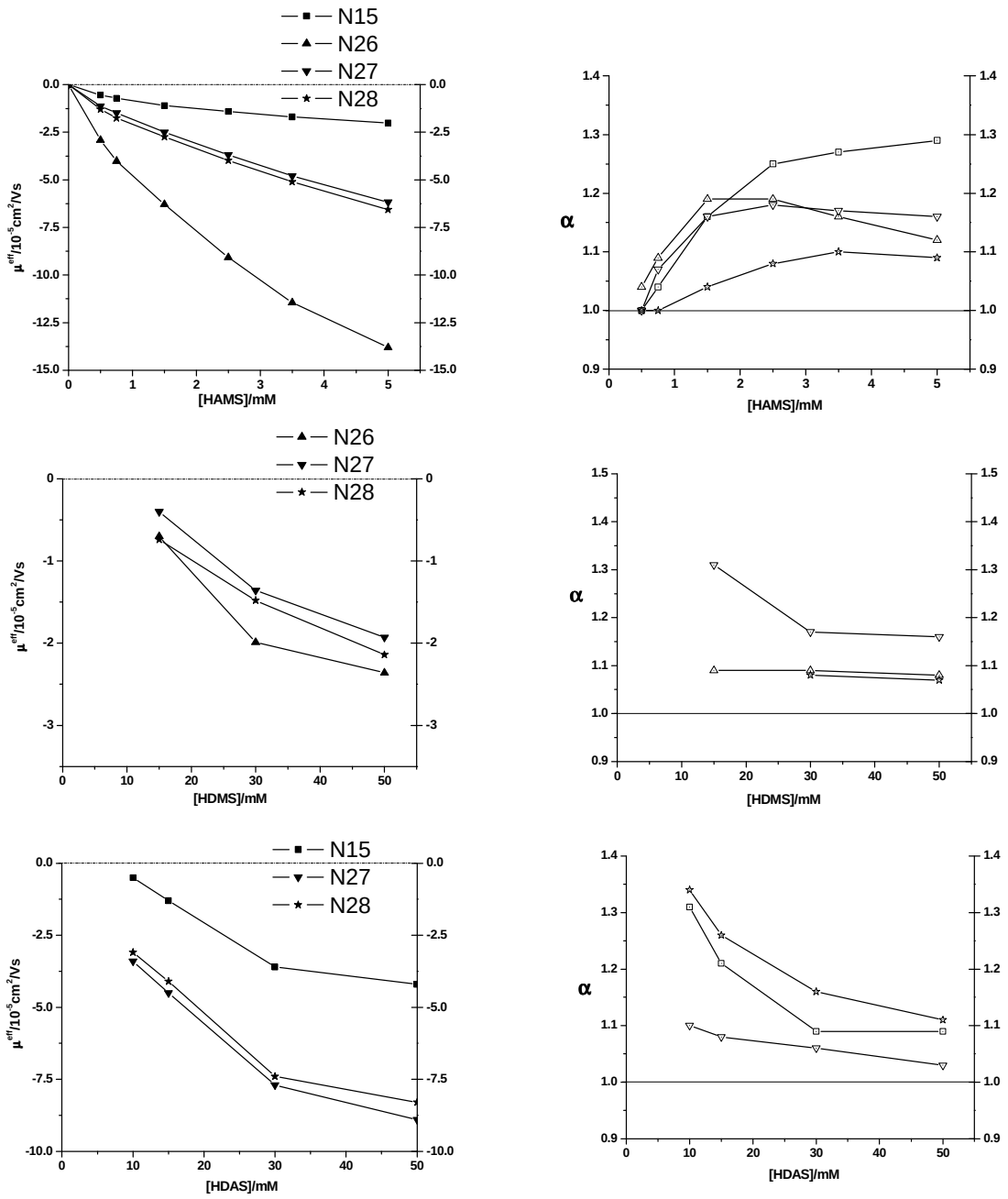

Figure 65. Effective mobilities (left panel) and separation selectivities (right panel) of N15, N26, N27 and N28 in pH 2.5 aqueous BGE with HAMS, HDMS and HDAS

3.6 Separations of the Enantiomers of Strong Electrolyte Analytes Using HAMS in Low pH BGEs

Although HAMS was designed for the separation of nonionic and cationic analytes, an attempt was made to separate the enantiomers of six strong electrolyte analytes shown in Figure 66. The set of strong electrolyte analytes used includes analytes with the sulfate moiety directly attached to the chiral carbon atom and either one or two bonds away from the aromatic ring. These analytes were synthesized and fully characterized by Nzeadibe.[84] The choice of these analytes was based on the excellent enantiorecognition observed for the corresponding nonionic aromatic alcohols. The results obtained are shown in Table 3. Since the charge of the strong electrolyte analyte is independent of the pH of the BGE, detailed studies were carried out in low pH BGEs by varying the concentration of HAMS from 0.5 mM to 5.0 mM. As expected, the monoanionic analytes have effective mobilities between -23 and -31 $\times$ 10^{-5} cm^2/Vs. The effective mobilities decreased in the absence of HAMS for the same substitution pattern as the length of the alkyl chain was increased; S01 compared to S07 and S02 compared to S05, due to the ratio of charge to hydrodynamic volume of the analytes.

Upon addition of HAMS to the BGE, the anionic effective mobilities increased to a shallow extremum and begin to approach zero as the concentration of HAMS increased. The observed decrease in effective anionic mobility could be due to increasing ionic strength and viscosity. The cause of this phenomenon is the interplay between the increased mole fraction of the anionic analytes-HAMS complex and the increased ionic strength brought about by the increased HAMS concentration. The former of these effects increases the contribution of the anionic complex to the effective mobility of the band which is greater at low HAMS concentrations, while the latter decreases the effective mobility of the anionic complex and its effect is greater at relatively high concentrations.[70] No separation was observed for the six strong electrolyte test analytes, although favorable β values were obtained. This may be due to ionic repulsion between the negatively charged analytes and the negatively charged chiral resolving agent with the sulfate group located on the chiral face of the SISCD.

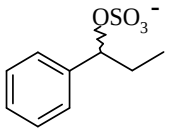

S01: 1-Phenyl-1-*O*-sulfo-propane

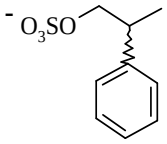

S02: 2-Phenyl-1-*O*-sulfo-propane

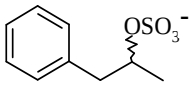

S03: 1-Phenyl-2-*O*-sulfo-propane

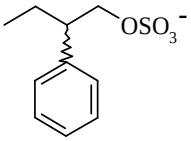

S05: 2-Phenyl-1-*O*-sulfo-butane

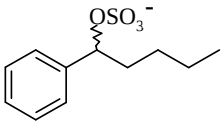

S07: 1-Pheny-1-*O*-sulfo-pentane

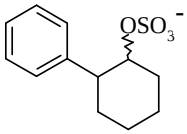

S10: trans-2-Phenyl-1-*O*-sulfo-cyclohexane

Figure 66. Names and structures of the strong electrolyte analytes tested

Table 3. Separation data for the strong electrolyte analytes in pH 2.5 aqueous HAMS BGE. (μ, in 10^{-5} cm^2/Vs units)

[CD]	0 mM	0.5mM				0.75mM			
U (KV)		20.0				20.0			
Analyte	μ	μ	α	β	Rs	μ	α	β	Rs
S01	-30.90	-34.90	1.00	-0.95	0.00	-34.62	1.00	-0.92	0.00
S02	-29.90	-35.95	1.00	-0.91	0.00	-35.63	1.00	-0.89	0.00
S03	-27.50	-35.01	1.00	-0.93	0.00	-34.70	1.00	-0.92	0.00
S05	-25.60	-30.31	1.00	-1.06	0.00	-30.10	1.00	-1.01	0.00
S07	-23.50	-28.90	1.00	-1.14	0.00	-28.70	1.00	-1.11	0.00
S10	-27.40	-31.90	1.00	-1.01	0.00	-31.50	1.00	-1.01	0.00

[CD]	1.5mM				2.5mM			
U (KV)	20.0				19.0			
Analyte	μ	α	β	Rs	μ	α	β	Rs
S01	-34.23	1.00	-0.88	0.00	-34.03	1.00	-0.90	0.00
S02	-35.25	1.00	-0.85	0.00	-34.90	1.00	-0.87	0.00
S03	-34.30	1.00	-0.88	0.00	-33.90	1.00	-0.90	0.00
S05	-29.84	1.00	-1.01	0.00	-29.53	1.00	-1.03	0.00
S07	-28.20	1.00	-1.06	0.00	-27.60	1.00	-1.10	0.00
S10	-30.80	1.00	-0.98	0.00	-30.16	1.00	-1.01	0.00

Table 3. Continued

[CD]		5.0mM		
U (KV)		15.0		
Analyte	μ	α	β	Rs
S01	-33.40	1.00	-0.92	0.00
S02	-34.01	1.00	-0.91	0.00
S03	-33.21	1.00	-0.91	0.00
S05	-28.90	1.00	-1.08	0.00
S07	-26.30	1.00	-1.13	0.00
S10	-29.01	1.00	-1.05	0.00

3.7 Summary

The first single-isomer β-CD derivative that is sulfated at the C2 position, the sodium salt of heptakis(2-*O*-sulfo-3-*O*-methyl-6-*O*-acetyl)cyclomaltoheptaose (HAMS) has been used to study the effective mobility and separation selectivity patterns of the enantiomers of structurally diverse weak base, nonionic and strong electrolyte analytes in acidic aqueous BGEs. The trends observed in all cases followed closely the predictions of the CHARM model. HAMS provided effective mobilities and separation selectivities that were complimentary to those obtained for the same analytes using other sulfated β-CDs.

CHAPTER IV

CONCLUSIONS

Several SISCDs have been synthesized and utilized as chiral resolving agents in capillary electrophoretic separation of enantiomers including acidic, basic, neutral and ampholytic analytes. All these SISCD derivatives carry the sulfate group at either the C3 or C6 positions of the glucopyranose moieties. Previous work has shown that the cavity size of the cyclodextrins and the types of the substituents including acetyl, hydroxyl and methyl groups contribute significantly to the enantiorecognition process. However, the influence of the attachment position of the sulfate group on the chiral recognition capabilities of CDs had not been fully investigated since a SISCD, carrying the sulfate group on the C2 position had not yet been synthesized. The need for this investigation to be carried out led to the synthesis of the first single-isomer β-CD derivative that is sulfated at the C2 position, the sodium salt of heptakis(2-*O*-sulfo-3-*O*-methyl-6-*O*-acetyl)cyclomaltoheptaose (HAMS). Apart from its potential for enantioresolution of both nonionic and ionic chiral analytes, introduction of negative charges on the β-CD enhances its solubility in aqueous media.

The synthetic methodology used to produce HAMS utilized protection and deprotection of the 2-, 3- and 6-hydroxyl groups of β-CD by using regioselective chemical processes. The first step, which has long been used as a means to bi-functionalize SISCDs, where the C2 and C3 positions are modified in a “one-pot” reaction with either methyl or acetyl groups, involve the protection of the C6 positions

with TBDMS. It is worth noting that one of the major steps leading to the successful synthesis of HAMS lies in the selective benzylation of the C2 position without concurrent modification at the C3 position. A conversion rate of over 80% was achieved under 3 hours. Methylation at C3 followed by selective desilylation at C6 gave good yields. Subsequent synthetic transformation began with acetylation of the hydroxyl group at C6, deprotection at C2 by selective removal of the benzyl group, the second major step leading to the successful synthesis of HAMS, and sulfation of the exposed hydroxyl groups at C2 to produce HAMS. The acetylation reaction proceeded with 98% conversion rate in less than 2 hours. Purification of each intermediate and the final product (HAMS) was accomplished using suitable recrystallization solvents and solvent mixtures.

The structural identities of the intermediates and the final product were verified by 1D ^{1}H, ^{13}C, 2D COSY and HMQC NMR spectroscopy, and also by high resolution MALDI-TOF mass spectrometry. Non-aqueous, gradient reversed-phase HPLC and HILIC-HPLC methods were developed for the determination of the purity of each synthetic intermediate and final product. Purities were typically in excess of 97% mol/mol. These complementary methods proved that HAMS is pure and has the desired structural characteristics of the targeted product.

HAMS was used to study the effective mobility and separation selectivity trends of weak base, nonionic and strong electrolyte analytes. The BGEs were made from a 25 mM phosphoric acid solution buffered to pH 2.5 with lithium hydroxide. The capillary

used was uncoated, bare fused silica and applied potentials were kept within the linear region of Ohm's Law plots.

Of the thirty-three weakly basic analytes tested, enantiomer separation was observed for twenty-seven over the HAMS concentration range used. Eighteen of these weak bases were baseline resolved (i.e., Rs > 1.5). In general, four types of separation trends were observed for the weak base analytes in the low pH BGEs. (1) For very strongly binding analytes, the effective mobilities became anionic at HAMS concentrations lower than 0.6 mM. (2) For strongly binding analytes, the effective mobilities became anionic at HAMS concentrations as low as 1.5 mM. (3) For the moderately strongly binding analytes, the effective mobilities of the analytes became anionic at some intermediate HAMS concentration ([HAMS] > 7.5 mM). (4) For weakly binding analytes, the effective mobilities did not become anionic over the HAMS concentration range tested. The effective mobility and separation selectivity trends for the weak bases agreed well with the predictions of the CHARM model.

Binding strength was found to be highly dependent on the structure of the analyte and the resolving agent. A group of structurally similar catecholamines showed that changes in substitution about the aromatic ring can result in significant changes in both effective mobility and separation selectivity trends. The effective mobilities of the analytes at 5 mM spanned from 2.3 to 8.2 10^{-5} cm^2/Vs. Metaproterenol, B30, the strongest binding analyte among them exhibits the best separation selectivity. In order to investigate the effect of the attachment position of the sulfate group on enantiorecognition, the effective mobility and separation selectivity trends observed for

homatropine, chlophedianol and metoprolol using HAMS as the chiral resolving agent in acidic aqueous BGEs, were compared to those observed with HMAS and HMdiSu. The binding strengths of the enantiomers of homatropine were the strongest for HMdiSu and decreased in the order HMdiSu > HAMS > HMAS. The binding strengths of the enantiomers of chlophedianol were strongest for HAMS and decreased in the order HAMS > HMdiSu > HMAS. The binding strength of metoprolol for HAMS was stronger compared to HMdiSu. While HMdiSu showed selectivity for all three weak base analytes, there was no resolution for homatropine and metoprolol using HMAS (homatropine) and HAMS (metoprolol) as chiral selectors. It is worth noting that although the position of attachment of the sulfate group significantly influences the enantiorecognition process, it is also dependent on the presence of the other substituents, including the acetyl and methyl groups.

Using HAMS for the separation of nonionic analytes, it was found that most analytes exhibit one of three specific mobility trends. The first group was called the group of weakly binding nonionic analytes: their effective anionic mobilities remained low, approaching -4.0×10^{-5} cm^2/Vs. The second group was called the group of moderately strongly binding analytes: their effective anionic mobilities increased to -10.0×10^{-5} cm^2/Vs. The third group was called the group of strongly binding analytes: their effective anionic mobilities increased beyond -10.0×10^{-5} cm^2/Vs.

The enantiomers of all fourteen nonionic analytes tested using HAMS were separated under the experimental conditions used. Experimental results show that

separation selectivity depended on (i) the structure of the analyte; and (ii) the polarity of the substituents of the β-CD.

(i) The effect of analytes structure on enantiorecognition is very significant. For example, the enantiomers of 2-phenylbutanol, 1-phenylbutanol and 2-phenyl-2-butanol showed significantly different separation selectivity behaviors from each other. These analytes have the same molecular formula but are different isomers. 1-phenylpropanol, 1-phenylbutanol and 1-phenylpentanol, which formed a homologous series, showed interesting separation selectivity patterns. The same can be said for the enantiomers of methylmandelate and ethylmandelate.

(ii) The type and position of attachment of the different substituents on β-CD led to different enantiomer separations. HDMS offered the best separation selectivity values for 1-phenyl-2-propanol compared to HDAS and HAMS. On the other hand, HDAS offered the best separation selectivity values for 2-phenyl-1-propanol compared with HAMS and HDMS. The binding strengths for 1-phenyl-2-propanol and 2-phenyl-1-propanol decreased in the order HDAS > HAMS > HDMS.

For the six anionic strong electrolytes, no enantioseparation was observed with HAMS over the concentration range studied. This lack of separation may be due to repulsion between the analytes and HAMS.

In conclusion, the first single-isomer, sulfated β-cyclodextrin carrying the sulfo group at the C2 position, the sodium salt of heptakis(2-*O*-sulfo-3-*O*-methyl-6-*O*-acetyl)cyclomaltoheptaose (HAMS) has been produced with isomeric purity greater than 97% mol/mol. It has been successfully used as a chiral resolving agent for the capillary

electrophoretic separations of the enantiomers of weak base and nonionic analytes in aqueous acidic BGEs. HAMS proved to be broadly useful and in many cases, had separation selectivity complimentary to that obtained with other single isomer sulfated cyclodextrins.

REFERENCES

(1) Millership, J. S.; Fitzpatrick, A. *Chirality* **1993**, *5*, 573-576.

(2) Ghanem, A.; Aboul-Enein, Y. H. *J. Liq. Chromatogr. & Rel. Technol.* **2005**, *28*, 2863-2874.

(3) Aboul-Enein, Y. H.; Abou-Basha, L. I. In *The Impact of Stereochemistry on Drug Development and Use*; Aboul-Enein, Y. H., Wainer, I. W., Eds.; John Wiley & Sons: New York, 1997, pp 3-102.

(4) Camp, E. W. *J. Pharm. Biomed. Anal.* **1993**, *11*, 1167-1172.

(5) Bicchi, C.; Brunelli, C.; Cravotto, G.; Rubiolo, P.; Galli, A. *J. Sep. Sci.* **2002**, *25*, 125-130.

(6) Granville, C. P.; Gehrcke, B.; Konig, W. A.; Wainer, I. W. *J. Chromatgr.* **1993**, *622*, 21-31.

(7) Mitchell, C.; Desai, M.; McCulla, R.; Jenks, W.; Armstrong, D. W. *Chromatographia* **2002**, *56*, 127-135.

(8) Kanazawa, H.; Kunito, Y.; Matusushima, Y.; Okubo, S.; Mashige, F. *J. Chromatogr. A* **2000**, *871*, 181-188.

(9) Blaschke, G. *J. Liq. Chromatogr. & Rel. Technol.* **1986**, *9*, 407-423.

(10) Skrdla, P. J.; Robertson, R.; Antonucci, V.; Lindemann, C. *J. Chromatogr. Sci.* **2003**, *41*, 117-122.

(11) Han, M. S.; Armstrong, D. W. *Chem. Anal.* **1990**, *108*, 81-85.

(12) Armstrong, D. W.; Faulkner, J.; Han, S. M. *J. Chromatgr.* **1988**, *452*, 323-330.

(13) Macaudiere, P.; Caude, M.; Rosset, R.; Tambute, A. *J. Chromatogr. Sci.* **1989**, *27*, 383-394.

(14) Hara, S.; Dobashi, A.; Kinoshita, K.; Hondo, T.; Saito, M.; Senda, M. *J. Chromatgr.* **1986**, *371*, 153-158.

(15) Porras, S.; Sarmini, K.; Fanali, S.; Kenndler, E. *Anal. Chem.* **2003**, *75*, 1645-1651.

(16) Natishan, K. T. *J. Liq. Chromatogr. & Rel. Technol.* **2005**, *28*, 1115-1160.

(17) Issaq, H. *J. Liq. Chromatogr. & Rel. Technol.* **2002**, *25*, 1153-1170.

(18) Knox, J. H.; Grant, I. H. *Chromatographia* **1987**, *24*, 135-143.

(19) Valko, I. E.; Siren, H.; Riekkola, M. L. *J. Microcol. Sep.* **1999**, *11*, 199-208.

(20) Pretorius, V.; Hopkins, B. J.; Schielke, J. D. *J. Chromatgr.* **1974**, *99*, 23-30.

(21) Beckers, J. L.; Bocek, P. *Electrophoresis* **2003**, *24*, 518-535.

(22) Ryslavy, Z.; Bocek, P.; Deml, M.; Janak, J. *J. Chromatgr.* **1977**, *144*, 17-25.

(23) Reijenga, J. C.; Kenndler, E. *J. Chromatgr. A* **1994**, *659*, 403-415.

(24) Armstrong, D. W.; Rundlett, K.; Reid, G. L. *Anal. Chem.* **1994**, *66*, 1690-1695.

(25) Gubitz, G.; Schmid, M. G. *J. Chromatogr. A* **1997**, *792*, 179-225.

(26) Fanali, S.; Aturki, Z.; Desiderio, C. *Forensic Sci. Int.* **1998**, *92*, 137-155.

(27) Ward, T. J.; Farris, A. B. *J. Chromatogr. A* **2001**, *906*, 73-89.

(28) Blanco, M.; Valverde, I. *Trends Anal. Chem.* **2003**, *22*, 428-439.

(29) Jiang, Z.; Kang, J.; Bischoff, D.; Bister, B. *Electrophoresis* **2004**, *25*, 2687-2692.

(30) Amini, A. *Electrophoresis* **2001**, *22*, 3107-3130.

(31) Gubitz, G.; Schmid, M. G. *Electrophoresis* **2000**, *21*, 4112-4135.

(32) Tanaka, Y.; Terabe, S. *J. Biochem. Biophys. Methods* **2001**, *48*, 103-116.

(33) Kuhn, R. *Electrophoresis* **1999**, *20*, 2605-2613.

(34) Nishi, H.; Izumoto, S.; Nakamura, K.; S., N.; Sato, T. *Chromatographia* **1996**, *42*, 617-630.

(35) Nishi, H. *J. Chromatogr. A* **1997**, *792*, 327-347.

(36) Eeckhaut, A. V.; Michotte, Y. *Electrophoresis* **2006**, *27*, 2880-2895.

(37) Francotte, E.; Junker-Buchheit, A. *J. Chromatogr.* **1992**, *576*, 1-45.

(38) Szejtli, J. *Chem. Rev.* **1998**, *98*, 1743-1754.

(39) Sepaniak, M. J.; Cole, R. O.; Clark, B. K. *J. Liq. Chromatogr. & Rel. Technol.* **1992**, *15*, 1023-1040.

(40) Fanali, S. *J. Chromatogr. A* **1989**, *474*, 441-446.

(41) Booth, D. T.; Wainer, I. W. *J. Chromatogr. A* **1996**, *737*, 157-169.

(42) Nardi, A.; Eliseev, A.; Bocek, P.; Fanali, S. *J. Chromatgr. A* **1993**, *638*, 247-253.

(43) Poole, F. C. In *The Essence of Chromatography*; Elsevier Science B. V.: Amsterdam, 2003, pp 25-200.

(44) Wedig, M.; Laug, S.; Christians, T.; Thunhorst, M.; Holzgrabe, U. *J. Pharm. Biomed. Anal.* **2002**, *27*, 531-540.

(45) Arai, T. *J. Chromatogr. B* **1988**, *717*, 295.

(46) Bjornsdottir, I.; Hensen, S. H. *Chirality* **1995**, *7*, 219-225.

(47) Williams, B.; Vigh, G. *J. Chromatogr. A* **1997**, *777*, 295-309.

(48) Weseloh, G.; Bartsch, H.; Konig, W. A. *J. Microcol. Sep.* **1995**, *7*, 355-363.

(49) Cravotto, G.; Palmisano, G.; Panza, L.; Tagliapietra, S. *J. Carbohydr. Chem.* **2000**, *19*, 1235-1245.

(50) Fujita, K.; Yamamura, H.; Matsunaga, A.; Imoto, T.; Mihashi, K.; Fujioka, T. *J. Am. Chem. Soc.* **1986**, *108*, 4509-4513.

(51) Takeo, K.; Uemura, K.; Mitoh, H. *J. Carbohydr. Chem.* **1988**, *7*, 293-308.

(52) Takahashi, K.; Hattori, K.; Toda, F. *Tetrahedron Lett.* **1984**, *25*, 3331-3334.

(53) Menger, F. M.; Dulany, M. A. *Tetrahedron Lett.* **1985**, *26*, 267-270.

(54) Takeo, K.; Mitoh, H.; Uemura, K. *Carbohydr. Res.* **1989**, *187*, 203-221.

(55) Rong, D.; D' Souza, V. T. *Tetrahedron Lett.* **1990**, *31*, 4275-4278.

(56) Gubitz, G.; Schmid, M. G. In *Chiral Separations by Capillary Electrophoresis*; Eeckhaut, A. V., Michotte, Y., Eds.; Taylor & Francis Group: Boca Raton, FL, 2010, pp 47-200.

(57) Li, S.; Vigh, G. *Electrophoresis* **2004**, *25*, 2657-2670.

(58) Li, S.; Vigh, G. *J. Chromatogr. A* **2004**, *1051*, 95-101.

(59) Vincent, J. B.; Sokolowski, T. V.; Nguyen, T. V.; Vigh, G. *Anal. Chem.* **1997**, *69*, 4226-4233.

(60) Vincent, J. B.; Kirby, D. M.; Nguyen, T. V.; Vigh, G. *Anal. Chem.* **1997**, *69*, 4419-4428.

(61) Cai, H.; Vigh, G. *J. Microcol. Sep.* **1998**, *10*, 293-299.

(62) Li, S.; Vigh, G. *Electrophoresis* **2003**, *24*, 2487-2498.

(63) Li, S.; Vigh, G. *Electrophoresis* **2004**, *25*, 1201-1210.

(64) Busby, B.; Lim, P.; Vigh, G. *Electrophoresis* **2003**, *24*, 351-362.

(65) Zhu, W.; Vigh, G. *Anal. Chem.* **2000**, *72*, 310-317.

(66) Zhu, W.; Wu, F.; Raushel, F. M.; Vigh, G. *J. Chromatogr. A* **2000**, *892*, 499-507.

(67) Zhu, W.; Vigh, G. *J. Microcol. Sep.* **2000**, *12*, 167-171.

(68) Busby, B.; Vigh, G. *Electrophoresis* **2005**, *26*, 1978-1987.

(69) Busby, B. M.; Vigh, G. *Electrophoresis* **2005**, *26*, 3849-3860.

(70) Maynard, D. M.; Vigh, G. *Electrophoresis* **2001**, *22*, 3152-3162.

(71) Wren, S. A. C.; Rowe, R. C. *J. Chromatogr. A* **1992**, *609*, 363-367.

(72) Wren, S. A. C.; Rowe, R. C. *J. Chromatogr.* **1992**, *603*, 235-241.

(73) Wren, S. A. C.; Rowe, R. C. *J. Chromatogr. A* **1993**, *635*, 113-118.

(74) Wren, S. A. C. *J. Chromatogr.* **1993**, *636*, 57-62.

(75) Russell, D. H.; Edmundson, R. D. *J. Mass Spectrom.* **1997**, *32*, 263-276.

(76) Russell, W. K.; Russell, D. H.; Busby, M. B.; Kolberg, K.; Li, S.; Maynard, D. K.; Sanchez-Vindas, S.; Zhu, W.; Vigh, G. *J. Chromatogr. A* **2001**, *914*, 325-330.

(77) Cai, H.; Nguyen, T. V.; Vigh, G. *Anal. Chem.* **1998**, *70*, 580-589.

(78) Angibeaud, P.; Utille, J.-P. *Synthesis* **1991**, 737-738.

(79) William, B.; Vigh, G. *Anal. Chem.* **1997**, *69*, 4445-4451.

(80) Busby, B. M. PhD Dissertation, Texas A&M University, College Station, 2005.

(81) Maynard, D. M. PhD Dissertation, Texas A&M University, College Station, 2001.

(82) Cai, H. PhD Dissertation, Texas A&M University, College Station, 1998.

(83) Vincent, J. B. PhD Dissertation, Texas A&M University, College Station, 1998.

(84) Nzeadibe, K. PhD Dissertation, Texas A&M University, College Station, 2006.

APPENDIX

SYNTHESIS PROTOCOL FOR SINGLE-ISOMER HAMS

Heptakis(2-*O*-benzyl-6-*O*-t-butyldimethylsilyl)cyclomaltoheptaose

1. Dry the pure, heptakis(6-*O*-t-butyldimethylsilyl)cyclomaltoheptaose ($TBDMS_7$-β-CD) in a vacuum oven at 80ºC to remove acetone, DMF and adsorbed water. Note: (i) Complete dryness of the material is critical for success of the reaction. (ii) Purity of the starting material is essential for the purity of the final product. Oversilylated and undersilylated CDs lead to the formation of byproducts that cannot be removed in the work-up of the final product.

2. In a well-ventilated hood, set up on a stir plate an oven-dried 500 ml three-neck round bottom flask, equipped with a 1″ Teflon-coated magnetic stir bar, a source of dry N_2 gas at one neck and, at another neck, an oil bubbler with 1″ of paraffin oil. Connect the oil bubbler to the reaction flask through a valve adapter with tabulation. Cap the third neck with a ground glass stopper of appropriate size. Thoroughly purge the set-up with dry N_2.

3. Place a clean, dry, flexible Teflon adapter, equipped with a female ground glass joint at one end and a male ground joint at the opposing end into an oven at 105ºC. While the adapter is being heated, weigh 2.7 g of NaH as 60% dispersion in oil into a 100 ml flask specially adapted at the neck to have a male ground glass joint. Next, cap the flask with a sealed, female ground glass joint and quickly seal the joint with Parafilm. Note: Do not use vacuum grease on any joint. Remove from the oven the flexible adapter that has been heating for no longer than 10 minutes. Remove the Parafilm seal from the flask, equip it with the flexible adapter and cap. Next, remove the cap from the flexible adapter and pour the hydride through the central neck of the reaction flask using female to male

ground glass joint adapters if necessary. Once transfer is complete, remove the flexible adapter from the reaction flask and quickly cap both the transport vessel and the reaction flask. Carefully quench the sodium hydride residue in the transport vessel with ethylene glycol.

4. The oil that coats the sodium hydride must be removed through a series of hexanes rinses accomplished using an air-free technique. Rubber septa should be wired down and ground glass joints should be equipped with Keck clamps to secure them. Transfer 30 ml of dried hexanes from its bottle into a septum-capped 100 ml graduated cyclinder. Next, canulate this volume to the reaction flask using a 24″ long, 12-gauge canula. Once the hexanes transfer is complete, stir the oily sodium hydride slurry for about 5 minutes, then allow sodium hydride to settle. Once sodium hydride has settled, canulate the hexanes to an open, 100 ml graduated cylinder by first closing off the oil bubbler. Once the first step is complete, repeat the hexanes rinse two more times. Care must be taken not to remove any sodium hydride that may become disturbed during the hexanes removal step. Measure 15 ml of dried THF and canulate it into the reaction flask.

5. In an oven-dried, 250 ml graduated addition funnel, with a standard taper top outer joint and lower inner joint, pressure equalizing arm and Teflon stopcock, transfer 60 ml of dried THF into the addition funnel. Next, weigh out 25 g of $TBDMS_7$-β-CD and transfer into the addition funnel using a polypropylene funnel. Dissolve the solid $TBDMS_7$-β-CD by swirling it in the addition funnel. Add 3 ml of dried DMF to the addition funnel followed by 1.8 g of TBAI. DMF helps with the dissolution of TBAI.

Next, pipette 11.5 ml of benzyl bromide into the addition funnel. Flush the addition funnel with dry N_2 and attach it to center neck of the 500 ml reaction flask.

6. While vigorously stirring the sodium hydride/THF slurry, add the solution from the addition funnel at the rate of a thin but steady stream over a period of 5-10 min. Hydrogen evolution will be observed at the oil bubbler in less than 1-2 minutes. During addition, monitor the rate of hydrogen evolution and the degree of foaming in the reaction mixture. Foaming should not be so intense that the entire surface of the reaction mixture is thickly covered. 30 minutes after addition of the TBDMS$_7$β-CD/TBAI/benzyl bromide/THF/DMF solution, take an aliquot of the reaction mixture using a long glass pipette with a drawn-out tip. Add two drops of the reaction mixture to a 2 ml glass vial. Fill the vial to the neck with HPLC grade methanol. Filter the clear solution through a 0.45 μm pore-size nylon membrane filter. Analyze the sample by isocratic, non-aqueous reversed-phase HPLC at room temperature using a 4.6 mm I.D, 250 mm HPLC column packed with 5 μm Luna C18 RP stationary phase and a 55: 45 MeOH : EtOAc mobile phase at a flow rate of 2 ml/min.

7. Once conversion rate reaches about 90 %, quench the reaction by slowly adding 5 ml of anhydrous ethanol through a clean addition funnel over a period of 10 to 15 minutes. Higher conversion rates lead to overbenzylation, the products of which are difficult to remove during work-up. Continue stirring the quenched reaction mixture for another 30 minutes.

8. Filter the quenched reaction mixture to remove the precipitated NaI. Rotavap the filtrate. Once the crude product begins to precipitate, continue to rotavap until no more

solvent condenses into the collection vessel. At this point it is safe to increase the temperature of the bath to 50ºC to rotavap all of the solvent away.

9. Add 20 ml of dichloromethane (1.25g/ml) to the crude product. Dissolve the crude material and place the flask on a stirrer plate. While stirring, add 380ml of MeOH (5%v/v) into the flask. A white precipitate begins to form after about 50% of the total volume of MeOH required has been added. Continue stirring for an additional 10 minutes after methanol addition is completed. Filter the precipitate. Analyze the precipitate by isocratic RP-HPLC as in step 6. Typical purity level for the target is > 99.6%. If purity of the target is lower than expected, repeat step 9.

Heptakis(2-*O*-benzyl-3-*O*-methyl-6-*O*-t-butyldimethylsilyl)cyclomaltoheptaose

1. Dry heptakis(2-*O*-benzyl-6-*O*-t-butyldimethylsilyl)cyclomaltoheptaose ($TBDMS_7Bn_7$-β-CD) in a vacuum oven at 80ºC to a constant weight.

2. In a well-ventilated hood, set up on a stir plate an oven-dried 500 ml three-neck round bottom flask, equipped with a 1″ Teflon-coated magnetic stir bar, a source of dry N_2 gas at one neck and, at another neck, an oil bubbler with 1″ of paraffin oil. Connect the oil bubbler to the reaction flask through a valve adapter with tabulation. Cap the third neck with a ground glass stopper of appropriate size. Turn on the N_2 flow to purge the 500 ml flask.

3. The procedure for transferring NaH into the reaction flask and the removal of oil from NaH is the same as described above for the synthesis of heptakis(2-*O*-benzyl-6-*O*-t-

butyldimethylsilyl)cyclomaltoheptaose. Lower the reaction flask into dry paraffin oil before proceeding further.

4. Transfer 60 ml of dried THF into an oven dried, 250 ml graduated addition funnel having a standard taper top outer joint, lower inner joint, pressure equalizing arm and Teflon stopcock. Next, weigh out 25 g of dry $TBDMS_7Bn_7$-β-CD and transfer into the addition funnel using a polypropylene funnel. Dissolve the added $TBDMS_7Bn_7$-β-CD by swirling the addition funnel. Add 8.5 ml of dried methyl iodide to the addition funnel. Flush the addition funnel with dry N_2 and attach it to the center neck of the reaction flask. Next, place the oil bubbler outlet onto a Liebig condenser and fit the condenser to the reaction flask. Equip the Liebig condenser with a recirculating ice water bath. Make certain that the oil bath has enough oil to exceed the height of the reaction solvent by a full 2″.

5. While stirring the sodium hydride/THF slurry, slowly begin to add the solution from the addition funnel. Bubble formation will begin instantaneously. Monitor the rate of hydrogen formation. About 5 minutes into the reaction, turn on the nitrogen flow for about 3 minutes, then turn it off again.

6. Once addition is completed, in about 15 min, stir the reaction mixture for about 2 hours. Take an aliquot of the reaction mixture using a long glass pipette and add the aliquot to a 2 ml glass vial. Add 1 ml of methanol to the vial and spot this solution onto a silica TLC plate. Use 2.5 × 10 cm aluminum-backed silica plates and an 8 : 1 mixture of hexanes : EtOAc as developing solvent. Once the solvent front migrated close to the top of the plate, air dry the plate for 5 minutes and then dip it into the α-naphtol staining

solution. Visualize the spots by placing the stained TLC plate into a 90ºC oven for 10 minutes.

6. As soon as the TLC plate indicates that the reaction is complete, add 6 ml of anhydrous ethanol to a clean addition funnel and begin to carefully drop it into the reaction mixture to quench the reaction.

7. Filter the NaI precipitate out of the reaction mixture. Transfer the filtrate into a round bottom flask and rotavap the solvent to obtain the crude product. Digest the crude product in 40 ml of dichloromethane and again filter the accumulated NaI precipitate. Rotavap dichloroemethane until no more solvent condenses into the collection vessel.

8. Add 250 ml of ethanol to the crude product in the flask. Place the flask in a heating mantle on a stirrer plate. Stir the mixture while warming the flask. Once the crude product is completely dissolved, turn off the heating mantle. Do not allow ethanol to boil. Slowly begin to add, dropwise, 50 ml of water. Once water addition is complete, stir the mixture for 5 minutes. Filter the gooey precipitate.

9. Analyze the precipitate by isocratic, non-aqueous reversed-phase HPLC at room temperature by using a 4.6 mm I.D., 250 mm long HPLC column packed with a 5 μm Luna C18 stationary phase, and a 55: 45 mixture of MeOH : EtOAc as the mobile phase, at a flow rate of 2 ml/min. The typical purity level for the target is > 99% mol/mol.

Heptakis(2-*O*-benzyl-3-*O*-methyl)cyclomaltoheptaose

1. Add 120 ml ethanol and 140 ml THF into a 600 ml polyethylene beaker. Add 50 g of the pure heptakis(2-*O*-benzyl-3-*O*-methyl-6-*O*-t-butyldimethylsilyl)cyclomaltoheptaose

to the solvent mixture. Let the cyclodextrin dissolve completely by stirring with 1″ Teflon coated magnetic stir bar. Slowly add 70 ml of 48% aqueous HF solution. Cover the beaker with aluminum foil and stir the solution for 24 hours. Check completeness of the desilylation reaction by TLC using 2.5 × 10 cm Silica 60 plates and a 50 : 10 : 1 mixture of $CHCl_3$: MeOH : H_2O as developing solvent.

2. When the desilylation reaction is complete, take a 10 ml aliquot and place it in a clean polyethylene beaker. Prepare a quenching solution by dissolving 60 g of NaOH pellets in 45 ml of deionized water. Cool the solution to room temperature. Next, add, drop-wise, the NaOH solution to 180 ml of ethanol. Place the reaction flask into an ice bath and allow it to cool for 30 minutes. Add a small amount of phenolphthalein indicator to the cyclodextrin solution. Quench the reaction by slowly adding the sodium hydroxide solution to the reaction mixture to neutralize excess HF. Use the aliquot taken in Step 2 to ensure that the reaction mixture is titrated to the proper endpoint indicted by the faintest detectable pink color.

3. Once the solution is completely neutralized, filter the NaF precipitate and wash the filter cake with ethanol. Rotavap the filtrate to dryness. Redissolve the white solid in dichloromethane and filter out the remaining NaF.

4. Add 50 ml acetone to a 250 ml round bottom flask and add the crude material. Add a Teflon-coated stir bar, attach a reflux condenser and reflux the mixture for 10 min. Transfer the flask into an ice bath and allow it to cool. Filter the crystals and take a ^1H NMR spectrum. Repeat Step 4 until the *t*-butyldimethyl silyl fluoride peaks are no longer observed in the ^1H NMR spectrum.

4. Analyze the precipitate by isocratic, aqueous reversed-phase HPLC at room temperature by using a 4.6 mm I.D., 250 mm long HPLC column packed with a 5 μm Luna C18 stationary phase and a solvent mixture of 95: 5 MeOH : H_2O as mobile phase at a flow rate of 2 ml/min. Typical purity level for the target is > 98%.

Heptakis(2-*O*-benzyl-3-*O*-methyl-6-*O*-acetyl)cyclomaltoheptaose

1. Dry the pure, heptakis(2-*O*-benzyl-3-*O*-methyl)cyclomaltoheptaose in a vacuum oven at 80ºC to constant weight.

2. Place a 500 ml, three-neck, round bottom flask with a 1 ″ Teflon coated stir bar and a stopper into an oven and dry overnight at 105ºC. Set up the 500 ml three-neck flask on a stir plate. Connect a N_2 line to one of the side necks on the flask. Connect a condenser to the central neck and an oil bubbler with 1″ of paraffin oil to the remaining neck. Place the flask into a paraffin oil bath on a stir plate. Flush the system with dry N_2 for approximately 5 minutes. Replace the N_2 line with a stopper.

3. Open the side neck and with minimum air exposure, add 100 ml of dry pyridine. Weigh out 25 g of heptakis(2-*O*-benzyl-3-*O*-methyl)cyclomaltoheptaose and transfer into the flask via a short-stem plastic funnel. Begin stirring the mixture with the stir bar. Once the cyclodextrin has completely dissolved, add 50 ml of acetic anhydride.

4. Regulate the temperature of the oil bath using a Variac so that the temperature of the reaction mixture is between 50ºC - 55ºC. Continue stirring for 30 minutes.

5. Take an aliquot of the reaction mixture using a long glass pipette with a drawn-out tip. Add two drops of the reaction mixture to a 2 ml glass vial. Fill the vial to the neck with

HPLC grade methanol. Filter the solution through a 0.45 μm pore-size nylon membrane filter. Analyze the sample by isocratic, aqueous reversed-phase HPLC at room temperature by using a 4.6 mm I.D., 250 mm long HPLC column packed with a 5 μm Luna C18 as stationary phase and a mixture of 95: 5 MeOH : H_2O as mobile phase at a flow rate of 2 ml/min.

6. Once the reaction is complete, replace the oil bath with a cork ring. While stirring, open the side neck and add 25 ml of ethanol that will consume the excess acetic anhydride. Rotovap the reaction solvent and acetic acid by-products until no more solvent distils over.

7. Redissolve the crude product in 450 dichloromethane. Into a 5 L round bottom flask add 3.5 L of hexanes and a Teflon-coated magnetic stirrer. Place the flask in a cork-ring on a stir plate. While stirring the hexanes solvent slowly add the concentrated cyclodextrin – dichloromethane solution. Upon complete addition, allow the mixture to stand for 10 minutes and filter the precipitate.

8. Check the purity of the product by isocratic, aqueous reversed-phase HPLC, at room temperature, by using a 4.6 mm I.D., 250 mm long HPLC column packed with a 5 μm Luna C18 RP stationary phase, and a 95: 5 mixture of MeOH : H_2O as the mobile phase, at a flow rate of 2 ml/min. Typical purity level for the target is > 99%.

Heptakis(3-*O*-methyl-6-*O*-acetyl)cyclomaltoheptaose

1. Dry the pure heptakis(2-*O*-benzyl-3-*O*-methyl-6-*O*-acetyl)cyclomaltoheptaose in a vacuum oven at 60ºC to constant weight.

2. Place a 250 ml, three-neck, round bottom flask with a 1″ Teflon coated stir bar and a stopper into an oven and dry overnight at 110ºC. Set up the 250 ml three-neck flask on a stir plate. Connect a N_2 line to one of the side necks on the flask and at another neck, an oil bubbler with 1″ of paraffin oil. Cap the third neck with a ground glass stopper of appropriate size. Flush the system with dry N_2 for approximately 5 minutes. Replace the N_2 line with a stopper.

3. Obtain a 10 ml syringe and a needle. Dispose the plunger and cut the finger flanges of the hollow barrel. Insert the cut end of the hollow barrel into a balloon and secure the balloon unto the barrel over Teflon tape. Next, insert the needle into a septum. Fill the balloon with hydrogen and as quickly as possible, fit the female luer-lock connector of the needle to the male luer-lock tip of the hollow barrel.

4. Add 50 ml of anhydrous MeOH and 50 ml of anhydrous dioxane into the reaction flask. With minimum exposure, transfer 20 g of heptakis(2-*O*-benzyl-3-*O*-methyl-6-*O*-acetyl)cyclomaltoheptaose into the flask using a short-stem plastic funnel. While stirring to dissolve the cyclodextrin, flush the system with N_2 for 5 minutes. Weigh out 7 g of 10 % Pd on activated charcoal and quickly transfer it into the reaction flask. Disconnect the N_2 line and insert the needle at the end of the hydrogen-filled balloon into the septum. Allow the hydrogen to flush the system for 5 minutes, then disconnect the oil bubbler line. Note: Efficiency of this reaction is highly dependent on the quality of the catalyst.

5. With a 1 ml syringe and a needle, draw out 0.3 ml of the reaction mixture. Release the 0.3 ml reaction mixture into a 2 ml glass vial. Fill the vial to the neck with ACN. Next, filter the solution through a 0.45 μm pore-size nylon membrane filter. Analyze the

sample by reversed-phase HPLC using a 4.6 mm I.D., 250 mm long HPLC column packed with a 5 μm Luna C18 RP stationary phase, and gradient elution at a flow rate of 1 ml/min. The initial mobile phase compostion is 80 : 20 H_2O : ACN that changes to 2 : 98 H_2O : ACN in 15 minutes, at 40ºC. The reaction time is between 22 – 24 hours.

6. Upon completion of the reaction, filter the catalyst and remove the reaction solvent under reduced pressure.

7. Redissolve the crude product in 200 ml dichloromethane. Into a 3 L round bottom flask add 1.5 L of hexanes and a Teflon-coated magnetic stirrer. Place the flask in a cork-ring on a stir plate. While stirring the hexanes solvent, slowly add (dropwise) the concentrated cyclodextrin–containing dichloromethane solution. Upon complete addition, allow the mixture to stand for 10 minutes and filter the precipitate.

8. Analyse the precipitate by the HPLC method described in step 5. Typical purity level for the target is > 98%.

Heptakis(2-*O*-sulfo-3-*O*-methyl-6-*O*-acetyl)cyclomaltoheptaose

1. Place heptakis(3-*O*-methyl-6-*O*-acetyl)cyclomaltoheptaose in a crystallizing dish and dry it in a vacuum oven at 60ºC to constant weight.

2. Place a 250 ml, three-neck, round bottom flask with a 1″ Teflon-coated stir bar and a stopper into an oven and dry overnight at 110ºC. Set up the 250 ml three-neck flask on a stir plate. Connect a N_2 line to one of the side necks on the flask. Connect a condenser to the central neck and to remaining neck, an oil bubbler with 1″ of paraffin oil. Place the

flask into a paraffin oil bath on a stir plate. Flush the system with dry N_2 for approximately 5 minutes. Replace the N_2 line with a stopper.

3. Open the side neck and with minimum air exposure, add 50 ml of dry pyridine and 35 ml of DMF to the flask. Close the system with the stopper. Weigh out 10 g of heptakis(3-*O*-methyl-6-*O*-acetyl)cyclomaltoheptaose and transfer it into the flask via a short-stem plastic funnel. Begin stirring with the stir bar. Continue stirring until a clear solution is obtained. Quickly weigh out 16 g of Py.SO3 and immediately transfer into the flask via a plastic funnel. Replace the stopper.

4. Regulate the temperature of the oil bath using a Variac so that the temperature of the reaction mixture is around 40ºC. Continue stirring for 2 hours.

5. Monitor the progress of the reaction by HPLC using a 4.6 mm I.D., 150 mm long column packed with a 3µm Luna HILIC stationary phase. Use gradient elution at a flow rate of 1 ml/min. The initial mobile phase composition is 100% A that changes to 50% A : 50% B in 30 min (A: 5 mM $HCOONH_4$ in 95% ACN, B: 5mM $HCOONH_4$ in H_2O) at room temperature.

6. Once the reaction is complete, prepare a slurry of 23 g $NaHCO_3$ in 30 ml water. Place the reaction flask in an ice bath on a stir plate and begin vigorous stirring. Slowly add the slurry in portions, waiting until there is no more bubble formation (CO_2) between additions. Be careful not to lose solution because of excessive foaming. After half the slurry has been added, begin checking the pH prior to the addition of each subsequent portion. Stop the addition of the slurry when the strip of the pH paper turns green. Filter off the solids.

7. Transfer the filtrate to a 1L round bottom flask with a 1″ Teflon-coated stir bar and rotavap the solution to dryness in a high vacuum rotavap at 50ºC.

8. Dissolve the solids in 100 ml MeOH. Into a 1 L round bottom flask add 725 ml of diethyl ether and a Teflon-coated magnetic stirrer. Place the flask in a cork-ring on a stir plate. While stirring the diethyl ether solvent, slowly add the concentrated cyclodextrin - MeOH solution. A precipitate will form. Filter and obtain the precipitate. Check its purity by HPLC (Step 5). Check the removal of DMF by ^{1}H NMR. If needed, repeat Step 8.

VITA

Name:	Edward Tutu
Address:	Department of Chemistry, Texas A&M University, 3255 TAMU College Station, TX 77843-3255
Email Address:	etutu@mail.chem.tamu.edu
Education:	B.S., Chemistry, University of Cape Coast, Cape Coast, Ghana, 1998 M.S., Chemistry, University of Minnesota, Duluth, Minnesota, 2003 Ph.D., Chemistry, Texas A&M University, College Station, Texas, 2010